

FINAL
11-02-96

DEPARTMENT OF MECHANICAL ENGINEERING
COLLEGE OF ENGINEERING & TECHNOLOGY
OLD DOMINION UNIVERSITY
NORFOLK, VIRGINIA 23529

16 REF
201
3-1-97

**VARIATIONAL METHODS IN SENSITIVITY ANALYSIS AND
OPTIMIZATION FOR AERODYNAMIC APPLICATIONS**

By

A. H. Ibrahim, G. J-W. Hou
and
S. N. Tiwari, Principal Investigator

Progress Report
For the period ended June 30, 1996

Prepared for
National Aeronautics and Space Administration
Langley Research Center
Hampton, VA 23681-0001

Under
Research Grant NCC1-68
Dr. Robert E. Smith, Jr., Technical Monitor
ISSD-Scientific Applications Branch

Submitted by the
Old Dominion University Research Foundation
P.O. Box 6369
Norfolk, VA 23508-0369

August 1996

DEPARTMENT OF MECHANICAL ENGINEERING
COLLEGE OF ENGINEERING & TECHNOLOGY
OLD DOMINION UNIVERSITY
NORFOLK, VIRGINIA 23529

**VARIATIONAL METHODS IN SENSITIVITY ANALYSIS AND
OPTIMIZATION FOR AERODYNAMIC APPLICATIONS**

By

A. H. Ibrahim, G. J-W. Hou
and
S. N. Tiwari, Principal Investigator

Progress Report
For the period ended June 30, 1996

Prepared for
National Aeronautics and Space Administration
Langley Research Center
Hampton, VA 23681-0001

Under
Research Grant NCC1-68
Dr. Robert E. Smith, Jr., Technical Monitor
ISSD-Scientific Applications Branch

Submitted by the
Old Dominion University Research Foundation
P.O. Box 6369
Norfolk, VA 23508-0369

August 1996



VARIATIONAL METHODS IN SENSITIVITY ANALYSIS AND OPTIMIZATION FOR AERODYNAMIC APPLICATIONS

By

A. H. Ibrahim¹, G. J-W. Hou², and S. N. Tiwari³
Department of Mechanical Engineering
Old Dominion University
Norfolk, Virginia 23529

ABSTRACT

Variational methods (VM) sensitivity analysis, which is the continuous alternative to the discrete sensitivity analysis, is employed to derive the costate (adjoint) equations, the transversality conditions, and the functional sensitivity derivatives. In the derivation of the sensitivity equations, the variational methods use the generalized calculus of variations, in which the variable boundary is considered as the design function. The converged solution of the state equations together with the converged solution of the costate equations are integrated along the domain boundary to uniquely determine the functional sensitivity derivatives with respect to the design function.

The determination of the sensitivity derivatives of the performance index or functional entails the coupled solutions of the state and costate equations. As the stable and converged numerical solution of the costate equations with their boundary conditions are *a priori* unknown, numerical stability analysis is performed on both the state and costate equations. Thereafter, based on the amplification factors obtained by solving the generalized eigenvalue equations, the stability behavior of the costate equations is discussed and compared with the state (Euler) equations. The stability analysis of the costate equations suggests that the converged and stable solution

¹Graduate Research Assistant

²Professor

³Eminent Professor

of the costate equation is possible only if the computational domain of the costate equations is transformed to take into account the reverse flow nature of the costate equations.

The application of the variational methods to aerodynamic shape optimization problems is demonstrated for internal flow problems at supersonic Mach number range. The study shows, that while maintaining the accuracy of the functional sensitivity derivatives within the reasonable range for engineering prediction purposes, the variational methods show a substantial gain in computational efficiency, i.e., computer time and memory, when compared with the finite difference sensitivity analysis.

ACKNOWLEDGMENTS

This is a progress report on the research project "Surface Modeling and Optimization Studies of Aerodynamic Configurations." Within the guidelines of the project, special attention was directed toward research activities in the area of "Variational Methods in Sensitivity Analysis and Optimization for Aerodynamic Application." The period of performance of this specific research ended June 30, 1996.

The authors wish to express their sincere thanks to Dr. Greg Burgreen, Dr. Mohammed Elehaky, Dr. K. P. Singh, Mr. James Lacasse, Mr. James Newman, III, and Dr. Gwen Wei Yen for their assistance during the entire period of this study. Also, sincere thanks are extended to Drs. A. O. Demuren, P. A. Newman, and A. C. Taylor, III for critical review and evaluation of this work. The basic concept for this research was suggested by Dr. O. Baysal and coworkers and by Dr. A. C. Taylor and coworkers.

This work, in part, was supported by the NASA Langley Research Center through Cooperative Agreement NCC1-68. The cooperative agreement was monitored by Dr. Robert E. Smith, Jr. of ISSD-Scientific Applications Branch, NASA Langley Research Center, Mail Stop 125.

TABLE OF CONTENTS

	<u>Page</u>
ABSTRACT	iii
ACKNOWLEDGMENTS	iv
LIST OF TABLES	xi
LIST OF FIGURES	xii
NOMENCLATURE	xiv
Chapter	
1. INTRODUCTION	1
1.1 Overview of Aerodynamic Design Optimization and Sensitivity	
Analysis	1
1.1.1 Nongradient Methods	1
1.1.2 Gradient-Based Methods (Numerical Design Optimization)	3
1.1.2.1 Finite Difference Sensitivity Analysis	4
1.1.2.2 Discrete Sensitivity Analysis	4
1.1.2.3 Variational Sensitivity Analysis	6
1.2 Stability Analysis of Euler and Costate Equations	8
1.3 Motivations	9
1.3.1 Computational Efficiency	9
1.3.2 Generality of the Variational Approach	10
1.4 Objectives	11
1.5 Prelude to Chapters 2 - 7	11

2. FLOW FIELD ANALYSIS	13
2.1 Rationale for Two-Dimensional Euler Equations	13
2.2 Governing Equations of Two-Dimensional Euler Equations	13
2.3 Solution Algorithm	16
2.3.1 Finite Volume Formulation	16
2.3.2 Inviscid Upwind Spatial Differencing	17
2.3.3 Van Leer flux Vector Splitting	19
2.3.4 Time Integration	20
2.4 Initial and Boundary Conditions of Two-Dimensional Euler Equations	23
2.5 Governing Equations of Quasi One-Dimensional Euler Equations	25
2.5.1 Quasi One-Dimensional Euler Equations in NonConservative Form.....	25
2.5.2 Quasi One-Dimensional Euler Equations in Conservative Form	26
2.6 Initial and Boundary Conditions of Quasi One-Dimensional Euler Equations.....	27
3. AERODYNAMIC DESIGN OPTIMIZATION AND SENSITIVITY ANALYSIS	28
3.1 General Scope	28
3.1.1 Sensitivity Information	28
3.1.2 Discrete Versus Variational Methods	30

3.2 Constrained Optimization Methodology	31
3.2.1 Design Variables in Variational Sense	31
3.2.2 Constraints	33
3.2.3 Objective Functional	34
3.3 Variational Formulation of Aerodynamic Optimization Problem ...	34
3.3.1 Standard Formulation of an Aerodynamic Optimization Problem	36
3.3.2 Derivation of Functional Sensitivity Equations	36
3.3.3 Derivation of Constraint Sensitivity Equations	42
3.4 Numerical Optimization	43
4. COSTATE EQUATIONS AND SOLUTION METHODS	46
4.1 Introduction to Numerical Integration of Costate Equations	46
4.2 Costate Equations	46
4.3 Boundary (Transversality) Conditions	47
4.4 Linearization of Costate(Adjoint) Equations	48
4.5 Time-Integration Methods to Costate Equations.....	49
5. STABILITY ANALYSIS OF TWO-DIMENSIONAL COSTATE AND EULER EQUATIONS	51
5.1 Rationale for Stability Analysis.....	51
5.2 Introduction to Stability Analysis	51
5.3 Objective and Motivation	53

5.4 One- and Two-Dimensional Euler Equations	54
5.4.1 One-Dimensional Euler Equations	54
5.4.2 One-Dimensional Costate Equations	55
5.4.3 Two-Dimensional Euler Equations	55
5.4.4 Two-Dimensional Costate Equations	57
5.5 Solution Algorithm	58
5.5.1 Complex Eigenvalue Equations of Euler and Costate Equations	59
5.5.2 One-Dimensional Euler-Fourier Symbols	59
5.5.3 One-Dimensional Costate Fourier Symbols	60
5.5.4 Two-Dimensional Euler-Fourier Symbols	60
5.5.5 Two-Dimensional Costate Fourier Symbols	60
5.6 Results, Discussion, and Recommendations.....	61
6. DESIGN OPTIMIZATION OF INTERNAL FLOWS USING QUASI ONE- DIMENSIONAL EULER EQUATIONS	70
6.1 Introduction to One-Dimensional Design Optimization	70
6.2 Model Problem	71
6.3 Approach1: Perturbed State Equations and Performance Indices in Nonconservative Variables	72
6.4 Approach 2: Perturbed State Equations and Performance Indices in Conservative Variables	77
6.5 Solution Algorithm and Surface Modification	81
6.6 Numerical Results and Discussion	82
6.7 Conclusions	83

7. RESULTS AND DISCUSSION ON DESIGN OPTIMIZATION OF INTERNAL FLOWS USING TWO-DIMENSIONAL. EULER EQUATIONS	98
7.1 Two-Dimensional Nozzle Optimization Problem	
Formulation	98
7.2 Two-Dimensional Nozzle Flow	99
8. CONCLUSIONS AND RECOMMENDATIONS	114
REFERENCES	117
APPENDICES	127
APPENDIX A: CONTINUOUS DOMAIN IN VARIATIONAL METHODS	128
APPENDIX B: DERIVATION OF THE SURFACE TRANSFORMATION JACOBIAN	131
APPENDIX C: VARIOUS MATRICES IN CONSERVATIVE FORMS FROM THE QUASI ONE-DIMENSIONAL EULER EQUATIONS	133
APPENDIX D: TWO-DIMENSIONAL JACOBIAN MATRICES THAT ARE USED FOR THE STABILITY ANALYSIS .	136
APPENDIX E: DERIVATION OF TWO-DIMENSIONAL CONSERVATIVE VAN LEER JACOBIAN MATRICES IN GENERALIZED COORDINATES	139

LIST OF TABLES

<u>Table</u>	<u>Page</u>
7.1 CPU Time and Memory for Four, Eight, and Twelve Design Variables with Variational Methods	103
7.2 Sensitivity Derivatives with Variational Methods and Finite Difference ..	103
7.3 Initial and Optimal Values of Functional and Constraint for Variational Methods and Finite Difference	104
7.4 Efficiency Comparison Between Variational Methods and Finite Difference	104

LIST OF FIGURES

Figure		Page
3.1	Variation of domain by one-parameter family of mapping.	45
3.2	Boundary variation normal to the original boundary $\partial\Omega$	45
5.1	Amplification of unfactored 2-D Euler equations.	63
5.2	Amplification of 1-D Euler equations.	64
5.3	Amplification of factored 2-D Euler equations.	65
5.4	Amplification of factored 1-D costate equations without space transformation.	66
5.5	Amplification of factored 2-D costate equations without space transformation.	67
5.6	Amplification of factored 1-D costate equations with space transformations.	68
5.7	Amplification of factored 2-D costate equations with space transformations	69
6.1	Thrust evolution for supersonic flow.	85
6.2	Thrust evolution for shock flow.	86
6.3	Thrust evolution for subsonic flow.	87
6.4	Area evolution for the shock flow.	88
6.5	Initial and optimized Mach number distributions for the shock flow.	89
6.6	Initial and optimized pressure distributions for the shock flow.	90
6.7	Area evolution for subsonic flow.	91
6.8	Initial and optimized pressure distributions for subsonic flow.	92

6.9	Initial and optimized Mach number distributions for subsonic flow.	93
6.10	Shape evolution for supersonic flow.	94
6.11	Initial and optimized Mach number distributions for supersonic flow.	95
6.12	Initial and optimized pressure distributions for supersonic flow.	96
6.13	Mass error for the shock flow.	97
7.1	Initial supersonic nozzle shape.	105
7.2	Effect of the number of design variables on the optimal shape. ...	106
7.3	Effect of the number of design variables on the optimal thrust. ...	107
7.4	History of the design variables for the variational methods.	108
7.5	History of the design variables for the finite difference.	109
7.6	Optimal shapes by variational methods and finite difference.	110
7.7	Optimal pressure contours by variational methods.	111
7.8	Pressure distributions on the solid and symmetry line by variational methods.	112
7.9	Optimal thrust history by the variational methods and finite difference.	113

NOMENCLATURE

a	local speed of sound
A, B	Jacobian matrices in the Cartesian coordinate system
\bar{A}, \bar{B}	Jacobian matrices in deformed space
\hat{A}, \hat{B}	Jacobian matrices in the generalized coordinate system
\hat{A}^\pm, \hat{B}^\pm	split Jacobians in generalized coordinate system
ADI	alternate directional implicit factorization
B_n	Jacobian of source terms in one-dimensional Euler equations
$B_{i,n}$	Bezier blending function
C	derivative of the pressure with respect to the conservative variables
$C(n,i)$	binomial coefficients
C_D	drag coefficient
C_L	lift coefficient
C_p	pressure coefficient
CFL	Courant-Friedrichs-Lewy number
D	objective function
E, F	inviscid flux components in Cartesian coordinates
\bar{E}, \bar{F}	inviscid flux components in deformed space
\hat{E}, \hat{F}	inviscid flux vectors in the generalized coordinate system
\bar{f}	Bezier generalized function
f_{energy}^\pm	Van Leer positive and negative energy flux
f_{mass}^\pm	Van Leer positive and negative mass flux
g_j	constraint functions

G	constraint functional
G	residual for quasi one-dimensional equations
H_s	vector of source terms
H, \bar{H}	boundary conditions
I	imaginary number
I	identity matrix
J	functionals or performance indices
J_{ar}	modified functional
J_s	space transformation Jacobian
k	constant parameter for upwind-biased formulation
L	nozzle length
\hat{L}	left side Fourier symbols
M_h	the derivative of the source term with respect to $\frac{dS}{dx}$
M_ξ	Mach number in generalized coordinate system
\bar{N}	unit vector in generalized coordinate
\bar{n}	unit vector in Cartesian coordinate
\hat{n}	unit vector in deformed space
nconf	number of generic fluid type constraints
ndv	number of design variables
n_x, n_y	unit vector components in the x and y directions
P	pressure
\bar{P}_0	initial constant vectors
\bar{q}	nonconservative variables
\bar{Q}	conservative variables in undeformed space
$\bar{\bar{Q}}$	conservative variables in deformed space
$\bar{\hat{Q}}$	conservative variables in generalized coordinates
\bar{r}	vector of spatial derivatives of One-Dimensional Euler equations

R	discrete residual in Cartesian coordinate system
\bar{R}	continuous residual in Cartesian coordinate system
\hat{R}	residual in generalized coordinates
\hat{R}	right side Fourier symbols
R_λ	costate residual
S	cross-sectional area
$s_x =$	the derivative of S with respect to x ($\frac{dS}{dx}$)
\bar{S}	search direction
u	velocity in the x direction
u_b	velocity at the boundary in the x direction
\bar{u}	normalized Bezier curve
U	normalized contravelocity in the ξ direction
\bar{U}	contravelocity in the ξ direction
v	velocity in the y direction
v_b	velocity at the boundary in the y direction
V	normalized contravelocity in the η direction
\bar{V}	contravelocity in the η direction
\bar{V}	eigenvectors
VM	variational methods
\bar{X}	spatial vector in the Cartesian coordinates
\bar{X}_D	vector of design variables

Greek symbols:

α	move parameter or step size for the search direction
α_i	constants for the Runge-Kutta time integration
β	parameter for upwind-biased approximation
γ	gas constant = 1.4

$\vec{\Gamma}$	vector of boundary components
δ	difference operator
δ	variational symbol
$\delta_{i,j}$	Kronecker delta
Δ	increment
Δ	forward operator
∇	backward operator
ε	step size for search direction
ε	small quantity for space transformation
ε	pressure ratio constant
ς	space transformation parameter
η, ξ	generalized curvilinear coordinate components
κ	curvature
$\vec{\lambda}$	vector of Lagrangian parameters
$\vec{\mu}$	vector of constant Lagrangian parameters
\vec{v}	vector of extremizing functions
\vec{v}^*	vector of optimal extremizing functions
$\vec{\xi}$	vector of generalized curvilinear coordinates
ρ	density
σ	smoothing factor
Σ	summation
τ	transformed time in the generalized curvilinear system
$\vec{\varphi}$	vector of amplification factors
$\vec{\omega}$	vector of extremizing functions
Ω	domain of integration in undeformed space
$\bar{\Omega}$	domain of integration in deformed space

Subscripts:

a	augmented value
b	values on the boundary
h	derivatives of the source terms
i, j	spatial indices
x, y	Cartesian coordinate components
s	source terms
t	time derivative in Cartesian system
τ	time derivative in generalized curvilinear system
Γ	on the boundary
\pm	right and left side MUSCL extrapolation
∞	reference values

Superscripts:

m	level of surface update
n	temporal level
T	transpose
\pm	positive and negative fluxes and Jacobians
$*$	optimum solutions; intermediate solutions

Special symbols:

$ $	absolute value
\in	inclusion or subdomain
\otimes	vector multiplication
\circ	inner or dot product
∂	partial derivatives

Chapter 1

INTRODUCTION

This chapter presents the global picture of design optimization and sensitivity analysis, briefly analyzes the historical and current state of optimization methodologies, outlines the motivations and objectives of the present research, and gives a short prelude to the remaining chapters .

1.1 Overview of Aerodynamic Design Optimization and Sensitivity Analysis

In the early times of flight, improvement of vehicle performance was mostly based first on intuition, empirically accumulated databases, and cut-and-try procedures [1,2]. Even recently, wind tunnel testing is being employed to perform optimization work to obtain airfoil performance criteria [3]. While this approach gave many valuable technical assistances, it was unable to furnish quick and reliable information to perform on-line design changes.

In recent years, aerodynamic performance has been analyzed by a method of mathematical optimization. Optimizations can be performed either by those methods which need no gradient evaluations or by those which require gradient information.

1.1.1 Nongradient Methods

Variational methods (VM) were widely used to replace nonlinear partial differential flow equations and their boundary conditions with nonlinear algebraic equations and their corresponding boundary conditions so that approximate

solutions could easily be obtained. Bateman [4] is known for his formulation of the irrotational compressible inviscid flow using variational principles. Rasmussen and Heys [5] have extensively applied the application of variational methods to potential flows.

Although the variational methods were used for the flow analysis in Refs. 4 and 5, their application for design purposes is also well documented. With the Newtonian flow assumption and the linearized supersonic flow analysis, Miele [6 - 11] used the variational methods (VM) to obtain the optimality criteria. Then, employing this optimality criteria, he determined the geometry of a slender body of revolution having minimum pressure drag, optimized a two-dimensional wing for minimum pressure drag, designed optimal airfoils for supersonic speeds, and computed the optimal path for vehicles flying in different mediums. This approach has been used in solving many interesting and complex engineering problems with application to diversified fields, such as atmospheric and oceanographic studies [12,13] and planetary sciences [14]. To design nozzle shapes, Rao [15] combined variational approach and characteristic methods. Shmyglevskii [16] used VM and methods of characteristics to predict wave drag of high Mach number flow. Mikhlin [17] treated many mathematical-physics problems using this same method. In line with Rao [15], Thompson and Murthy [18] combined the characteristics methods and VM to design a three-dimensional rocket motor nozzle. In this class of optimization [6 - 18], the complete form of the Euler-Lagrangian equations and their boundary conditions are derived from the augmented Lagrangian and, thereafter, they are solved for the extremizing functions or curves until the measure of criteria is satisfied.

From the combination of wide range of experiences in flow physics and wind tunnel techniques, the other category of optimization, i.e., the inverse design approach, has made immense contributions to design optimization. Lighthill [19],

in his pioneer work of optimization, showed how to numerically optimize a two-dimensional airfoil for a prescribed pressure distribution using an inverse design approach. An ample number of researchers [20 - 24] have also applied this same method from lower subsonic to hypersonic flow regimes in two-and three-dimensional problems. Using a stream-line curvature method, Campbell [25] has also applied this approach to solve constrained optimization to design airfoils. The inherent problems with this approach, though, are the limitations in casting all relevant design problems in the form amenable to the inverse design optimization procedure and the requirement of high level of expertise to determine *a priori* the target objective functions. For this approach to work, the physics of the flow must be determined *a priori* in terms of the pressure or other quantities, and thereafter, the geometry that matches the above physical criterion must be sought.

The other categories are the neural-network optimization approaches [26 - 29]. While their applications are gaining momentum, they also have drawbacks due to the need for an extensive database, prior ideas about the optimal solution, intensive computations, and large computer memory.

Note that all the design approaches mentioned previously do not require gradient computations. Therefore, they are efficient for moderate optimization problems. The limitations, though, are that those approaches are restricted to a certain class of problems with large databases and immense expertise and are confined to simplified geometries and flow field equations.

1.1.2 Gradient-Based Methods (Numerical Design Optimization)

With the advantage of modern hardware and software computer technologies, numerical design optimization and sensitivity analysis are currently solving

complete aircraft design in two-dimensional Navier-Stokes and three-dimensional Euler equations of the fluid flow.

1.1.2.1 Finite Difference Sensitivity Analysis

The simplest, but the most expensive, sensitivity analysis technique used by gradient-based optimization methods is the finite difference approach. This method uses the one-sided or central-difference alternative to evaluate the sensitivities of performance functionals, and consequently, the computational time invested would increase with the increment of the number of design variables. This is due to the requirement to perturb each design variable by an appropriate step size and then compute the flow field variable for each new perturbed design variable with the chosen flow solver. This approach has an additional problem to determine the correct step size *a priori* so that the correct gradient is predicted within a given degree of accuracy. Despite its shortcomings, Huddelston and Mastin [30], and others, have applied this approach in their design procedure with Euler and Navier-Stokes equations as their flow field approximations. In the optimization package for general purposes optimizations, Vanderplaats [31] has also incorporated finite difference as an alternative to acquire the gradient information.

1.1.2.2 Discrete Sensitivity Analysis

The other category of sensitivity analysis technique is the discrete analysis approach. The computation of the sensitivity equations is based on the Implicit Function Theorem. Due to the implicit dependence of the functional (objective function) and constraints on the flow field quantities, the determination of the sensitivity derivatives is related to obtaining the derivatives of the flow field vector with respect to the design variables. As the flow field equations are in most cases

solved in a computational domain, the functional dependence of the metric terms and the coordinate points with respect to the design variables are also required. This approach first calls upon the multiplication and assembly of various terms to a very large sparse linear algebraic equations, which depends on the number of design variables, and then solution of these sparse system of algebraic equations for the derivatives of the solution vector with respect to the design variables. Despite the large computational intensity and huge memory requirements of this approach, the versatility to incorporate many types of constraints, the need to perform multidisciplinary designs of moderate geometrical complexity, and the flexibility to incorporate it with any existing optimization algorithm make it attractive to perform design and shape optimizations.

A wealth of literature can be found for this category. Hicks [32] and Vanderplaats [33,34] have used the discrete approach to design airfoils in transonic flow regimes. Pittman [35] has also used this procedure for supersonic flow conditions. Using the small perturbation equations in two dimensional flows, Elbana and Carlson [36] have also employed the technique. Recently Baysal and Eleshaky [37,38] and Eleshaky and Baysal [39] used this method for both internal and external flow problems. They also integrated the domain decomposition method in solving the sensitivity equations. Burgreen and Baysal [40,41] and Burgreen [42] further extended the methodology to the three-dimensional wing optimization and introduced an efficient way of parameterizing the curves and surfaces using the Bezier polynomials. Lacasse [43] applied the method to optimize multielement airfoils for two-dimensional, thin-layer, Navier-Stokes laminar equations. With a variant of approximation to the fluid flow, Taylor et al. [44,49], Newman et al. [45], Korivi et al. [46,48], and Hou et al. [47] introduced an incremental iterative technique to obtain the gradient information. In doing so, they have applied this new approach not only to the two-dimensional Euler and

thin-layer Navier-Stokes turbulent equations for internal and external flows but also to the three-dimensional Euler equations in supersonic flow regimes.

1.1.2.3 Variational Sensitivity Analysis

The new emerging sensitivity analysis technique for gradient-based optimization methodology within the optimization community is the continuous sensitivity (variational sensitivity) analysis which fully exploits the variational methods. From the modified functional, this approach derives a set of partial differential equations (PDEs), i.e. the costate equations with their boundary conditions and the sensitivity equations. In computing the sensitivity derivatives with respect to the control points or design variables, this approach makes use of the converged solution of the state and costate equations.

In recent years, variational sensitivity analysis has significantly contributed to the progress of aerodynamic design optimization. Lions [50], Pironneau [51], and Glowinski and Pironneau [52] showed the usefulness of the variational approach in fluid mechanical problems by illustrating how to compute the minimum drag profile in two-dimensional viscous and laminar flows. Chen and Seinfeld [53] developed a methodology to compute the performance sensitivity derivatives using optimal control theory. Koda et al. [54] used this procedure to solve atmospheric diffusion problems. Koda [55 - 57] further developed this approach and outlined a numerical algorithm for the computation of functional derivatives. This approach is well suited to solving the optimum design problems in fluid mechanics. Meric [58,59] treated optimal control problems governed by parabolic and elliptic partial differential equations and solved them numerically using variational methods. In their effort to compare the gradients obtained by "implicit" and "variational" approaches, Shubin and Frank [60] implemented VM to optimize the shape of a nozzle of a variable cross-sectional area for steady

one-dimensional Euler equations. Hou and Sheen [61] used a class of VM to derive second-order shape sensitivity equations of heat conduction problems. Jameson [62] regarded the boundary of the flow domain as a control parameter and then designed airfoils using the potential as well as the two- and three-dimensional compressible inviscid flows. Cabuk and Modi [63] implemented a perturbation method to compute the optimum profile of a diffuser for a maximum static pressure in a two-dimensional steady viscous incompressible flow. Ta'asan et al. [64] have successfully implemented variational methods and optimized an airfoil in the potential flow field. Quite recently, Ibrahim and Baysal [65] demonstrated the versatility of the variational methods to solve aerodynamical design problems for internal flows in different Mach number regimes including shock flows. Following the same approach as Jamson [62], Reuter and Jameson [66] optimized airfoils in potential flows. Also following the same solution method of Ta'asan et al. [64], Kurivila et al. [67] used the potential equations as their state equations and optimized the NACA 0012 airfoil for a given pressure distribution. Iollo and Salas [68] used variational methods to solve two-dimensional internal flow optimization problem with embedded shock to match a pressure distribution. In addition to the general application of VM, many researchers have also proposed a numerical algorithm to accelerate convergence and improve efficiency for optimal design problems [69,70]. In this class of optimization, the functional sensitivity derivatives are directly coupled to the solution of a set of linear partial differential equations, i.e., the costate equations and their boundary or transversality conditions that result from the variation of the augmented Lagrangian function. The success of any optimization by this approach is, therefore, destined to a stable and converged solution of the costate equations.

1.2 Stability Analysis of Euler and Costate Equations

The most popular schemes to advance any PDE, such as the Euler equations to steady-state solutions, are the implicitly factored time integration schemes (ADI). Unfortunately, approximate factorizations introduce errors that propagate throughout the computational domain. As a result of this, the stability limit is drastically reduced and the convergence rate deteriorates. To propose the range of Courant-Friedrichs-Lewy (CFL) numbers for which the allowable maximum eigenvalues are predicted, a stability analysis of the Euler and costate equations for the optimization purposes is conducted.

Jespersen and Pulliam [71] studied the stability characteristics of the Euler equations for different flux-splitting methods. Anderson and Thomas [72] further conducted stability analysis on the complete three-dimensional Euler equations. Demuren and Ibraheem [73] have also pursued an extensive and complete stability analysis of one-, two-, three-dimensional Euler and two- and three-dimensional Navier-Stokes equations. The common conclusion of these researchers [71 - 73] is that the stability solutions of state equations are impaired because of factorization and are dependent on the types of splitting and flux approximations. Also, the stability deteriorates as the dimensionality of the fluid equations increases. The stability problem associated with the numerical integrations of the costate equations was reported in Ibrahim and Baysal [65]. Although no stability analysis was performed for the costate equations in Ref. 65, its convergence and stability were assured by taking into account the reverse flow nature of the costate equations.

1.3 Motivations

The advantage and disadvantage of the various approaches to perform design optimizations and sensitivity analysis are briefly discussed in Sec. 1.1. The main thrust of the exposition is intended to understand the complexities involved in each approach and to take advantage of the best of each approach as complementary to the others to realize a certain level of optimization goals.

The major problems associated with any gradient-based numerical optimization are the penalties incurred because of the computational **memory** and **time** in obtaining the sensitivity gradients. These bottle-necks can be attributed to the repetitive need to solve the flow analysis for a change of any design variable and the huge memory allocation needed to store the derivatives of the objective function and constraints with respect to the design variables. This problem becomes more acute when one wants to design complex geometry using full Navier-Stokes equations at many design points in a multidisciplinary mode. While enjoying wide popularity and applicability, discrete sensitivity analysis has the previously mentioned potential limitations. Although no methodology exists which would overcome the aforementioned pitfalls of numerical optimization problems with the current state of computing facilities, sensitivity analysis by the variation methods (VM) is proposed in this study to partially alleviate the problems associated with huge memory allocation for moderate two-dimensional Navier-stokes and three-dimensional Euler equations. In this study, the motivation can be streamlined into three sub groups: efficiency in memory, efficiency in time, and generality in application.

1.3.1 Computational Efficiency

Independent of the approach one adopts, the complete optimization of gradient-based approach requires a repetitive solution of the state equations.

This being common to all, one is also concerned with the computational intensity and memory efficiency in the pursuits of the optimal solution. Here, efficiency is measured by the number of mathematical operational counts (time) associated with the computation and the computer memory saved in using the new proposed approach. The sensitivity analysis by the variational methods (VM) proposed in this study overcomes some of the critical issues by having some flexibility. First, the sensitivity analysis by VM involves the solution of the costate equations with their boundary conditions for already converged solution of the state equations. Also, because there are no metric and grid sensitivities as a result of a unique feature of the sensitivity analysis by variational methods, a substantial saving in computer memory is achieved. This is detrimental in large two-dimensional Navier-stokes and three-dimensional Euler equations.

1.3.2 Generality of the Variational Approach

First, since the costate equations are once and for all derived from the continuous PDE of the state equation, any robust solution method can be adopted to furnish the converged solution so that the costate equations can be solved until convergence is attained. This means that one does not necessarily have to solve the original state equation from which the costate equations are derived. Secondly, any other convenient discretization methods different from the type of discretization one uses for the state equations can be selected for the costate equations. The requirement that the costate equations be discretized exactly the same way as the state equations is shown not to be necessary, at least for quasi one-dimensional Euler equations [74]. Thirdly, any time integration method different from the time integration method used for the state equation can be selected to advance the costate equations to steady state. The fourth point to mention is the design variables. In the approach proposed, note that the shape of

the domain is considered as the design parameter, and its contribution to the functional sensitivity derivatives is directly incorporated as shown in Chap. 3 and Appendices B and C.

1.4 Objectives

From the short motivations mentioned in Sec. 1.3, one would set the following objectives for the this study:

- (1) Develop a design optimization methodology based on sensitivity computed by the variational methods (VM), which is computationally efficient and general for aerodynamic optimization applications.
- (2) Investigate the causes of slow convergence and establish stability criteria for the costate equations by performing a complete stability analysis of the costate and Euler equations.
- (3) Demonstrate the concept on quasi one-dimensional Euler flow problems.
- (4) Extend the methodology to two-dimensional Euler equations of internal flows.

1.5 Prelude to Chapters 2 - 7

Chapter 2 presents the general two-dimensional Euler equations of the fluid flow in conservative forms as used in the general purpose CFL3D computer code [75] and the quasi one-dimensional Euler equations in conservative and nonconservative forms [76]. Chapter 3 gives a detailed procedure for aerodynamic sensitivity analysis of a two-dimensional nozzle problem by the

variational methods including the pertinent formulations and, finally, the derivation of the costate equations, their boundary conditions, and the sensitivity equations. Chapter 4 addresses the numerical approximations, discretizations, and time integrations of the costate equations. As the numerical solution of the costate equations are the prerequisite to obtain the gradient information, a complete numerical stability analysis is presented, and the results are discussed in Chap. 5 for the one- and two-dimensional equations of the costate and Euler equations. Chapter 6 demonstrates the applications of variational methods for sensitivity analysis by applying it to the quasi one-dimensional Euler equations for conservative and nonconservative flow field quantities. Chapter 7 discusses the optimization results for two-dimensional internal flow problem of the proposed approach for aerodynamic sensitivity analysis, and Chap. 8 finalizes the proposed theme (variational methods) and gives some recommendations for the future work in this particular area.

Chapter 2

FLOW FIELD ANALYSIS

2.1 Rationale for Two-Dimensional Euler Equations

One of the integral parts of an optimization procedure is the correct approximation of the state equations. Depending on the simplicity, efficiency, and accuracy of the optimization procedure, any level of approximation to the flow physics can be adopted. To demonstrate the proposed optimization methodology, i.e., the variational methods (VM), we have chosen the Euler equations in conservative form. The choice of the state equations in conservative form renders it simpler to derive the costate equations along with their auxiliary conditions and sensitivity coefficients.

2.2 Governing Equations of Two-Dimensional Euler Equations

The Two-Dimensional, unsteady, Euler equations can be written in an integral form as [75,77]

$$\iiint_{\Omega} \frac{\partial \bar{Q}}{\partial t} dV + \iint_{\partial \Omega} \bar{G} \cdot \bar{N} dS = \bar{0} \quad (2.1)$$

where \bar{G} represents the vector of fluxes that is represented by

$$\bar{G} = E \circ \bar{i} + F \circ \bar{j} \quad (2.2)$$

Here, E , and F are the cartesian flux components and \vec{i} , and \vec{j} are the unit vectors in the x and y directions, respectively. In Eq. (2.1), \vec{N} is the unit normal pointing outward at the boundary and is defined as

$$\vec{N} = [n_x, n_y]^T \quad (2.3)$$

The conservative dimensionalized solution vector and fluxes of the two-dimensional Euler equations in the Cartesian coordinate systems are given as

$$\vec{Q} = [\rho, \rho u, \rho v, \rho e_t]^T \quad (2.4)$$

$$E = [\rho u, \rho u^2 + p, \rho uv, (\rho e_t + p)u]^T \quad (2.5)$$

$$F = [\rho v, \rho vu, \rho v^2 + p, (\rho e_t + p)v]^T \quad (2.6)$$

where ρ , u , v , e_t , p , E , and F are the density, velocity in the x direction, velocity in the y direction, total internal energy, pressure, flux in the x direction, and, flux in the y direction, respectively.

By an assumption of a smooth continuity on the integrand and application of the divergence theorem, Eq. (2.1) can be transformed to its mathematically equivalent differential form as

$$\frac{\partial \vec{Q}}{\partial t} + \frac{\partial E}{\partial x} + \frac{\partial F}{\partial y} = \vec{0} \quad (2.7)$$

Given the reference length L , the free-stream density ρ_∞ , and the free-stream speed of sound a_∞ the dimensional solution vector \vec{Q} , and the other relevant

dimensional quantities in Eq. (2.7) are nondimensionalized with the help of the following definitions:

$$x = \frac{\tilde{x}}{L} \quad y = \frac{\tilde{y}}{L} \quad (2.8a)$$

$$u = \frac{\tilde{u}}{a_\infty} \quad v = \frac{\tilde{v}}{a_\infty} \quad (2.8b)$$

$$\rho = \frac{\tilde{\rho}}{\rho_\infty} \quad P = \frac{\tilde{P}}{\rho_\infty a_\infty^2} \quad (2.8c)$$

where the tilda denotes a dimensionalized quantity. To perform time integration in uniform meshes, Eq. (2.7) is further transformed to a boundary-conforming space by use of stationary generalized curvilinear coordinate transformation as follows:

$$\xi = \xi(x, y) \quad \eta = \eta(x, y) \quad \tau = t \quad (2.9)$$

With the help of Eqs. (2.8) and (2.9), Eq. (2.7) is transformed to

$$\frac{\partial \tilde{Q}}{\partial \tau} + \frac{\partial \hat{E}}{\partial \xi} + \frac{\partial \hat{F}}{\partial \eta} = \bar{0} \quad (2.10)$$

where

$$J = \frac{\partial(\xi, \eta)}{\partial(x, y)} = (x_\xi y_\eta - x_\eta y_\xi)^{-1} \quad (2.11)$$

$$\tilde{Q} = \frac{\bar{Q}}{J} = J^{-1}[\rho, \rho u, \rho v, \rho e_t]^T \quad (2.12)$$

$$\bar{U} = \xi_x u + \xi_y v \quad (2.13a)$$

$$\bar{V} = \eta_x u + \eta_y v \quad (2.13b)$$

$$\hat{E} = J^{-1} [\rho \bar{U}, \rho u \bar{U} + P \xi_x, \rho v \bar{U} + P \xi_y, (P + e_t) \bar{U}]^T \quad (2.14a)$$

$$\hat{F} = J^{-1} [\rho \bar{V}, \rho u \bar{V} + P \eta_x, \rho v \bar{V} + P \eta_y, (P + e_t) \bar{V}]^T \quad (2.14b)$$

In Eqs. (2.12) - (2.14), \bar{Q} is the vector of conservative variables, \hat{E} and \hat{F} are the fluxes, \bar{U} and \bar{V} are the contravariant velocities in the new coordinate systems, and J is the Jacobian of transformation. The pressure P is related to the field variables through

$$P = (\gamma - 1) \rho \{e_t - 0.5(u^2 + v^2)\} \quad (2.15)$$

The various metric terms in Eqs. (2.9) - (2.14) are computed as

$$\xi_x = J y_\eta \quad \eta_x = -J y_\xi \quad \xi_y = -J x_\eta \quad \eta_y = J x_\xi \quad (2.16)$$

2.3 Solution Algorithm

The basic governing equations and their formulations in the finite volume sense are presented in this section. Also, the various steps in approximating and advancing the solution to the steady state are briefly discussed.

2.3.1 Finite Volume Formulation

The guarantee to satisfy the mass, momentum, and energy across the cell faces, the ease with which to deal with complex geometries and discontinuities,

and the choice to work either on the physical or computational domain make the finite volume approach preferable to the finite difference approach. In this two-dimensional approach, the conserved field variables are cell-area averaged and computed at the cell center while the fluxes are computed at the cell faces with these cell-centered quantities. If one integrates Eq. (2.6) over the control volume bounded by lines of constant ξ and η , then the resulting semidiscrete equations become:

$$\left(\frac{\partial \bar{Q}}{\partial t}\right)_{i,j} + \hat{E}_{i+\frac{1}{2},j} - \hat{E}_{i-\frac{1}{2},j} + \hat{F}_{i,j+\frac{1}{2}} - \hat{F}_{i,j-\frac{1}{2}} = \bar{0} \quad (2.17)$$

where i and j are the grid points. We have also taken

$$\Delta \xi = 1 \quad \Delta \eta = 1 \quad (2.18)$$

and the cell-averaged $\bar{Q}_{i,j}$ is computed as

$$\bar{Q}_{i,j} = \frac{1}{V} \left\{ \iint_V \bar{Q}(x,y,t) dV \right\}_{i,j} \quad (2.19)$$

2.3.2 Inviscid Upwind Spatial Differencing

A Monotone Upstream Centered Scheme for Conservation Law (MUSCL) is generally adopted in the CFL3D computer code [75]. For instance, the derivative in the ξ direction is

$$\left(\frac{\partial \hat{E}}{\partial \xi}\right)_{i,j} = \hat{E}_{i+\frac{1}{2},j} - \hat{E}_{i-\frac{1}{2},j} \quad (2.20)$$

where the cell-face fluxes are constructed from the cell-center solution variables, which are located on the left and right sides of the cell faces. Mathematically, the fluxes can be expressed as

$$\hat{E}_{i+\frac{1}{2},j} = \hat{E}(\bar{q}^-, \bar{q}^+)_{i+\frac{1}{2},j} \quad (2.21)$$

where \bar{q}^\mp are the nonconservative variables constructed from the upwind biased interpolations given by

$$\bar{q}_{i+\frac{1}{2},j}^- = \bar{q}_{i,j} + \left\{ \frac{1}{4} [(1-k)\bar{\Delta}_- + (1+k)\bar{\Delta}_+] \right\}_{i,j} \quad (2.22a)$$

$$\bar{q}_{i+\frac{1}{2},j}^+ = \bar{q}_{i+1,j} - \left\{ \frac{1}{4} [(1-k)\bar{\Delta}_+ + (1+k)\bar{\Delta}_-] \right\}_{i+1,j} \quad (2.22b)$$

with k assuming three different values depending on the order of approximation. For instance, $k = 1$ for central difference, $= 1/3$ for the third-order upwind-biased, and $= -1$ for the second-order fully upwind. For flows with large flow field discontinuities, such as shocks, flux limiting of Chakravarthy-Osher [77] are used to maintain monotonicity. This can be achieved by

$$\bar{\Delta}_+ = \max[0, \min(\Delta_+ \text{sgn}\Delta_-, \beta\Delta_- \text{sgn}\Delta_+)] \text{sgn}\Delta_+ \quad (2.23a)$$

$$\bar{\Delta}_- = \max[0, \min(\Delta_- \text{sgn}\Delta_+, \beta\Delta_+ \text{sgn}\Delta_-)] \text{sgn}\Delta_- \quad (2.23b)$$

with

$$\beta = \frac{(3-k)}{(1-k)} \quad (2.24)$$

and

$$\bar{q} = [\rho, u, v, P]^T \quad (2.25)$$

Also, a number of other upwind-biased interpolations are available in the literature, such as the Spekreijse, ENO, Venkat, and Superbee [78].

2.3.3 Van Leer Flux-Vector Splitting

The most popular flux-vector-splitting schemes in Computational Fluid Dynamics (CFD) are the Beam-Warming [79] and Van Leer [80] flux-vector splittings. The Beam-Warming fluxes are constructed from the approximate fluxes. The Van Leer fluxes, on the other hand, are computed from the exact fluxes that fulfill definite criteria to maintain continuous differentiability at sonic and stagnation points. Because of this advantage over the Beam-Warming flux-vector-splitting method, the Van Leer method is adopted in this analysis. In practical computation, the Van Leer fluxes and flux Jacobians are split into positive and negative contributions by use of the local Mach number computed normal to the cell face. The local Mach number, in the ξ direction for instance, is computed as

$$U = \frac{\bar{U}}{|\nabla(\xi)|} \quad M_\xi = \frac{U}{a} \quad (2.26)$$

where a is the local speed of sound and \bar{U} is the contravariant velocity. For a supersonic flow where $|M_\xi| > 1$, the positive and negative fluxes are expressed as

$$\hat{E}^+ = \hat{E}, \quad \hat{E}^- = 0 \quad \text{for } M_\xi \geq 1 \quad (2.27a)$$

$$\hat{E}^- = \hat{E} \quad \hat{E}^+ = 0 \quad \text{for } M_\xi \leq -1 \quad (2.27b)$$

For subsonic flow where $|M_\xi| < 1$, the flux in the normal direction of the cell for constant ξ is given by

$$\hat{E} = \hat{E}^+(\bar{Q}^-) + \hat{E}^-(\bar{Q}^+) \quad (2.28)$$

The split fluxes in the η direction can be likewise obtained by replacing ξ with η .

From Eqs. (2.24) - (2.28), the split Jacobians in the ξ and η directions, respectively, are obtained from the Van Leer fluxes, which are given in Appendix E, as

$$\hat{A}^+ = \frac{\partial \hat{E}^+(\bar{Q}^-)}{\partial \bar{Q}} \quad \hat{A}^- = \frac{\partial \hat{E}^-(\bar{Q}^+)}{\partial \bar{Q}} \quad \hat{A} = \hat{A}^+ + \hat{A}^- \quad (2.29)$$

$$\hat{B}^+ = \frac{\partial \hat{F}^+(\bar{Q}^-)}{\partial \bar{Q}} \quad \hat{B}^- = \frac{\partial \hat{F}^-(\bar{Q}^+)}{\partial \bar{Q}} \quad \hat{B} = \hat{B}^+ + \hat{B}^- \quad (2.30)$$

2.3.4 Time Integration

Numerical integration in time can be accomplished by either explicit or implicit schemes. The choice of the type of time integration depends mostly on convergence, stability, efficiency with computer memory, and the flow physics. Implicit schemes are robust and stable for any type of flow and are not restrictive in the range of Courant-Friedrechs-Lewy (CFL) numbers. However, the explicit

schemes are inexpensive but restrictive with the allowable CFL numbers. To increase the range of the CFL number and assure stability, either dissipations are added or a sort of residual smoothing is performed [81]. In the case where the flow is unsteady, time-accurate explicit schemes are preferable even though implicit schemes with large time steps are often used as well. Note that, even for steady flow cases, the solution is marched in pseudo-time where the time is used as a relaxation factor.

The application of backward Euler linearization in time whereby the higher-order terms are neglected, the flux \hat{E} in the ξ direction can be approximated as

$$\hat{E}^{n+1}(\bar{Q}) = \hat{E}^n(\bar{Q}) + \frac{\partial \hat{E}^n(\bar{Q})}{\partial \tau} \cdot \Delta \tau \quad (2.31)$$

Equation (2.31) can be simplified further as

$$\hat{E}^{n+1}(\bar{Q}) = \hat{E}^n(\bar{Q}) + \frac{\partial \hat{E}^n(\bar{Q})}{\partial \bar{Q}} \cdot \frac{\partial \bar{Q}}{\partial \tau} \cdot \Delta \tau \quad (2.32)$$

Now, the partial derivative of \bar{Q} with respect to time in Eq. (2.32) is approximated by

$$\frac{\partial \bar{Q}}{\partial \tau} = \frac{\bar{Q}^{n+1} - \bar{Q}^n}{\Delta \tau} = \frac{\Delta \bar{Q}^n}{\Delta \tau} \quad (2.33)$$

Eq. (2.31) is simplified to

$$\hat{E}^{n+1}(\bar{Q}) = \hat{E}^n(\bar{Q}) + \frac{\partial \hat{E}^n(\bar{Q})}{\partial \bar{Q}} \cdot \Delta \bar{Q}^n \quad (2.34)$$

where n is the time level. If one does the same type of linearization and approximations for the fluxes in the η direction and puts the approximate equations into Eq. (2.7), one obtains the following equations in the delta form:

$$\left\{ I + \Delta\tau \left[\delta_{\xi}^+ \hat{A}^- + \delta_{\xi}^- \hat{A}^+ + \delta_{\eta}^- \hat{B}^+ + \delta_{\eta}^+ \hat{B}^- \right] \right\} \Delta \bar{Q}^n = -\Delta\tau \cdot \hat{R}^n(\bar{Q}) \quad (2.35)$$

where

$$\hat{R}^n(\bar{Q}) = \left[\delta_{\xi}^+ \hat{E}^- + \delta_{\xi}^- \hat{E}^+ + \delta_{\eta}^+ \hat{F}^- + \delta_{\eta}^- \hat{F}^+ \right]^n \quad (2.36)$$

is the residual and

$$\Delta \bar{Q}^n = \bar{Q}^{n+1} - \bar{Q}^n \quad (2.37)$$

is the increment in the solution vector at each time level.

For an initially guessed solution which is close to the final solution, integration methods like Newton's method or its variations can be used to drive the solution close to zero. But when the initial solution is far from the final solution, this method does not reach the quadratic convergence within an acceptable iteration count. This restriction can be partially alleviated if one uses the alternating directional implicit (ADI) method [76,77, 82]. This method operates on the principle of first factoring Eq. (2.35) into easily manageable unidimensional operators and then sweeping once in the ξ direction and next in the η direction or vice versa until a steady-state solution is achieved. If one applies the ADI method to Eq. (2.35) one obtains

$$\{I + \Delta\tau[\delta_{\xi}^+ \hat{A}^- + \delta_{\xi}^- \hat{A}^+]\} \Delta \bar{Q}^* = -\Delta\tau \cdot \hat{R}^n(\bar{Q}) \quad (2.38a)$$

$$\{I + \Delta\tau[\delta_{\eta}^- \hat{B}^+ + \delta_{\eta}^+ \hat{B}^-]\} \Delta \bar{Q}^n = \Delta \bar{Q}^* \quad (2.38b)$$

For the steady-state computation, Eqs. (2.38a) and (2.38b) are advanced by a local time step $\Delta\tau$ which is computed for the given CFL number as [82]

$$\Delta\tau \leq CFL \cdot \left[|\bar{U}| + |\bar{V}| + a \sqrt{(|\nabla(\xi)| + |\nabla(\eta)|)} \right]^{-1} \quad (2.39)$$

where CFL is the Courant-Friedrich-Lewy number.

2.4 Initial and Boundary Conditions of Two-Dimensional Euler Equations

Although the initial condition can be arbitrarily assigned, the usual practice in the steady-state computation is to initiate the computational domain with the reference values of the state variables. On the other hand, the boundary condition cannot be arbitrarily assigned because the solution depends on the unique determination of the boundary condition that stems from the physical reasoning of the flow. The far-field boundary condition of the Euler equations, for example, is derived from the propagation of information along the characteristics defined by the Riemann invariants as

$$R^{\pm} = U \pm \frac{2a}{\gamma - 1} \quad (2.40)$$

Then with the help of Eq. (2.40), the normal velocities and the speed of sound at the body surfaces can be computed. Consequently, the inflow and respectively

the outflow Cartesian components of the velocities on the outer boundary can be computed as

$$\bar{v} = \bar{v}_\infty + (\bar{V} - \bar{v}_\infty \cdot \hat{n}) \hat{n} \quad (2.41a)$$

and

$$\bar{v} = \bar{v}_{exit} + (\bar{V} - \bar{v}_{exit} \cdot \hat{n}) \hat{n} \quad (2.41b)$$

where

$$\bar{V} = [U, V]^T \quad \bar{v} = [u, v]^T \quad \hat{n} = [\xi_x, \xi_y]^T \quad (2.41c)$$

In Eq. (2.41c), $\hat{\xi}$ can be either in the ξ direction or in the η direction.

For inviscid flow with impermeable and adiabatic wall conditions, the contravariant velocity normal to the wall, and the normal derivatives of the density and pressure at the wall are assumed to be identically zero. Mathematically, this can be expressed by

$$V = 0 \quad \frac{\partial P}{\partial n} = 0 \quad \frac{\partial \rho}{\partial n} = 0 \quad (2.42)$$

The extrapolated density and pressure from Eq. (2.39) are then imposed explicitly on the boundary and updated at every iteration until the solution converges.

2.5 Governing Equations of Quasi One-Dimensional Euler Equations

The time-dependent, compressible, quasi one-dimensional Euler equations [76] are formulated both in the nonconservative and conservative form to elucidate two design sensitivity approaches, i.e., sensitivity equations derived from one-dimensional nonconservative field variables and sensitivity equations from one-dimensional conservative variables.

2.5.1 Quasi One-Dimensional Euler Equations in NonConservative Form

The quasi one-dimensional Euler equations in nonconservative forms are commonly expressed in terms of the conservation of mass, momentum, and energy. These conserved quantities of mass, momentum, and energy can be given, respectively, as

$$\frac{\partial(\rho S)}{\partial t} + \frac{\partial(\rho u S)}{\partial x} = 0 \quad (2.43)$$

$$\frac{\partial(\rho u S)}{\partial t} + \frac{\partial(\rho u^2 + P)S}{\partial x} - P \frac{dS}{dx} = 0 \quad (2.44)$$

and

$$\frac{\partial(\rho S e_i)}{\partial t} + \frac{\partial[(P + \rho e_i)u S]}{\partial x} = 0 \quad (2.45)$$

For the first approach (nonconservative field variables), Eqs. (2.43) - (2.45) are put in their vector form as

$$\frac{\partial(S\bar{Q})}{\partial t} = \bar{r} \quad (2.46)$$

where

$$\bar{Q} = [\rho, \rho u, \rho e_t]^T \quad (2.47)$$

S is the cross-sectional area, u is the velocity, p is the pressure, e_t is the total internal energy, ρ is the density, and \bar{r} denotes the vector of the spatial derivatives.

2.5.2 Quasi One-Dimensional Euler Equations in Conservative Form

Unlike the nonconservative approach, this approach deals directly with the variation of the conservative fluxes with respect to the conservative field variables. To realize this objective, let us recast Eqs. (2.43) - (2.45) in a form amenable to conservative formulation. If one follows this procedure, the time-dependent quasi one-dimensional Euler equations in conservative forms are given as

$$\frac{\partial(S\bar{Q})}{\partial t} + \frac{\partial E}{\partial x} - H_s = \bar{0} \quad (2.48)$$

where

$$H_s = H_s(S, \bar{Q}) = \left[0, p \frac{dS}{dx}, 0 \right]^T \quad (2.49)$$

are the source terms.

In Sec. 2.4.1, the one-dimensional fluxes and Jacobians are computed by both the Beam-Warming and Van Leer flux-vector-splitting techniques. In Sec.

2.4.2, however, the Van Leer flux-vector-splitting techniques are only adopted. The discretization, and time integration of both approaches are performed as given in [76].

2.6 Initial and Boundary Conditions of Quasi One-dimensional Euler Equations

For the purely supersonic flow case, the flow properties ρ , u , and e_t are specified at the inflow boundary; whereas, at the outflow boundary they are numerically computed from the interior points using a second-order extrapolation. For the supersonic-inflow and subsonic-outflow conditions, the inflow boundary is specified as in the supersonic conditions. However, at the outflow boundary location, the pressure is specified whereas the density and velocity are computed from the interior by a second-order extrapolation.

In the purely subsonic flow condition, the density and the velocity are specified at the inflow, and the pressure is specified at the outflow boundary. During the numerical experimentation on the various ways to specify the numerical and physical boundary conditions that produce stable and converged solutions, it was generally observed that using first-order extrapolations of the numerical boundary conditions both at the inflow and outflow boundaries produced either spurious or non-convergent solutions. However, switching the inflow boundary to a first-order extrapolation seemed to give comparable results.

Chapter 3

AERODYNAMIC DESIGN OPTIMIZATION AND SENSITIVITY ANALYSIS

The work done with regard to general aerodynamic optimization problems is discussed in this chapter. The pertinent elements of aerodynamic shape design optimization and sensitivity analysis by the application of the variational methods (VM) are also presented.

3.1 General Scope

Since the 1950's, design and shape optimization for bodies and the numerical algorithms to improve analysis and optimization processes steadily grew. Now, with the latest supercomputers and software technology, many design problems are being solved in a matter of hours. Therefore, the question today is not whether researchers want to design numerically complex parts, but rather, which is the most reliable design and shape optimization tool. This quest ultimately culminates in devising an algorithm to get better gradient or sensitivity information of the functional or system responses to the change of design variables or control functions.

3.1.1 Sensitivity Information

At the present time, three main avenues exist to get the gradient information. The first, and the oldest one, is the finite difference approach. Depending on the type of approximation and number of design variables, this method requires a substantial number of converged solutions and is also dependent on the step

size, which is always arbitrary. The gradient information is commonly obtained by either forward, backward, or central difference approximations. With the use of the central difference alternative, for example, the gradient is computed as

$$\frac{\partial D}{\partial \bar{X}_D} \approx \frac{D[\bar{Q}(\bar{X}_D + \Delta \bar{X}_D), \bar{X}_D + \Delta \bar{X}_D] - D[\bar{Q}(\bar{X}_D - \Delta \bar{X}_D), \bar{X}_D - \Delta \bar{X}_D]}{2\Delta \bar{X}_D} \quad (3.1)$$

The second category is the discrete approach. This is widely used and is computationally intensive. In its standard form, it also requires huge computer memory allocation, especially, for the two-dimensional complete Navier-Stokes equations and, generally, for three-dimensional equations. This can be attributed to the large and sparse matrices obtained from the sensitivity of the solution vector and grid terms with respect to the design variables. Generally, the sensitivity coefficient is derived [83] by the chain rule for implicit functions, for instance, as

$$\frac{\partial D}{\partial \bar{X}_D} = \left(\frac{\partial D}{\partial \bar{X}_D} \right)_{\bar{Q}} + \left(\frac{\partial D}{\partial \bar{Q}} \right)^T \circ \frac{\partial \bar{Q}}{\partial \bar{X}_D} \quad (3.2)$$

The derivative of the solution vector with respect to the vector of the design variables $\frac{\partial \bar{Q}}{\partial \bar{X}_D}$ can be obtained by the implicit differentiation of discrete residual

which is defined as

$$R(\bar{Q}(X_d), X_d) = \bar{0} \quad (3.3)$$

The determinations of $\left(\frac{\partial R}{\partial X_d} \right)_{\bar{Q}}$ and $\left(\frac{\partial D}{\partial X_d} \right)_{\bar{Q}}$, which are needed in the computation

of the total gradient or sensitivity coefficients of the objective functional, are

computed by use of the chain rule for implicit functions of the discrete residual and objective functional with respect to the metric terms and the derivative of the metric terms with respect to the design variables. This process is also done for the gradients of the constraint functionals.

The third way of obtaining the sensitivity gradient is through the variational methods. Unlike the discrete approach, variational methods derive the derivatives of the functional based upon the calculus of variations. The optimal control theory is an example of using the variational methods to derive the optimality conditions whereby the extremizing functions (design variables) are solved for. In general, variational design optimization blends the concepts of optimal control theory and calculus of variations [84]. The optimal control theory states the conditions under which the control variables, parameters, and functions or the combinations of them can be continuously altered to meet the desired criteria. The optimal control theory particularly focuses on the following: (1) determination of a mathematical model of the dynamical or physical system, (2) determination of the admissible control variables or functions, (3) specification of the performance index or functional that can be extremized, (4) identification of the physical constraints that produce unique and converged solutions, and (5) construction of the augmented functional that consists of the objective functional and the constraints. After the optimal control problem is explicitly formulated, the fundamental principles of calculus of variations determines the variation of the augmented functional to the variation of the admissible control variables or functions or design variables.

3.1.2 Discrete Versus Variational Methods

The discrete approach describes the local behavior of the functional that is to be differentiated in an infinitesimal region. The variational approach, on the otherhand, integrates the functional that is to be differentiated over the

continuous domain or boundary. While both procedures are mathematically equivalent, the discrete approach is based on differentiation and the variational approach on the integration. Conceptually, differentiation is an inductive process, whereas integration is a deductive process. Computationally, integration is a smoothing operation, i.e., many weak integral (variational) forms can be stated, whereas differential (discrete) approach is a *noisy* operation. In short, the discrete sensitivity analysis involves prior discretization of the continuous flow field equations and boundary conditions before they are differentiated with respect to the design variables. On the other hand, in the variational sensitivity analysis, the continuous state equation in the weak form of the integral is first differentiated by use of the principle of calculus of variations and optimal control theory to derive the costate equations, transversality conditions, and functional sensitivity derivatives, and then they are discretized.

3.2 Constrained Optimization Methodology

A constrained optimization method in general encompasses three elements of optimization, i.e., design variables, constraints, and objective function.

3.2.1 Design Variables in Variational Sense

In most aerodynamic optimization problems, the design variables are generally of a geometric nature, such as the coefficients of some geometric functions, surface grid points [83], aerofunctions [85], or polynomial functions such as Bezier-Bernstein functions [42, 86] and spline functions [87].

Variational methods treat the boundary of the domain in a continuous fashion, and therefore, the boundary is considered as part of the solution to the design problem. With the assumption that the domain Ω is sufficiently regular, the location of points on the boundary \bar{X}_r can be considered as a continuous design

variable (Figs. 3.1 and 3.2). Mathematically, the coordinates of the varying boundary in the continuous sense can be expressed as

$$\bar{X}_r = \bar{f}(\bar{X}_d) \quad (3.4)$$

where \bar{X}_d are the design variables. In aerodynamic optimization problems, the vector of design variables is provided for very limited and simplified geometries, for instance, 4 digit NACA airfoils and some nozzles. However, for general-purpose geometries, these control points must be determined through iterative methods from certain functional relationships such as the Bezier-Bernstein polynomials [42]. Because these polynomial functions are known to generate smooth curves and surfaces for a minimal number of control points, the function \bar{f} which describes the curve for the two-dimensional problem, is given by [86]

$$\bar{f}(\bar{u}) = \sum_{i=0}^n \bar{X}_{d,i} B_{i,n}(\bar{u}) \quad \text{for } \bar{u} \in [0,1] \quad (3.5)$$

where

$$B_{i,n}(\bar{u}) = C(n,i) \bar{u}^i (1-\bar{u})^{n-i} \quad (3.6)$$

$$C(n,i) = \frac{n!}{i!(n-i)!} \quad (3.7)$$

In Eqs. (3.5) - (3.7), $B_{i,n}(\bar{u})$ are the blending functions, which are key to the behavior of the curve, $C(n,i)$ are the binomial coefficients, \bar{u} is the normalized arc length and n is the order of the Bezier-Bernsten polynomials. In this study, with the use of Eqs. (3.4) - (3.7), the location of the control points can be considered as the design variables.

3.2.2 Constraints

Constraints are the integral parts of the optimization procedure that influence the final outcome of the functional. They can be geometrical, flow-type, equality or inequality constraints, or a combination of all or some that depends on the particular optimization problem one wants to address.

In the design optimization process, certain constraints are bound to be satisfied while the others are violated. Those which are satisfied encompass the feasible domain, while the violated constraints belong to the infeasible domain.

In the variational formulation of design optimization problems, the flow-type constraints are expressed in the integral forms. The geometrical and side constraints, on the other hand, can be formulated either in the integral or discrete forms. For the general variational approach, generic flow-type constraints are expressed as

$$G_j(\bar{Q}, \bar{n}) = \int_{\bar{\Gamma}} g_j(\bar{Q}, \bar{n}) d\bar{\Gamma} \leq 0 \quad \text{for } j = 1, 2, \dots, \text{nconf} \quad (3.8)$$

where $\bar{\Gamma}$, is the deformed boundary and nconf is the number of generic fluid-type constraints. The generic geometric-type and the side constraints can also be given as

$$G_j(\bar{X}_D) \leq 0 \quad \text{for } j = \text{nconf}+1, \text{nconf}+2, \dots, \text{ncon} \quad (3.9)$$

and

$$X_{iD}^{lower} \leq X_{iD} \leq X_{iD}^{upper} \quad \text{for } i = 1, 2, \dots, \text{ndv} \quad (3.10)$$

where n_{con} is the total number of constraints, and n_{dv} is the number of design variables, respectively.

3.2.3 Objective Functional

In the variational methods (VM), the objective functional is defined in the form of a definite integral involving an unknown state function \bar{Q} , which can be dependent on some normal vectors \bar{n} and other problem parameters. Then, the objective functional is extremized at the converged state solution over the curve of the surface described by the vector of design variables. Mathematically, a generic functional on the boundary $J_{\bar{\Gamma}}$, is defined as

$$J_{\bar{\Gamma}}(\bar{Q}, \bar{n}) = \int_{\bar{\Gamma}} D(\bar{Q}, \bar{n}) d\bar{\Gamma} \quad (3.11)$$

where D , for the two-dimensional problem, is the objective function specified on the curve or boundary. The selection of the objective function is mostly dictated by the flow physics.

3.3 Variational Formulation of Aerodynamic Optimization Problem

In a design optimization where the constraints are absent, the necessary condition for the objective function to reach its optimal solution is when the partial derivatives of the function with respect to the design variables are all identically zero. The sufficient condition for optimality can be further augmented by requiring the Hessian matrix of the function to be positive-definite at the design points. Realistic optimization problems involve constraints which have functional relationships to the functional through the design variables or state variables. When constraints are involved in the optimization problem, the partial derivatives of the functional and the constraints cannot be zero at the same time since they

are functionally related to each other through the optimality criteria [84, 88]. One common practice is to cast the constrained optimization to unconstrained optimization through the introduction of the weighting functions or Lagrange multipliers $\tilde{\lambda}(\bar{X})$. The other is to sequentially solve a linear or quadratic programming problem, which is an approximation of the original constrained minimization problem. In the later approach, one needs to derive the sensitivities of the performance functional.

In the following paragraph, the objective functional defined in Eq. (3.11) will be used as an example to facilitate the discussion of the procedure to derive the aerodynamic sensitivity equations by the variational methods. To start the derivation, the steady state solution of Eq. (2.6), i.e., the residual $\bar{R}(\bar{Q})$, is written as

$$\bar{R}(\bar{Q}) = \bar{E}_x + \bar{F}_y = \bar{0} \quad (3.12)$$

and the generic boundary conditions are expressed as

$$\bar{H}(\bar{Q}, \bar{n}) = \bar{0} \quad (3.13)$$

Without changing its value, the objective functional $J_{\bar{F}}$ can now be modified as

$$J_{\bar{F}_a}(\bar{Q}, \bar{n}, \tilde{\lambda}, \tilde{\mu}) = J_{\bar{F}} + \int_{\bar{\Omega}} \tilde{\lambda}^T(\bar{X}) \bar{R}(\bar{Q}) d\bar{\Omega} + \int_{\bar{\Gamma}} \tilde{\mu}^T \bar{H}(\bar{Q}, \bar{n}) d\bar{\Gamma} \quad (3.14)$$

where $\bar{\Gamma}$ and $\bar{\Omega}$ are the deformed boundary and domain, and $\tilde{\lambda}$ and $\tilde{\mu}$ are vectors to be determined.

3.3.1 Standard Formulation of an Aerodynamic Optimization Problem

A mathematical formulation of the constrained optimization problem can be expressed as

$$\min_{\Gamma} \{J_{\Gamma}\} \quad (3.15)$$

subject to

$$G_j(\bar{Q}, \bar{n}) = \int_{\Gamma} g_j(\bar{Q}, \bar{n}) d\bar{\Gamma} \leq 0 \quad \text{for } j = 1, 2, \dots, \text{nconf} \quad (3.16)$$

$$G_j(\bar{X}_D) \leq 0 \quad j = \text{nconf}+1, \text{nconf}+2, \dots, \text{ncon} \quad (3.17)$$

and

$$X_{iD}^{lower} \leq X_{iD} \leq X_{iD}^{upper} \quad i = 1, 2, \dots, \text{NDV} \quad (3.18)$$

where the flow field variables \bar{Q} are the solution to the state equations, $\bar{R}(\bar{Q})$.

The problem statement clearly indicates that the state equations are the integral parts of the optimization process and, therefore, must be represented by the highest level of flow field approximations and solved by the most efficient numerical techniques as discussed in Chap. 2.

3.3.2 Derivation of Functional Sensitivity Equations

In the derivation of the sensitivity derivatives for the functional and constraints, the spirit of Ref. 65 is still kept in implementing the variational methods. But unlike Ref. 65 the variation is performed on the conservative variables and fluxes with respect to the variation of a variable domain. Let us define the following expressions for later use:

$$\frac{\partial \bar{E}}{\partial \bar{Q}} = \bar{A} \quad \text{and} \quad \frac{\partial \bar{F}}{\partial \bar{Q}} = \bar{B} \quad (3.19)$$

to be the Jacobian matrices in the x and y directions. The variation of the fluxes (to the first order) can be written as

$$\delta \bar{E} = \bar{A} \delta \bar{Q} \quad \text{and} \quad \delta \bar{F} = \bar{B} \delta \bar{Q} \quad (3.20)$$

Then the fluxes on the deformed space due to the variation of the boundary can be approximated as

$$\bar{E}(\bar{\bar{Q}}) = \bar{E}(\bar{Q}) + \delta \bar{E}(\bar{Q}) \quad \text{and} \quad \bar{F}(\bar{\bar{Q}}) = \bar{F}(\bar{Q}) + \delta \bar{F}(\bar{Q}) \quad (3.21)$$

By application of the principles of calculus of variations and use of the results in Appendices A and B, the variation of the modified functional can be approximated by [84]

$$\Delta J_{\Gamma_a} = J_{\bar{\Gamma}_a}(\bar{\bar{Q}}(\bar{\bar{X}}), \bar{\bar{\lambda}}(\bar{\bar{X}}), \bar{\bar{\mu}}(\bar{\bar{X}})) - J_{\Gamma_a}(\bar{Q}(\bar{X}), \bar{\lambda}(\bar{X}), \bar{\mu}(\bar{X})) \quad (3.22)$$

where $\bar{\bar{X}}$ and \bar{X} are position vectors of the deformed and undeformed coordinate systems, respectively. Then, with Eqs. (3.19) - (3.21) and Eqs. (A.2), (A.6), and (B.5) from Appendices A and B, the Taylor expansion of the integrand of Eq. (3.22) [84] is computed (the linear part relative to ε) as [84,88,89]

$$\begin{aligned}
\delta J_{\Gamma_a} = & \int_{\Gamma} \left\{ D + D_{\rho} \delta \bar{Q} + D_n \delta n + D \kappa \delta n \right\} d\Gamma \\
& + \int_{\Gamma} (\bar{\mu}^T + \delta \bar{\mu}^T) \left\{ \bar{H} + \bar{H}_{\rho} \delta \bar{Q} + \bar{H}_n \delta n + \bar{H} \kappa \delta n \right\} d\Gamma \\
& + \int_{\Omega} \left\{ (\bar{\lambda}^T + \delta \bar{\lambda}^T) \left[\bar{E}_x(\bar{Q}) + (\delta \bar{E}(\bar{Q}))_x + \bar{F}_y(\bar{Q}) + (\delta \bar{F}(\bar{Q}))_y \right] \right\} |J_s| d\Omega \\
& - \int_{\Omega} \bar{\lambda}^T \left[\bar{E}_x(\bar{Q}) + \bar{F}_y(\bar{Q}) \right] d\Omega - \int_{\Gamma} [D + \bar{\mu}^T \bar{H}] d\Gamma
\end{aligned} \tag{3.23}$$

where ε is a small parameter, J_s is the space transformations matrix that is given in Eq. (B.5) as $|J_s| = |I + \bar{\nabla} \cdot \delta \bar{X}|$ and the quantity κ in Eq. (3.27) is the curvature and can be calculated as [88]

$$\kappa = -\bar{\nabla} \circ \bar{n} \tag{3.24}$$

where \circ denotess a dot or inner product and \bar{n} is the unit normal which can be computed from the grid generating routine or from the analytical derivatives of the Bezier-Bernstein polynomials as [86]

$$\kappa = \left[\frac{\partial \bar{f}}{\partial \bar{u}} \otimes \frac{\partial^2 \bar{f}}{\partial \bar{u}^2} \right] \left\{ \left| \frac{\partial \bar{f}}{\partial \bar{u}} \right|^3 \right\}^{-1} \tag{3.25}$$

where \otimes is a vector multiplication sign and $\bar{f}(\bar{u})$ is defined in Eq. (3.9). In Eq. (3.23), δn is defined as

$$\delta n = \delta \bar{X} \circ \bar{n} \tag{3.26}$$

Now, by taking only the linear terms of Eq. (3.23), one obtains

$$\begin{aligned}
\delta J_{\Gamma_a} = & \int_{\Gamma} \left\{ D_Q \delta \bar{Q} + D_n \delta n + D_\kappa \delta n + \bar{\mu}^T \left[\bar{H}_Q \delta \bar{Q} + \bar{H}_n \delta n + \bar{H}_\kappa \delta n \right] \right\} d\Gamma \\
& + \int_{\Omega} \left\{ \bar{\lambda}^T \left[(\delta \bar{E}(\bar{Q}))_x + (\delta \bar{F}(\bar{Q}))_y \right] \right\} d\Omega + \int_{\Omega} \left\{ (\delta \bar{\lambda})^T \left[\bar{E}_x(\bar{Q}) + \bar{F}_y(\bar{Q}) \right] \right\} d\Omega \\
& + \int_{\Gamma} \delta \bar{\mu}^T \bar{H} d\Gamma + \int_{\Gamma} \bar{\lambda}^T \left[\bar{E}_x + \bar{F}_y \right] \delta n d\Gamma \quad (3.27)
\end{aligned}$$

With Eq.(3.20) and performing integration by parts, the second term in Eq. (3.27) is expressed as

$$\begin{aligned}
\int_{\Omega} \left\{ \bar{\lambda}^T \left[(\delta \bar{E}(\bar{Q}))_x + (\delta \bar{F}(\bar{Q}))_y \right] \right\} d\Omega = & \int_{\Omega} \left\{ -\bar{\lambda}_x^T \bar{A} - \bar{\lambda}_y^T \bar{B} \right\} \delta \bar{Q} d\Omega + \\
\int_{\Gamma} \left\{ \bar{\lambda}^T \left[\bar{A} n_x + \bar{B} n_y \right] \delta \bar{Q} \right\} d\Gamma \quad (3.28)
\end{aligned}$$

Where \bar{A} and \bar{B} are defined in Eq. (3.19). Substitution of Eq. (3.28) into Eq. (3.27) gives

$$\begin{aligned}
\delta J_{\Gamma_a} = & \int_{\Gamma} \left\{ D_Q \delta \bar{Q} + D_n \delta n + D_\kappa \delta n + \bar{\mu}^T \left[\bar{H}_Q \delta \bar{Q} + \bar{H}_n \delta n + \bar{H}_\kappa \delta n \right] \right\} d\Gamma \\
& + \int_{\Gamma} \left\{ \bar{\lambda}^T \left[\bar{A} n_x + \bar{B} n_y \right] \delta \bar{Q} \right\} d\Gamma + \int_{\Omega} \left\{ -\bar{\lambda}_x^T \bar{A} - \bar{\lambda}_y^T \bar{B} \right\} \delta \bar{Q} d\Omega \\
& + \int_{\Omega} \left\{ (\delta \bar{\lambda})^T \left[\bar{E}_x(\bar{Q}) + \bar{F}_y(\bar{Q}) \right] \right\} d\Omega + \int_{\Gamma} \delta \bar{\mu}^T \bar{H} d\Gamma + \int_{\Gamma} \bar{\lambda}^T \left[\bar{E}_x + \bar{F}_y \right] \delta n d\Gamma \quad (3.29)
\end{aligned}$$

Note that for the arbitrary variations of $\delta \bar{\lambda}$ and $\delta \bar{\mu}$ and with Eqs. (3.12) and (3.13), the last two terms in Eq. (3.29) are identically zero. Then Eq. (3.29) reduces to

$$\begin{aligned}
\delta J_{ra} = & \int_{\Gamma} \left\{ D_Q \delta \bar{Q} + D_n \delta n + D_\kappa \delta n + \bar{\mu}^T \left[\bar{H}_Q \delta \bar{Q} + \bar{H}_n \delta n + \bar{H}_\kappa \delta n \right] \right\} d\Gamma \\
& + \int_{\Gamma} \left\{ \bar{\lambda}^T \left[\bar{A} n_x + \bar{B} n_y \right] \delta \bar{Q} \right\} d\Gamma + \int_{\Omega} \left\{ -\bar{\lambda}_x^T \bar{A} - \bar{\lambda}_y^T \bar{B} \right\} \delta \bar{Q} d\Omega + \int_{\Gamma} \bar{\lambda}^T \left[\bar{E}_x + \bar{F}_y \right] \delta n d\Gamma
\end{aligned} \tag{3.30}$$

In Eq. (3.30), the vectors $\bar{\lambda}$, and $\bar{\mu}$ can now be determined to eliminate the terms associated with $\delta \bar{Q}$. Consequently, the costate (adjoint) equations are given as

$$-\bar{A}^T \bar{\lambda}_x - \bar{\lambda}_y \bar{B}^T = \bar{0} \quad \text{in } \Omega \tag{3.31}$$

Upon the combination of Eqs. (3.30) and (3.31), the variation of the functional becomes

$$\begin{aligned}
\delta J_{ra} = & \int_{\Gamma} \left\{ D_Q \delta \bar{Q} + D_n \delta n + D_\kappa \delta n + \bar{\mu}^T \left[\bar{H}_Q \delta \bar{Q} + \bar{H}_n \delta n + \bar{H}_\kappa \delta n \right] \right\} d\Gamma \\
& + \int_{\partial\Omega} \left\{ \bar{\lambda}^T \left[\bar{A} n_x + \bar{B} n_y \right] \delta \bar{Q} \right\} d\Gamma + \int_{\Gamma} \bar{\lambda}^T \left[\bar{E}_x + \bar{F}_y \right] \delta n d\Gamma
\end{aligned} \tag{3.32}$$

With Eq. (A.11) in Appendix A, we now express $\delta \bar{Q}$ in terms of $\delta \bar{X}$ to get

$$\delta \bar{Q} = \delta \bar{Q} - \frac{\partial \bar{Q}}{\partial \bar{X}} \delta \bar{X} \tag{3.33}$$

For the sake of computational simplification, the variation of $\delta \bar{X}$ on the boundary is limited only to the y component in this study, i.e.,

$$\delta \bar{X} = [0, \delta y]^T \tag{3.34}$$

and Eq. (3.33) is simplified as

$$\delta\bar{Q} = \delta\bar{Q} - \frac{\partial\bar{Q}}{\partial y} \delta y \quad (3.35)$$

Also an approximation of Eq. (3.26) and use of Eq. (3.34), Eq. (3.26) can be written as

$$\begin{aligned} \delta n &= \delta\bar{X} \circ \bar{n} \\ &= [0, \delta y]^T \circ [n_x, n_y] \\ &= n_y \circ \delta y \end{aligned} \quad (3.36)$$

By use of Eqs. (3.33) - (3.36), Eq. (3.32) is now given as

$$\begin{aligned} \delta J_{\Gamma_a} &= \int_{\Gamma} \left\{ D_Q \delta\bar{Q} + n_y D_n \delta y + n_y D_\kappa \delta y - n_y D_Q \bar{Q}_y \delta y + \right\} d\Gamma \\ &\quad + \int_{\Gamma} \left\{ \bar{\mu}^T [\bar{H}_Q \delta\bar{Q} + n_y \bar{H}_n \delta y + n_y \bar{H}_\kappa \delta y - n_y \bar{H}_Q \bar{Q}_y \delta y] \right\} d\Gamma \\ &\quad + \int_{\Gamma} \left\{ \bar{\lambda}^T [\bar{A} n_x + \bar{B} n_y] (\delta\bar{Q} - n_y \bar{Q}_y \delta y) \right\} d\Gamma + \int_{\Gamma} \bar{\lambda}^T [\bar{E}_x + \bar{F}_y] n_y \delta y d\Gamma \end{aligned} \quad (3.37)$$

For arbitrary $\delta\bar{Q}$ and the variation of y on the boundary Γ , Eq. (3.37) gives the boundary conditions for the costate equations and the sensitivity equations, respectively, as

$$\left\{ [\bar{A} n_x + \bar{B} n_y]^T \bar{\lambda} + D_Q^T + \bar{H}_Q^T \bar{\mu} \right\} = \bar{0} \quad \text{on } \Gamma \quad (3.38)$$

and

$$\begin{aligned} \delta J_{\Gamma_a} = & \int_{\Gamma} \left\{ D_n + D\kappa - D_Q \bar{Q}_y + \bar{\mu}^T [\bar{H}_n + \bar{H}\kappa - \bar{H}_Q \bar{Q}_y] \right\} n_y \delta y d\Gamma \\ & - \int_{\Gamma} \left\{ \bar{\lambda}^T [\bar{A}n_x + \bar{B}n_y] \bar{Q}_y \right\} n_y \delta y d\Gamma + \int_{\Gamma} \bar{\lambda}^T [\bar{E}_x + \bar{F}_y] n_y \delta y d\Gamma \end{aligned} \quad (3.39)$$

The unique determination of Eq. (3.39), therefore, demands the unique and converged solutions of Eqs.(3.12) and (3.13), (3.31), and (3.38).

3.3.3 Derivation of Constraint Sensitivity Equations

With the constraints defined in Eq. (3.16), the residual, and the boundary conditions, Eqs. (3.12) and (3.13), one can formulate the modified constraints as

$$\begin{aligned} G_{j\bar{\Gamma}_a}(\bar{Q}, \bar{n}, \bar{\lambda}_j, \bar{\mu}_j) = & \int_{\bar{\Gamma}} g_j(\bar{Q}, \bar{n}) d\bar{\Gamma} + \int_{\bar{\Omega}} \bar{\lambda}_j^T [\bar{E}_x + \bar{F}_y] d\bar{\Omega} + \int_{\bar{\Gamma}} \bar{\mu}_j^T \bar{H}(\bar{Q}, \bar{n}) d\bar{\Gamma} \\ & \text{for } j = 1, 2, \dots, \text{nconf} \end{aligned} \quad (3.40)$$

By following the same procedure as was done for the objective functional, the costate equations, boundary conditions, and the constraint derivative coefficients, respectively, can be expressed as

$$\left\{ -\bar{A}^T \bar{\lambda}_{j_x} - \bar{B}^T \bar{\lambda}_{j_y} \right\} = \bar{0} \quad \text{for } j = 1, 2, \dots, \text{nconf} \quad \text{in } \Omega \quad (3.41)$$

$$\left\{ [\bar{A}n_x + \bar{B}n_y]^T \bar{\lambda}_j + g_{j\bar{Q}}^T + \bar{H}_Q^T \bar{\mu}_j \right\} = \bar{0} \quad \text{for } j = 1, 2, \dots, \text{nconf} \quad \text{on } \Gamma \quad (3.42)$$

$$\begin{aligned} \delta G_{j\bar{\Gamma}_a} = & \int_{\Gamma} \left\{ g_{j_n} + g_{j\kappa} - g_{j_Q} \bar{Q}_y + \bar{\mu}_j^T [\bar{H}_n + \bar{H}\kappa - \bar{H}_Q \bar{Q}_y] \right\} n_y \delta y d\Gamma \\ & - \int_{\bar{\Omega}} \left\{ \bar{\lambda}_j^T [\bar{A}n_x + \bar{B}n_y] \bar{Q}_y \right\} n_y \delta y d\Gamma + \int_{\Gamma} \bar{\lambda}_j^T [\bar{E}_x + \bar{F}_y] n_y \delta y d\Gamma \\ & \text{for } j = 1, 2, \dots, \text{nconf} \end{aligned} \quad (3.43)$$

As can be discerned from Eq. (3.43), the computation of the constraint sensitivity equations requires the solution of a new set of costate equations and boundary conditions as many times as the number of constraints.

3.4 Numerical Optimization

In Sec. 3.2, the elements of gradient-based constrained optimization, i.e., the parameterization of the boundary, objective and constraint functionals, and the sensitivity derivatives for an aerodynamic design optimization problem, are presented. The next logical step is to specify a numerical optimization technique to search for a better design. The feasible direction method developed by Vanderplaats and Moses [90] and used by Haftka and Gurdal [91] is implemented in our study. Two steps are essentially followed in this approach. The first step is to determine the search direction, \bar{s} , and the second is to compute the magnitude of the step size α . These two quantities can be computed as proposed in Refs. 90 and 91. A typical computation of the feasible direction starts at the boundary of the feasible domain, and its magnitude and directions are kept constant as long as the search direction keeps the design variables in the feasible domain while improving the performance index. Otherwise, a new search direction and step size are recomputed with the new gradient information and this process continues until the optimality is met. Mathematically, the feasible direction can be formulated as

$$\bar{s}^T \circ \nabla g_i \leq 0, \quad (3.44)$$

where i is part of the active constraints and the usable direction at a point is given by

$$\bar{s}^T \circ \nabla J_{\Gamma} \leq 0 \quad (3.45)$$

The change in design must be sought along the combination of the useable and feasible directions so that the functional or the performance index is reduced as much as possible, and the design is kept away from the constrained boundary as much as possible. By use Eqs. (3.44) and (3.45) in the method of feasible directions, the new design variables are updated as

$$\bar{X}_D^{n+1} = \bar{X}_D^n + \alpha \bar{s} \quad (3.46)$$

where n is the iteration number. The values of the design variables are continuously altered until the criteria for the optimal solution of the performance index are satisfied.

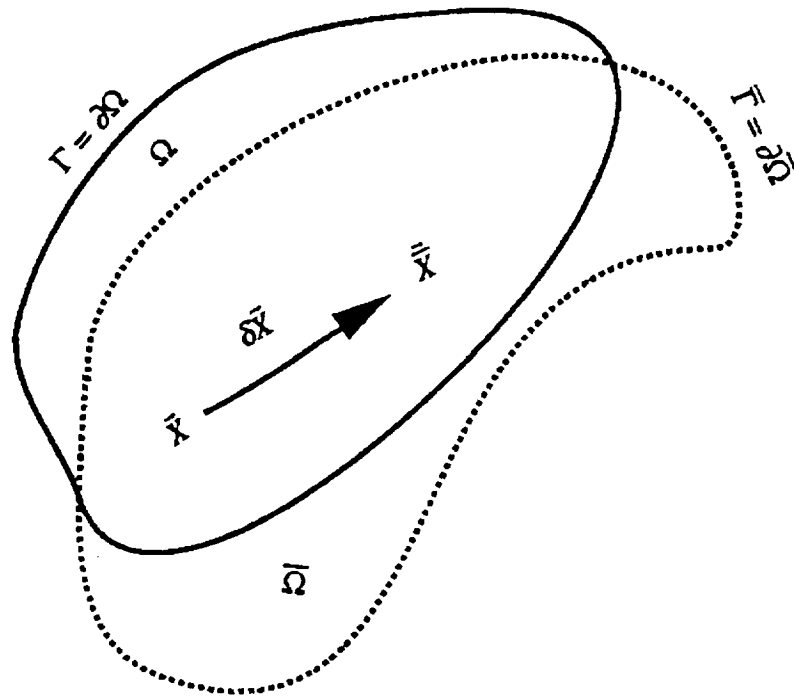


Fig. 3.1 Variation of domain by a One-parameter family of mapping

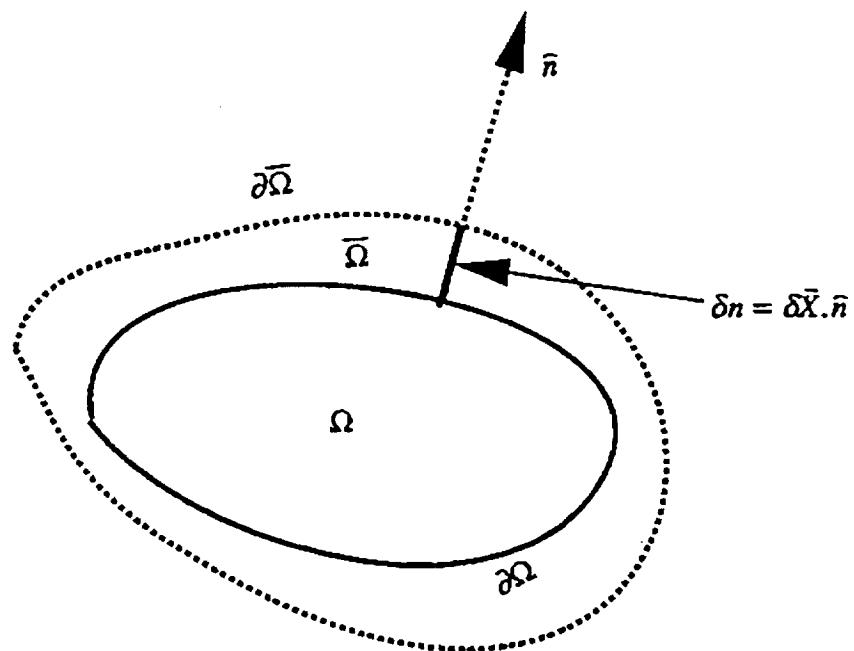


Fig. 3.2 Boundary variation normal to the original boundary, $\partial\Omega$

Chapter 4

COSTATE EQUATIONS AND SOLUTION METHODS

4.1 Introduction to the Numerical Integration of Costate Equations

The coefficients of the costate equations are constant matrices whose components are derived from the converged solution of the state equations. (See Appendix E). They are globally constant in time and locally constant in space. But the interpretation of *constant* matrices must be understood in a sense that, during the time integration of the costate equations, only the costate variables evolve in space and time to convergence. The costate equations are identical to the Euler equations in form, but mathematically, they are different in the sense that they do not meet the homogeneity requirement to put them in a conservative form like the Euler equations. From the numerical view point, one can adopt any solution algorithm, which is used for the Euler equations, to the costate equations. This can be explained by the fact that the fluxes on the cell faces or at grid points can be artificially constructed by approximating the solution vector of the costate equations either on the cell face from the right and left sides of the cell centers or at the grid points in exactly the same way one does for the state fluxes and solution vector.

4.2 Costate Equations

The costate equations, like the state equations, are solved by use of the time dependent techniques. The Eqs. (3.31) and (3.41) are, therefore, modified to include the unsteady term with the proper signs so that this time dependent

technique is fully exploited. Thus, for instance, Eq. (3.35) in the generalized coordinates system is expressed as

$$\pm \bar{\lambda}_\tau - \hat{A}^T \bar{\lambda}_\xi - \hat{B}^T \bar{\lambda}_\eta = \bar{0} \quad (4.1)$$

The proper sign selection of the time term is dependent on the complementary property of the well-posed boundary conditions of the state and costate equations. For Eq. (4.1) to be well-posed, the positive sign of the time term is selected, and Eq. (4.1) becomes

$$\bar{\lambda}_\tau - \hat{A}^T \bar{\lambda}_\xi - \hat{B}^T \bar{\lambda}_\eta = \bar{0} \quad (4.2)$$

4.3 Boundary (Transversality) Conditions

The objective functional boundary conditions, i.e. Eq. (3.38), in their general forms are again for the sake of convenience presented here as

$$\left\{ \delta \bar{Q}^T [\bar{A} n_x + \bar{B} n_y]^T \bar{\lambda} + D_Q^T + \bar{H}_Q^T \bar{\mu} \right\} = \bar{0} \quad \text{on } \Gamma \quad (4.3)$$

The objective functional and the no-mass penetration conditions are defined only on the solid boundary, and hence their derivative contributions in Eq. (4.3) are identically zero. Therefore, the boundary conditions for the inlet, exit, and center-line reduce to

$$\left\{ \delta \bar{Q}^T [\bar{A} n_x + \bar{B} n_y]^T \bar{\lambda} \right\} = \bar{0} \quad \text{on } (\Gamma_{inlet}, \Gamma_{center}, \Gamma_{exit}) \quad (4.4)$$

For the supersonic flow flow, the inlet condition is known, and hence the variation of the vector of the flow field is identically zero. Therefore, with Eq. (4.4),

the values of the costate variables at the inlet boundary can be approximated from the internal stencils. Because the the vector of the flow field is computed from the internal grids at the exit plane, Eq. (4.4) gives four linear independent equations for the costate variables, which result in all the costate variables to be identically zero. On the centerline, the normal velocity is known to be zero, and one of the costate variables, for instance λ_3 , is assigned a value, and the remaining flow field quantities are to be determined from the resulting 3 x 3 system of equations as given in Eq. (4.4)

One way of treating the boundary conditions, i.e. Eq. (4.3), is to use Eq. (3.13) and to find a relationship between the conservative field variables \bar{Q} by taking the variation of Eq. (3.13). This procedure eliminates the constant Lagrange multipliers $\bar{\mu}$ and modifies the functional sensitivity derivatives, Eqs. (3.39) and (3.43) by a term resulting from the variation of the normal vector \bar{n} at the solid boundary.

On the solid boundary, on the other hand, the costate variables are determined by use of the complete form of the compatibility relationships and the sign of the eigenvalues of the costate Jacobian matrices. Once the values of the costate variables on the solid boundary are computed, the constant Lagrange multipliers $\bar{\mu}$ of the no-mass penetration condition can be calculated by solving the complete set of the boundary condition. The results presented in this study are obtained by solution of the complete boundary conditions as given in Eq. (3.42).

4.4 Linearization of Costate (Adjoint) Equations

By the same linearization procedure we used for the state equations, Eq. (4.2) can be approximated as follows:

$$\bar{\lambda}_\tau - \Delta\tau \frac{\partial}{\partial\tau} \left\{ \hat{A}^T \bar{\lambda}_\xi + \hat{B}^T \bar{\lambda}_\eta \right\} = \left\{ \hat{A}^T \bar{\lambda}_\xi + \hat{B}^T \bar{\lambda}_\eta \right\}^n \quad (4.5)$$

$$\bar{\lambda}_\tau - \Delta\tau \frac{\partial}{\partial\tau} \left\{ \left[\hat{A}^T \delta_\xi + \hat{B}^T \delta_\eta \right] \bar{\lambda} \right\} = \left\{ \hat{A}^T \bar{\lambda}_\xi + \hat{B}^T \bar{\lambda}_\eta \right\}^n \quad (4.6)$$

$$\bar{\lambda}_\tau - \Delta\tau \frac{\partial}{\partial\lambda} \left\{ \left[\hat{A}^T \delta_\xi + \hat{B}^T \delta_\eta \right] \bar{\lambda} \right\} \frac{\partial \bar{\lambda}}{\partial\tau} = \left\{ \hat{A}^T \bar{\lambda}_\xi + \hat{B}^T \bar{\lambda}_\eta \right\}^n \quad (4.7)$$

By approximation of the time and space terms, Eq. (4.7) then becomes

$$\Delta \bar{\lambda}^n - \Delta\tau \left[\hat{A}^T \delta_\xi + \hat{B}^T \delta_\eta \right] \Delta \bar{\lambda}^n = \Delta\tau \left\{ \left[\hat{A}^T \delta_\xi + \hat{B}^T \delta_\eta \right] \bar{\lambda} \right\}^n \quad (4.8)$$

4.5 Time-Integration Methods

In this study we have used both the implicit and explicit, i.e., the ADI and Runge-Kutta time-integration, respectively, methods to drive costate equations to steady state. For the implicit method, the ADI factorization of Eq. (4.8) is used to split it into the ξ and η sweeps. Let us define the right side R_λ of Eq. (4.8) as

$$R_\lambda = \Delta\tau \left\{ \left[(\hat{A}^-)^T \delta_\xi^+ + (\hat{A}^+)^T \delta_\xi^- + (\hat{B}^-)^T \delta_\eta^+ + (\hat{B}^+)^T \delta_\eta^- \right] \bar{\lambda} \right\}^n \quad (4.9)$$

where R_λ is the residual for the costate equations. Also, Eq. (4.8) can be put in its split form of Jacobians and fluxes as

$$\left\{ I - \Delta\tau \left[(\hat{A}^+)^T \delta_\xi^- + (\hat{A}^-)^T \delta_\xi^+ + (\hat{B}^+)^T \delta_\eta^- + (\hat{B}^-)^T \delta_\eta^+ \right] \right\} \Delta \bar{\lambda}^{n*} = R_\lambda \quad (4.10)$$

Then the ξ and η sweeps of Eq. (4.10) are given as

$$\left\{ I - \Delta \tau \left[(\hat{A}^+)^T \delta_{\xi}^- + (\hat{A}^-)^T \delta_{\xi}^+ \right] \right\} \Delta \bar{\lambda}^{n*} = R_{\lambda} \quad (4.11)$$

and

$$\left\{ I - \Delta \tau \left[(\hat{B}^+)^T \delta_{\eta}^- + (\hat{B}^-)^T \delta_{\eta}^+ \right] \right\} \Delta \bar{\lambda}^n = \Delta \bar{\lambda}^{n*} \quad (4.12)$$

For the explicit method, the four stage Runge-Kutta algorithm [81] is adopted to compute the vector of the costate variables as

$$\bar{\lambda}^{(1)} = \bar{\lambda}^n \quad (4.13)$$

$$\bar{\lambda}^{(2)} = \bar{\lambda}^n + \alpha_2 \Delta \tau R_{\lambda}^{(1)} \quad (4.14)$$

$$\bar{\lambda}^{(3)} = \bar{\lambda}^n + \alpha_3 \Delta \tau R_{\lambda}^{(2)} \quad (4.15)$$

$$\bar{\lambda}^{(4)} = \bar{\lambda}^n + \alpha_4 \Delta \tau R_{\lambda}^{(3)} \quad (4.16)$$

$$\bar{\lambda}^{n+1} = \bar{\lambda}^n + \frac{\Delta t}{6} \left[R_{\lambda}^{(n)} + 2R_{\lambda}^{(2)} + 2R_{\lambda}^{(3)} + R_{\lambda}^{(4)} \right] \quad (4.17)$$

where

$$\alpha_2 = 1/2 \quad \alpha_3 = 1/2 \quad \alpha_4 = 1 \quad (4.18)$$

In advancing the costate equations in time, both the implicit ADI and explicit Runge-Kutta methods are employed. The results, however, will be presented only for the ADI method.

Chapter 5

STABILITY ANALYSIS OF THE TWO DIMENSIONAL COSTATE AND EULER EQUATIONS

5.1 Rationale for Stability Analysis

The most popular schemes to advance the Euler equations to steady-state solutions are, among others, the implicitly factored time-integration schemes. Approximate factorizations unfortunately introduce errors which propagate throughout the computational domain. As a result of this, the stability limit is drastically reduced, and the convergence rate deteriorates. To propose the range of the CFL numbers for which the allowable maximum eigenvalues are predicted, a stability analysis of the Euler and costate equations are conducted.

5.2 Introduction to Stability Analysis

In solving coupled time-dependent partial differential equations like the Euler equations, one takes advantage of the hyperbolic nature of the equations. Because of this fact, numerical upwind methods are devised according to the direction of the flow information along the characteristics. The most common upwind methods that take into account the hyperbolicity of the equations are the Beam-Warming, Van Leer vector-splitting, and the Roe flux-differencing methods [92]. On the basis of the eigenvalue decompositions, the fluxes and Jacobians of these methods are split into the backward and forward contributions. The Van Leer vector-splitting method [80] is shown to produce sharper shocks than the Beam - Warming flux - vector - splitting approach [79]. In this analysis, the

Beam-Warming splitting for the one-dimensional Euler equations has been used for the purpose of comparison only. Otherwise, the Van Leer vector-splitting technique has been adopted throughout for both the one-dimensional and two-dimensional Euler equations.

As mentioned in Sec. 1.2, Jespersen and Pulliam [71] studied the stability characteristics of the Euler equations for different flux-splitting methods. Anderson and Thomas [72] further conducted stability analysis on the complete three-dimensional Euler equations. In their analysis, they have investigated specifically three kinds of splittings: three-factor spatially split, two-factor eigenvalue split, and two-factor combination split. All three splittings have different levels of factorization errors. During derivation of the generalized complex eigenvalue equations, they have also used first-order differencing on the implicit side (leftside) and fully upwind second-order differencing for the residual (right side) part. For a Mach number of 0.8 and an angle of attack of 0° , they found out that the three-factor splitting has lower CFL stability ($CFL = 20$), whereas the other two-factor splittings are stable for all CFL numbers considered.

In their pursuit to optimize the PROTEUS code with multigrid methods, Demuren and Ibraheem [73] have conducted an extensive and complete stability analysis of one-, two-, and three-dimensional Euler and two-, and three-dimensional Navier-Stokes equations. They have looked at not only the ADI factorization but also the LU approximation factorization for Euler equations and Navier-Stokes equations with various levels of dissipation terms. These inclusions, in fact, encompass the most recent and commonly used approximation numerical methods, specifically, the upwind and central difference approximations. Their conclusions are in line with Ref. 72, i.e., the CFL range over which the maximum eigenvalues are optimized decrease as the dimensionality of the problem increases. The stability deterioration is dependent

or augmented by the type of discretizations and factorizations employed in the numerical computations.

5.3 Objective and Motivation

In the preceding section, the main features of different schemes are analyzed with the help of the amplification factors for the complex eigenvalue boundary equations [71 - 73]. The objective of the present stability analysis is not to revisit the complete stability analysis of different upwind schemes of the Euler and costate equations with varying approximations. Rather, the main thrust is to investigate the stability analysis of the costate equations with only the spatial upwind factorization scheme and the Euler equations are included for comparison reasons. This procedure is necessary because the costate equations are similar to the Euler equations, and consequently, one will adopt the same numerical technique for the costate equations. The numerical stability and quick convergence of the costate equations are very detrimental because the computation of the sensitivity gradient is directly influenced by the converged solution of the costate equations, which ultimately controls the whole analysis and optimization process. For this obvious reason, one has to investigate the CFL range over which the maximum, average, and L2-normed eigenvalues are extremized.

Like the previous researchers [71 - 73], first-order difference approximation on the left side and second-order upwind differencing on the right side of the Euler and costate equations are used. To investigate the stability limits of the PDE for the stated factorization of the Van Leer schemes, one solves the generalized complex eigenvalue boundary value problems given in Secs. 5.4.1 and 5.4.2. In doing so, one computes the maximum, average, and L2-normed eigenvalues in the range of $0 \leq \omega_x, \omega_y \leq 2\pi$ for the desired series of CFL number. Also the

smoothing factor σ , which is related to the damping of the high frequencies in the multigrid methods, is computed as the absolute value of the maximum amplification in the range of $\frac{\pi}{2} \leq \max(\omega_x, \omega_y) \leq \frac{3\pi}{2}$. Following Anderson and Thomas [72], the time step which is used in the computation of the amplification factors for the two-dimensional case is given by

$$\Delta t \leq CFL \cdot \left[\frac{|u|}{\Delta x} + \frac{|v|}{\Delta y} + a \sqrt{\left(\frac{1}{\Delta x^2} + \frac{1}{\Delta y^2} \right)} \right]^{-1} \quad (5.1)$$

5.4 One- and Two-Dimensional Euler Equations

The one- and two-dimensional Euler equations in conservative forms and in Cartesian coordinate systems are given first. Then, they are discretized in the upwind fashion depending on the positive and negative fluxes and Jacobians. For the one-dimensional Euler flow, the source terms are included to investigate their eventual influence in the stability limit of the flow characteristics. Finally, the approximations and discretizations of the one- and two-dimensional costate equations in Cartesian coordinate systems are given for completeness.

5.4.1 One-Dimensional Euler Equations

$$\frac{\partial(S\bar{Q})}{\partial t} + \frac{\partial E}{\partial x} - H_s = \bar{0} \quad (5.2)$$

By an application of the Euler backward approximation in time on Eqs. (5.2), one obtains

$$\left\{ SI + \Delta t \cdot \left[\frac{\partial}{\partial x} (A^+ + A^-) - B_h \right] \right\} \Delta \bar{Q} = -\Delta t \cdot \left[\frac{\partial}{\partial x} (E^+ + E^-) - H_s \right] \quad (5.3)$$

$$\{SI + \Delta t \cdot [(\delta_x^- A^+ + \delta_x^+ A^-) - B_h]\} \Delta \bar{Q} = -\Delta t \cdot [(\delta_x^- E^+ + \delta_x^+ E^-) - H_s] \quad (5.4)$$

The use of $E^\pm = A^\pm \bar{Q}$; into Eq. (5.4) results in

$$\{SI + \Delta t \cdot [(\delta_x^- A^+ + \delta_x^+ A^-) - B_h]\} \Delta \bar{Q} = -\Delta t \cdot [\delta_x^- (A^+ \bar{Q}) + \delta_x^+ (A^- \bar{Q}) - H_s]^n \quad (5.5)$$

where the fluxes, the Jacobians, and the source terms are given in Appendix C.

5.4.2 One-Dimensional Costate Equations

From Eq. (2.48), the one-dimensional costate equations in Cartesian coordinate systems are derived (see the detail in Chap. 6) as

$$\bar{\lambda}_t - A^T \bar{\lambda}_x - B_h^T \bar{\lambda} + SC^T = \bar{0} \quad (5.6)$$

where B_h , and C are given in Appendix C. By the same procedure as for the Euler equations (Eqs. (5.3) - 5.5)), the following approximations for the costate equations are obtained.

$$\{I - \Delta t \cdot [\delta_x^- (A^+)^T + \delta_x^+ (A^-)^T]\} \Delta \bar{\lambda}^n = \Delta t \cdot [\delta_x^- (A^+)^T + \delta_x^+ (A^-)^T + B_h^T] \bar{\lambda}^n \quad (5.7)$$

Although the Jacobian matrices of the costate equations are transposed, they are given in Appendix C.

5.4.3 Two-Dimensional Euler Equations

From Eq. (2.7), the conservative two-dimensional Euler equations in Cartesian coordinates are expressed as

$$\frac{\partial \bar{Q}}{\partial t} + \frac{\partial E}{\partial x} + \frac{\partial F}{\partial y} = \bar{0} \quad (5.8)$$

By application of the Euler backward approximation in time on Eqs. (5.2) and (5.7), one gets

$$\left\{ I + \Delta t \cdot \left[\frac{\partial}{\partial x} (A^+ + A^-) + \frac{\partial}{\partial y} (B^+ + B^-) \right] \right\} \Delta \bar{Q}^n = -\Delta t \cdot R^n \quad (5.9)$$

where

$$R^n = \frac{\partial}{\partial x} (E^+ + E^-) + \frac{\partial}{\partial y} (F^+ + F^-) \quad (5.10)$$

Then, further representation of Eqs. (5.4) and (5.5) in the delta form gives

$$\left\{ I + \Delta t \cdot \left[(\delta_x^- A^+ + \delta_x^+ A^-) + (\delta_y^- B^+ + \delta_y^+ B^-) \right] \right\} \Delta \bar{Q}^n = -\Delta t \cdot R^n \quad (5.11)$$

where

$$R^n = (\delta_x^- E^+ + \delta_x^+ E^-) + (\delta_y^- F^+ + \delta_y^+ F^-) \quad (5.12)$$

By use of $E^\pm = A^\pm \bar{Q}$; and $F^\pm = B^\pm \bar{Q}$ in Eq. (5.12), Eq. (5.12) assumes the form of

$$\begin{aligned} \left\{ I + \Delta t \cdot \left[\delta_x^- A^+ + \delta_x^+ A^- + \delta_y^- B^+ + \delta_y^+ B^- \right] \right\} \Delta \bar{Q}^n = \\ -\Delta t \cdot \left\{ \delta_x^- (A^+ \bar{Q}) + \delta_x^+ (A^- \bar{Q}) + \delta_y^- (B^+ \bar{Q}) + \delta_y^+ (B^- \bar{Q}) \right\}^n \end{aligned} \quad (5.13)$$

Factorization of the left side of Eq. (5.13) results in:

$$\begin{aligned} \{I + \Delta t \cdot (\delta_x^- A^+ + \delta_x^+ A^-)\} \{I + \Delta t \cdot (\delta_y^- B^+ + \delta_y^+ B^-)\} \Delta \bar{Q}^n = \\ -\Delta t \cdot \{ \delta_x^- (\bar{A}^+ \bar{Q}) + \delta_x^+ (\bar{A}^- \bar{Q}) + \delta_y^- (\bar{B}^+ \bar{Q}) + \delta_y^+ (\bar{B}^- \bar{Q}) \}^n \end{aligned} \quad (5.14)$$

5.4.4 Two-Dimensional Costate Equations

With Eq. (3.31) and addition of time term with its appropriate sign, the two-dimensional costate equations are

$$\bar{\lambda}_t - A^T \bar{\lambda}_x - B^T \bar{\lambda}_y = \bar{0} \quad (5.15)$$

Adoption of the same method as for the two-dimensional Euler equations (Eqs. (5.9) and (5.13)) results in

$$\{I - \Delta t \cdot [\delta_x^- (A^+)^T + \delta_x^+ (A^-)^T + \delta_y^- (B^+)^T + \delta_y^+ (B^-)^T]\} \Delta \bar{\lambda}^n = \Delta t \cdot R_\lambda^n \quad (5.16)$$

where

$$R_\lambda^n = \{ \delta_x^- [(A^+)^T \lambda] + \delta_x^+ [(A^-)^T \lambda] + \delta_y^- [(B^+)^T \lambda] + \delta_y^+ [(B^-)^T \lambda] \}^n \quad (5.17)$$

Similarly as for Eq. (5.13), factorization of the left side of Eq. (5.16) gives

$$\begin{aligned} \{I - \Delta t \cdot [\delta_x^- (A^+)^T + \delta_x^+ (A^-)^T]\} \{I - \Delta t \cdot [\delta_y^- (B^+)^T + \delta_y^+ (B^-)^T]\} \Delta \bar{\lambda}^n = \\ R_\lambda^n = \{ \delta_x^- [(A^+)^T \lambda] + \delta_x^+ [(A^-)^T \lambda] + \delta_y^- [(B^+)^T \lambda] + \delta_y^+ [(B^-)^T \lambda] \}^n \end{aligned} \quad (5.18)$$

For the time increment of the flow and costate field variables, respectively, the following approximations are used:

$$\Delta \bar{Q}^n = \bar{Q}^{n+1} - \bar{Q}^n \quad (5.19)$$

$$\Delta \bar{\lambda}^n = \bar{\lambda}^{n+1} - \bar{\lambda}^n \quad (5.20)$$

5.5 Solution Algorithm

To perform the Von Neumann stability analysis of the Euler and costate equations, the flow field quantities are considered to be constant in the Cartesian coordinate system. For a constant flow field, the Jacobians are also assumed to be constant. With this assumption, the flow quantities can be expressed in terms of wave fronts [72, 77]. Thus, the wave fronts for the Euler and costate flow variables are represented, respectively, by

$$\bar{Q}^n = \bar{\varphi}^n \bar{P}_0 e^{I(i\omega_x + j\omega_y)} \quad (5.21)$$

and

$$\bar{\lambda}^n = \bar{\varphi}^n \bar{P}_0 e^{I(i\omega_x + j\omega_y)} \quad (5.22)$$

where I is the imaginary number defined by $I = \sqrt{-1}$ and ω_x , ω_y are the x and y modes, and $\bar{\varphi}$, \bar{P}_0 are the amplification factors and initial constant vectors, respectively. Now Eq. (5.21) is substituted into Eqs. (5.5) and (5.14), and Eq. (5.22) into Eqs. (5.7) and (5.18). If the resulting equations are simplified, then the

generalized eigenvalue equations of the Euler and costate equations are obtained, and these are given in the next subsections.

5.5.1 Complex Eigenvalue Equations of Euler and Costate Equations

The one- and two-dimensional complex eigenvalue boundary problems of the Euler and costate equations can be generally represented as

$$(\hat{L} \pm \hat{R})\bar{V} = \hat{L}\bar{\varphi}\bar{V} \quad (5.23)$$

where \bar{L} and \hat{R} are the left and right side Fourier symbols and \bar{V} are the eigenvectors. Here the positive sign corresponds to the costate equations and the negative sign to the Euler equations. The various matrices defined in the one-dimensional Euler and costate equations are given in Appendix C, and the matrices for the two-dimensional analysis are given in Appendix D.

5.5.2 One-Dimensional Euler-Fourier Symbols

The insertion of the one-dimensional form of Eq. (5.21) into Eq. (5.5) gives the one-dimensional Fourier symbols of the Euler equations as

$$\hat{L} = SI - \Delta t \cdot B_h + \left\{ \frac{\Delta t}{\Delta x} \left[(A^+ - A^-)(1 - \cos \omega_x) + (A^+ + A^-)I \sin \omega_x \right] \right\} \quad (5.24)$$

$$\begin{aligned} \hat{R} = & \frac{\Delta t}{2\Delta x} \left[(A^+ - A^-)(3 + \cos 2\omega_x - 4\cos \omega_x) + (A^+ + A^-)(4\sin \omega_x - \sin 2\omega_x)I \right] \\ & - \Delta t B_h \end{aligned} \quad (5.25)$$

5.5.3 One-Dimensional Costate Fourier Symbols

The insertion of the one-dimensional form of Eq. (5.22) into Eq. (5.7) gives the one-dimensional Fourier symbols of the costate equations as

$$\hat{L} = \mathbf{I} - \left\{ \frac{\Delta t}{\Delta x} \left[(A^+ - A^-)^T (1 - \cos \omega_x) + (A^+ + A^-)^T I \sin \omega_x \right] \right\} \quad (5.26)$$

$$\begin{aligned} \hat{R} = & \frac{\Delta t}{2\Delta x} \left[(A^+ - A^-)^T (3 + \cos 2\omega_x - 4 \cos \omega_x) + (A^+ + A^-)^T (4 \sin \omega_x - \sin 2\omega_x) I \right] \\ & + \Delta t B_h^T \end{aligned} \quad (5.27)$$

5.5.4 Two-Dimensional Euler-Fourier Symbols

The insertion of Eq. (5.21) into Eq. (5.14) gives the two-dimensional Fourier symbols of the Euler equations as

$$\begin{aligned} \hat{L} = & \left\{ \mathbf{I} + \frac{\Delta t}{\Delta x} \left[(A^+ - A^-)(1 - \cos \omega_x) + (A^+ + A^-) I \sin \omega_x \right] \right\} \\ & \left\{ \mathbf{I} + \frac{\Delta t}{\Delta y} \left[(B^+ - B^-)(1 - \cos \omega_y) + (B^+ + B^-) I \sin \omega_y \right] \right\} \end{aligned} \quad (5.28)$$

$$\begin{aligned} \hat{R} = & \frac{\Delta t}{2\Delta x} \left[(A^+ - A^-)(3 + \cos 2\omega_x - 4 \cos \omega_x) + (A^+ + A^-)(4 \sin \omega_x - \sin 2\omega_x) I \right] \\ & + \frac{\Delta t}{2\Delta y} \left[(B^+ - B^-)(3 + \cos 2\omega_y - 4 \cos \omega_y) + (B^+ + B^-)(4 \sin \omega_y - \sin 2\omega_y) I \right] \end{aligned} \quad (5.29)$$

5.5.5 Two-Dimensional Costate Fourier Symbols

The insertion of Eq. (5.22) into Eq. (5.18) gives the two-dimensional Fourier symbols of the costate equations as

$$\hat{L} = \left\{ \mathbf{I} - \frac{\Delta t}{\Delta x} \left[(A^+ - A^-)^T (1 - \cos \omega_x) + (A^+ + A^-)^T I \sin \omega_x \right] \right\} \\ \left\{ \mathbf{I} - \frac{\Delta t}{\Delta y} \left[(B^+ - B^-)^T (1 - \cos \omega_y) + (B^+ + B^-)^T I \sin \omega_y \right] \right\} \quad (5.30)$$

$$\hat{R} = \frac{\Delta t}{2\Delta x} \left[(A^+ - A^-)^T (3 + \cos 2\omega_x - 4 \cos \omega_x) + (A^+ + A^-)^T (4 \sin \omega_x - \sin 2\omega_x) I \right] \\ + \frac{\Delta t}{2\Delta y} \left[(B^+ - B^-)^T (3 + \cos 2\omega_y - 4 \cos \omega_y) + (B^+ + B^-)^T (4 \sin \omega_y - \sin 2\omega_y) I \right] \quad (5.31)$$

5.6 Results, Discussion, and Recommendations

To confirm that factorization indeed puts a restriction on how to choose the CFL range for the stable solution of the approximated PDE, a stability investigation of two-dimensional Euler equations in unfactored form is performed. Figure 5.1 clearly depicts that the maximum allowable amplification factor is stable at all CFL numbers considered. As the case of solving Euler equations in unfactored form is computationally prohibitive, one would rather revert to solving the factored and easily invertible operators in a unidimensional mode.

To gain insight and confidence in solving numerically adjoint equations for optimization purposes, a systematic stability analysis is performed on the one- and two-dimensional adjoint equations along with the corresponding one- and two-dimensional Euler equations. In addition to the usual analysis of the quasi one-dimensional Euler equations without the source terms, stability characteristics with the source terms are also conducted. The study shows that the range of the CFL number for which the upwind schemes are stable is not basically affected by the source terms (Fig. 5.2). Note that the costate equations have two distinguishing features. The first one is that the transposed Jacobians

are constructed from the converged solution of the Euler equations. This indicates that those matrices are globally constant in time even though they vary in space. The second feature is that the matrices have negative entries. Mathematically, and from the stability view point of a matrix, the eigenvalues of a transposed matrix are no different from the eigenvalues of the nontransposed matrices. Therefore, transposition of the matrices has no bearing on the stability characteristics of the costate equations. Rather, the deterioration of the stability limit of the costate equations stems from the negative sign of the transposed matrices (Figs 5.4 and 5.5). Therefore, the correct direction of the flow for the costate equations is imperative. As can be discerned from Figs. 5.2, 5.3, 5.6, and 5.7, the trends of the stability of the adjoint equations are similar to those of Euler equations if the flow field is transformed as presented in Ibrahim and Baysal [65]. When the direction of the flow is not taken into account, which is the case with the costate equations, the stability is limited to very small CFL numbers (Figs. 5.4 and 5.5). This low-stability problem becomes especially apparent when there is high flow discontinuity in the flow field as mentioned in Ibrahim and Baysal [65]. Therefore, a transformation of the flow field or another numerical approach to account for the reverse flow direction of the costate equations is highly recommended.

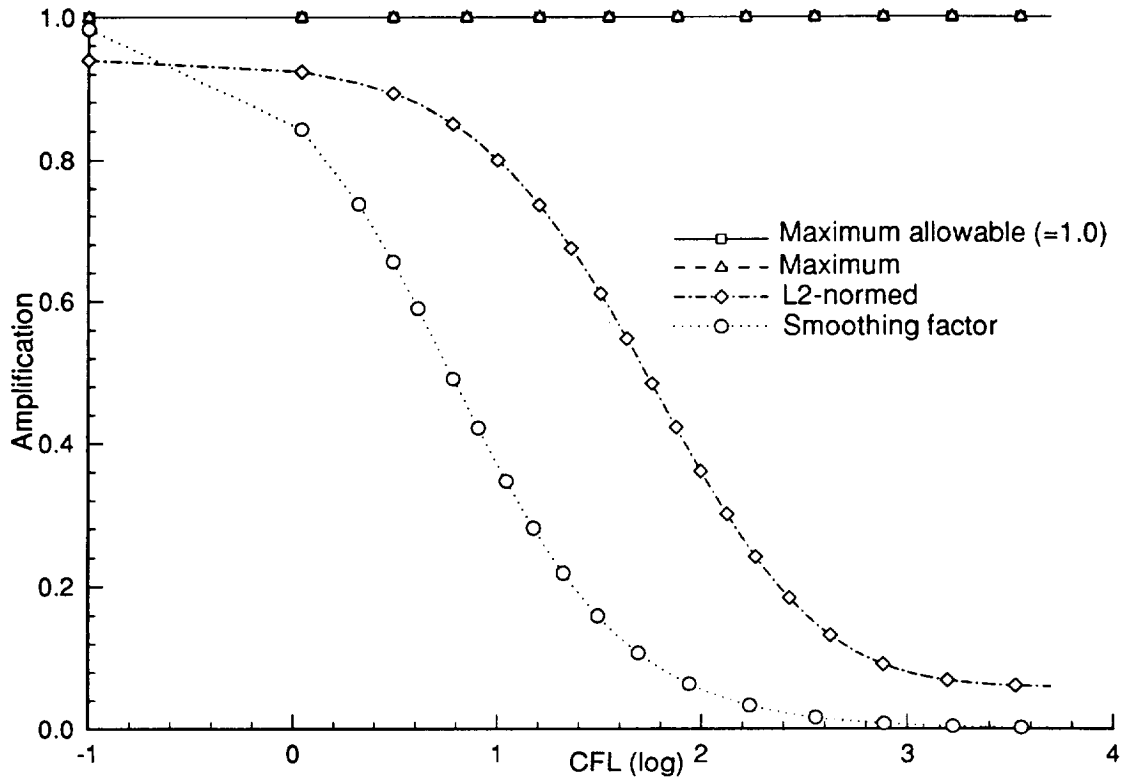


Fig. 5.1 Amplification of unfactored 2-D Euler equations.

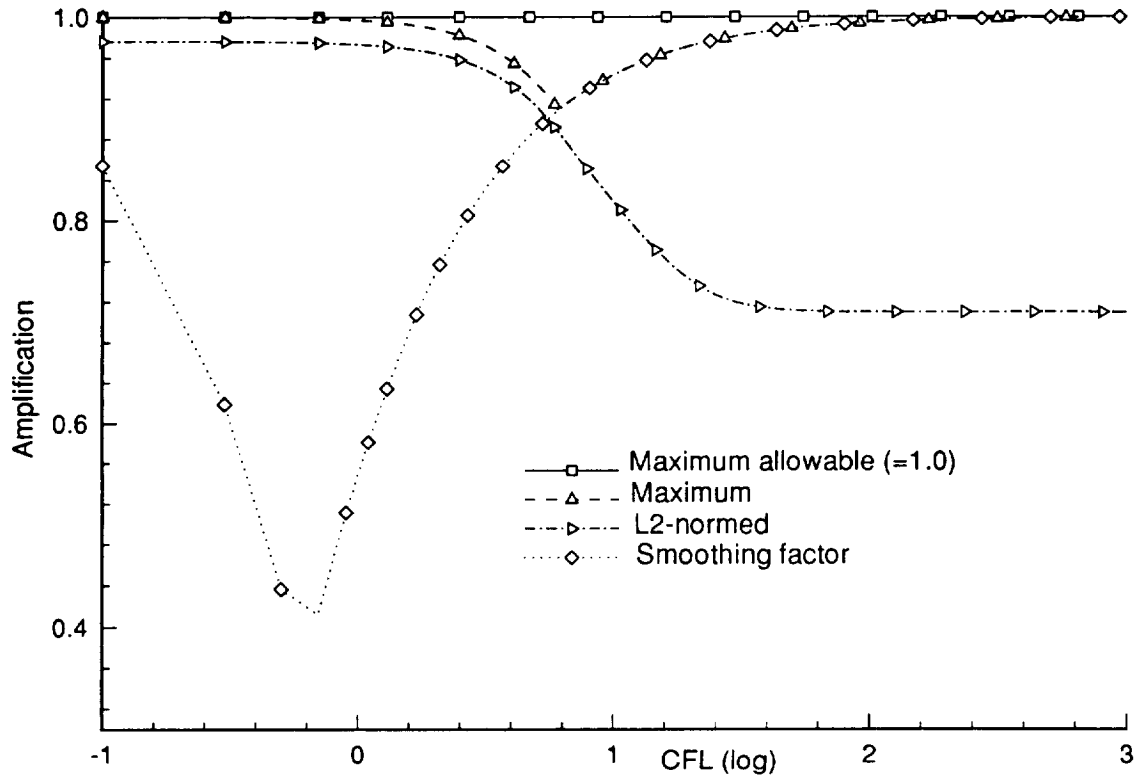


Fig 5.2 Amplification factor for 1-D Euler equations.

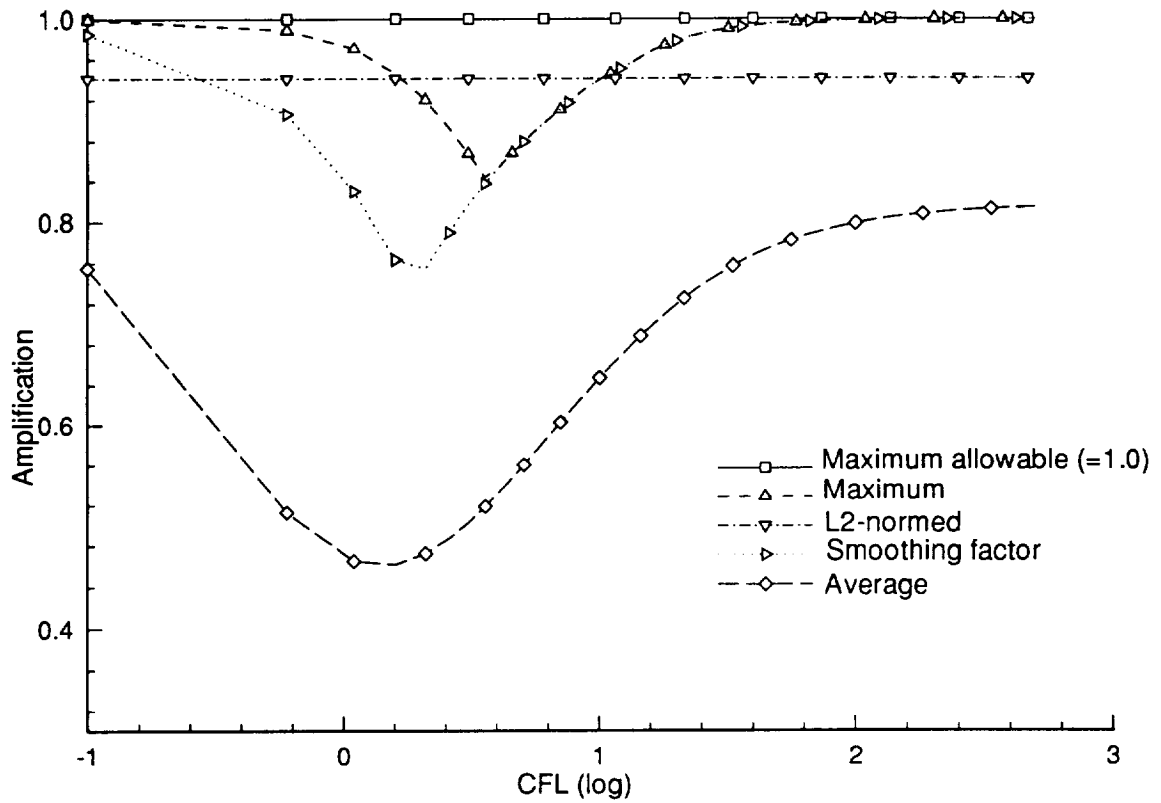


Fig. 5.3 Amplification of factored 2-D Euler equations.

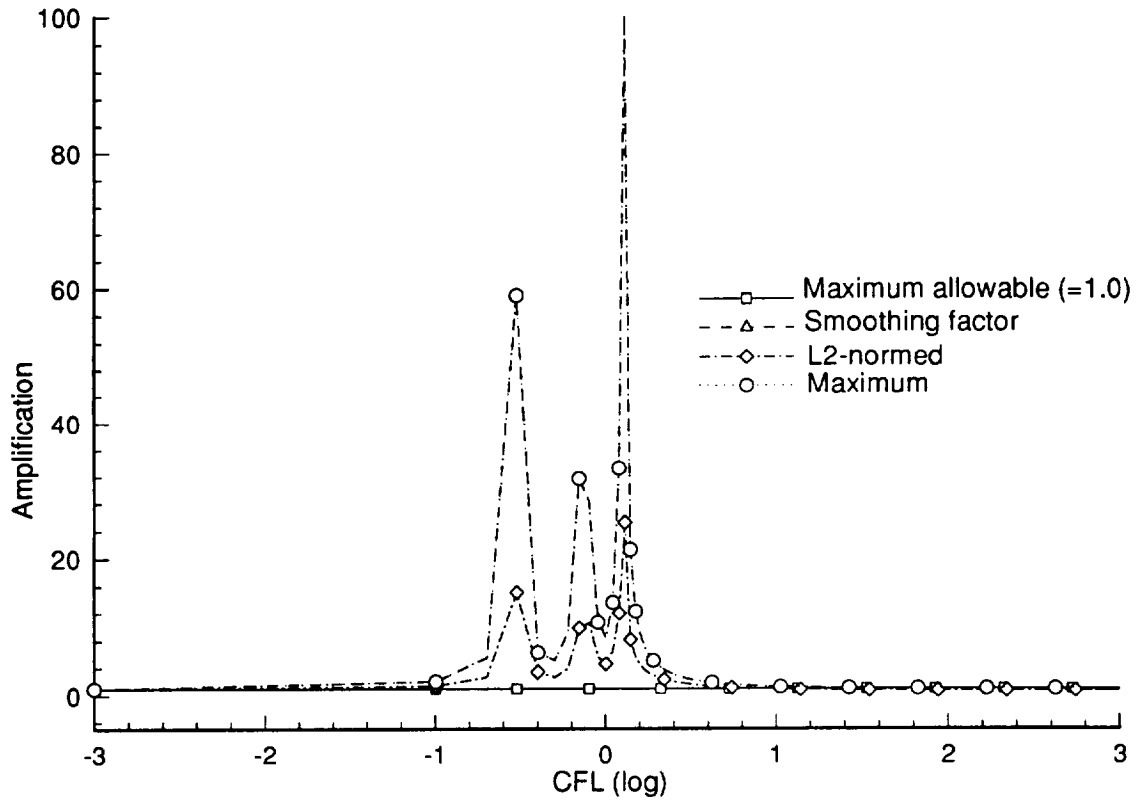


Fig. 5.4 Amplification of factored 1-D costate equations without space transformation.

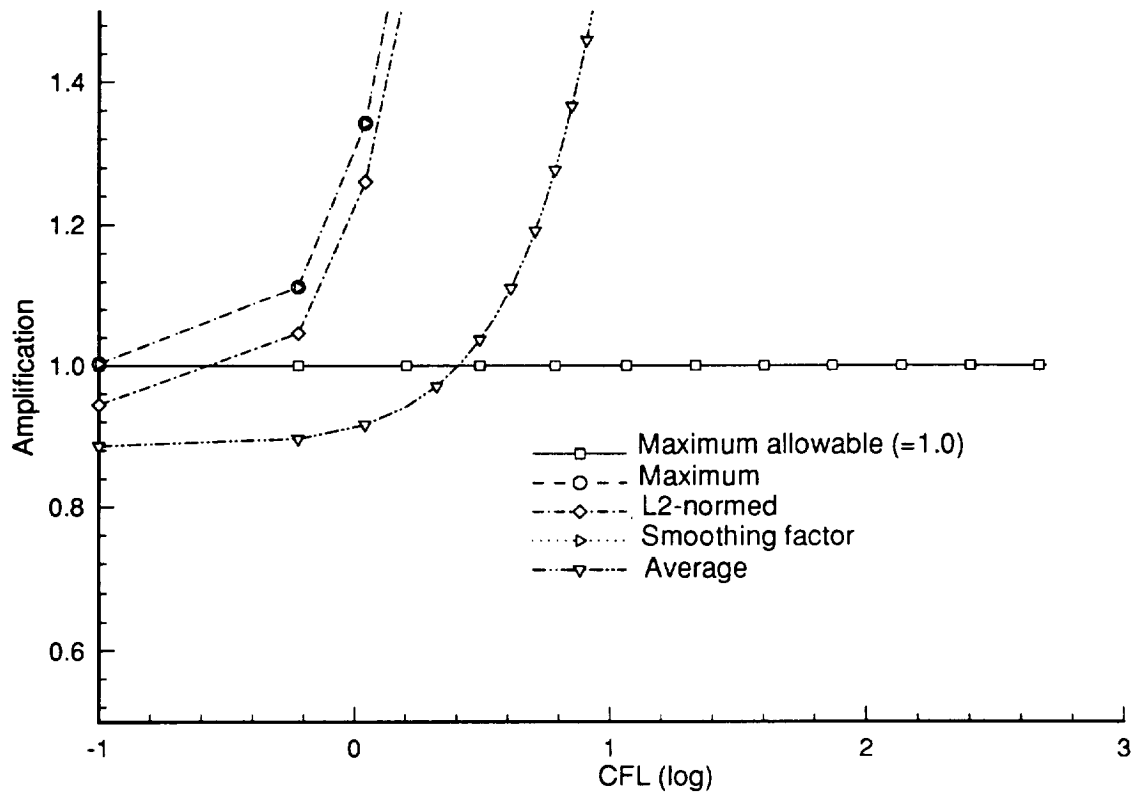


Fig. 5.5 Amplification of factored 2-D costate equations without space transformation.

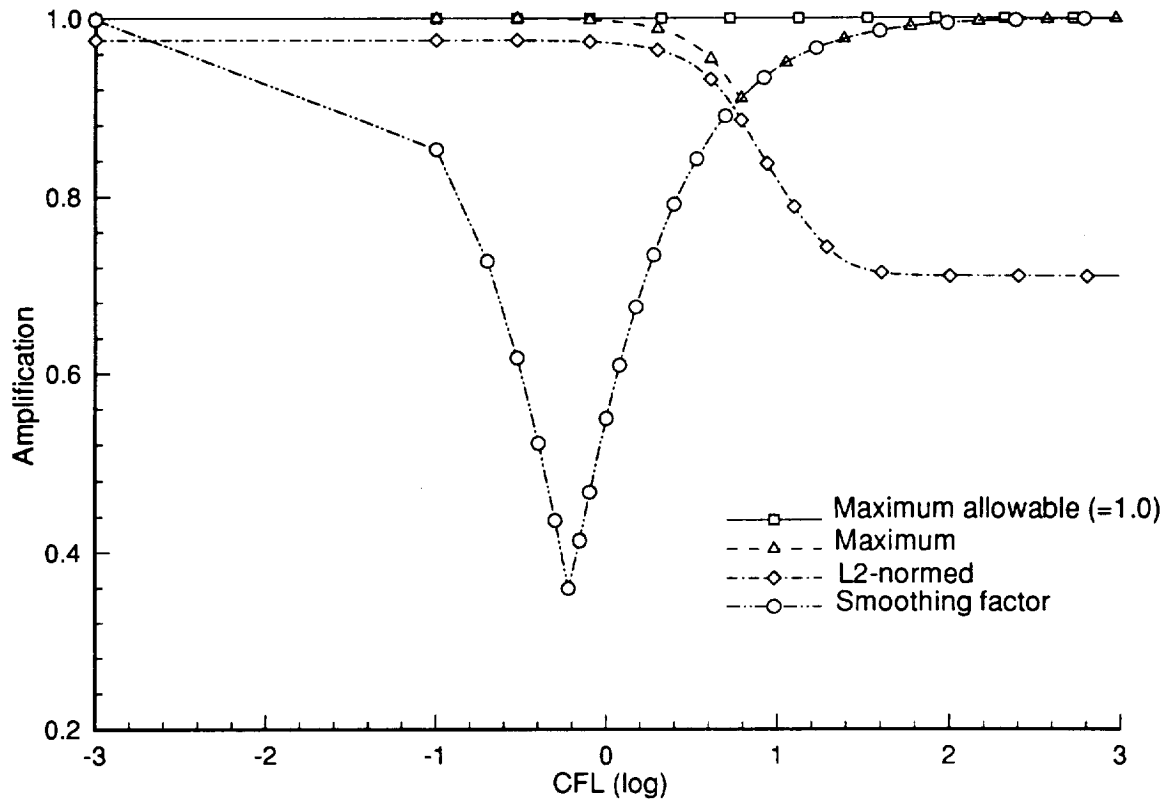


Fig. 5.6 Amplification of factored 1-D costate equations with space transformation.

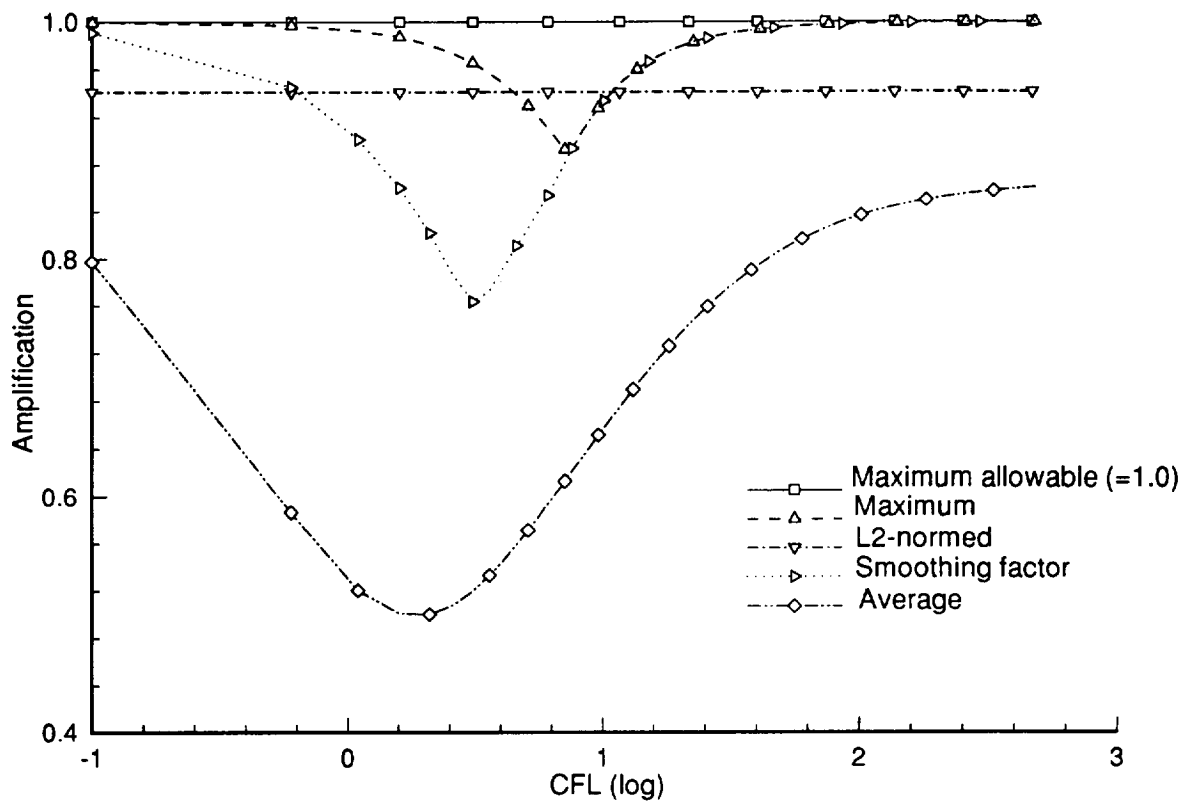


Fig. 5.7 Amplification of factored 2-D costate equations with space transformations.

Chapter 6

DESIGN OPTIMIZATION OF INTERNAL FLOWS USING QUASI ONE-DIMENSIONAL EULER EQUATIONS

6.1 Introduction to One-Dimensional Design Optimization

Two approaches, one based on the nonconservative and the other one on conservative flow field variables, are developed for quasi one-dimensional Euler equations. In addition to the difference in the representation of the flow field variables, the first approach incorporates time integration while the second approach neglects the role of time and only takes the converged residual part of the solution. These approaches, which are based on the variational methods (VM), are used to derive the costate(adjoint) partial differential equations and their transversality (boundary) conditions from the differential equations of the fluid flow. The costate equations coupled with the flow field equations are solved iteratively to get the functional derivative coefficients. Then, these derivative coefficients, combined with the flow field variables, are used to find the boundary shape which minimizes the performance index (objective functional).

To demonstrate the method through examples, the shape of the nozzle is optimized for the maximum thrust. For this maximization problem, different inlet and outlet flow conditions are considered. In the supersonic flow case, the gain in thrust is remarkably high. Even in the shock and the subsonic flows, the improvement of the thrust is found to be substantial. As demonstrated through the cases investigated, a new improvement is that the present variational shape optimization approach is capable of resolving flows with shocks.

6.2 Model Problem

To demonstrate the versatility of the proposed approach, the time-dependent, compressible, quasi one-dimensional Euler equations are chosen as the state equations. The corresponding adjoint equations (costate) with their transversality (boundary) conditions are derived by variational methods. In this design optimization problem, the objective functional is the thrust which is given in Eq. (6.7), where the cross-sectional area S is the design variable and the governing equations of the model fluid problem are given in Sec. 2.5 which are

$$\frac{\partial(\rho S)}{\partial t} + \frac{\partial(\rho u S)}{\partial x} = 0 \quad (6.1)$$

$$\frac{\partial(\rho u S)}{\partial t} + \frac{\partial(\rho u^2 + P)S}{\partial x} - P \frac{dS}{dx} = 0 \quad (6.2)$$

and

$$\frac{\partial(\rho S e_t)}{\partial t} + \frac{\partial[(P + \rho e_t)uS]}{\partial x} = 0 \quad (6.3)$$

The eqs. (6.1), (6.2), and (6.3) are mass, momentum and energy, respectively, and ρ , u , e_t , and S , are density, velocity, total energy and cross-sectional area.

The example problem here is to find $S(x)$ where $0 \leq x \leq L$ to maximize

$$J(\bar{Q}, S) = \int_0^T \int_0^L \{PS\} dx dt \quad (6.4)$$

subject to

$$S(0) \leq S_0 \text{ and } S(L) \leq S_i \quad (6.5)$$

where L is the dimension of the geometry and T is the maximum time of integration.

6.3 Approach 1: Perturbed State Equations and Performance Indices in NonConservative Variables

In this approach, we make use of Eqs. (6.1) - (6.3) and the cross-sectional area S , which is expressed as

$$S(x, x_D) = a + b[\tanh(0.8x - 4)] \quad (6.6)$$

A change of the design function S perturbs the flow variables, which in turn gives rise to the variation of the functional. Then, the functional derivatives (sensitivity coefficients) are obtained by perturbation techniques, for which the primitive variables are redefined as

$$\rho = \bar{\rho} + \delta\rho \quad u = \bar{u} + \delta u \quad e_i = \bar{e}_i + \delta e_i \quad (6.7)$$

and the variation of the boundary is similarly approximated as

$$S = \bar{S} + \delta S \quad (6.8)$$

where $\bar{\rho}$, \bar{u} , \bar{e}_i , and \bar{S} are the nominal values and $\delta\rho$, δu , δe_i , and δS are the perturbed values. First, Eqs. (6.7) and (6.8) are inserted into Eqs. (6.1) - (6.4). In

the resulting equation, only the first-order terms in the perturbed quantities are retained. Recalling that the nominal flow values satisfy the flow equations, the perturbed flow equations are obtained as (the overbar signs are dropped for convenience)

$$\frac{\partial(S\delta\rho + \rho\delta S)}{\partial t} = -\frac{\partial(uS\delta\rho + \rho S\delta u + \rho u\delta S)}{\partial x} \equiv r_1 \quad (6.9)$$

$$\begin{aligned} \frac{\partial(uS\delta\rho + \rho S\delta u + \rho u\delta S)}{\partial t} = & -\frac{\partial[S(u^2\delta\rho + 2\rho u\delta u + \delta P) + (\rho u^2 + P)\delta S]}{\partial x} \\ & + \frac{dS}{dx}\delta\rho + \rho\delta\left(\frac{dS}{dx}\right) \equiv r_2 \end{aligned} \quad (6.10)$$

and

$$\frac{\partial(Se_i\delta\rho + \rho S\delta e_i + \rho e_i\delta S)}{\partial t} = -\frac{\partial[uS(e_i\delta\rho + \rho\delta e_i + \delta P) + (P + \rho e_i)(S\delta u + u\delta S)]}{\partial x} \equiv r_3 \quad (6.11)$$

Similarly, the functional J in Eq. (6.7) is perturbed. Because the nominal functional values along with the nominal flow variables satisfy the flow equations, the perturbed functional is reduced to the following forms for the maximization problem:

$$\delta J = \int_0^T \int_0^L \{S\delta P + P\delta S\} dx dt \quad (6.12)$$

Note that the variation of x is not considered in the previous derivations because the length of the nozzle is not changed in the design process. For this approach, Eqs. (6.1) - (6.3) are put in their vector form as

$$\frac{\partial(s\bar{Q})}{\partial t} = \bar{r} \quad (6.13)$$

where

$$\bar{Q} = [\rho, \rho u, \rho e_t]^T \quad (6.14)$$

\bar{r} denotes the vector of the spatial derivatives as given in Eqs. (6.9) - (6.11), and \bar{Q} is the vector of conserved variables. Then Eq. (6.13) can be used to define the residual for the nonconservative approach as

$$G(x, t, S, \bar{Q}) = \frac{\partial(s\bar{Q})}{\partial t} - \bar{r} = \bar{0} \quad (6.15)$$

To eliminate δP , from Eq. (6.15), one may augment J with the flow equation as

$$J_a(\bar{Q}, \bar{\lambda}, S) = J(\bar{Q}, S) + \int_0^T \int_0^L \bar{\lambda}^T(x, t) G(x, t, S, \bar{Q}) dx dt \quad (6.16)$$

where G is given in Eq. (6.15). Then, the variation of Eq. (6.16) is given as

$$\delta J_a(\bar{Q}, \bar{\lambda}, S) = \delta J(\bar{Q}, S) + \delta \int_0^T \int_0^L \bar{\lambda}^T(x, t) G(x, t, S, \bar{Q}) dx dt \quad (6.17)$$

Because the length of the nozzle is unchanged and $G \delta \bar{\lambda}$ is equal to zero, then Eq. (6.17) is simplified to

$$\delta J_a(\bar{Q}, \bar{\lambda}, S) = \delta J(\bar{Q}, S) + \int_0^T \int_0^L \bar{\lambda}^T(x, t) \delta G(x, t, S, \bar{Q}) dx dt \quad (6.18)$$

The substitution of the variational expressions from Eqs. (6.9) - (6.12) into Eq. (6.18), gives the following equation for the maximization problem.

$$\begin{aligned} \delta J_a(\bar{Q}, \bar{\lambda}, S) = & \int_0^T \int_0^L \left\{ (S \delta P + P \delta S) - \lambda_1 \left[\frac{\partial (u S \delta \rho + \rho S \delta u + \rho u \delta S)}{\partial x} + \frac{\partial (S \delta \rho + \rho \delta S)}{\partial t} \right] \right\} dx dt \\ & - \int_0^T \int_0^L \left\{ \lambda_2 \left[\frac{\partial [S u^2 \delta \rho + 2 \rho u S \delta u + S \delta P + (P + \rho u^2) \delta S]}{\partial x} + \frac{\partial (u S \delta \rho + S \rho \delta u + \rho u \delta S)}{\partial t} \right] \right\} dx dt \\ & + \int_0^T \int_0^L \lambda_2 \left[\frac{dS}{dx} \delta P + P \delta \left(\frac{dS}{dx} \right) \right] dx dt \\ & - \int_0^T \int_0^L \left\{ \lambda_3 \left[\frac{\partial [u S e_i \delta \rho + S (P + \rho e_i) \delta u + u (P + \rho e_i) \delta S]}{\partial x} + \frac{\partial (S e_i \delta \rho + \rho S \delta e_i + \rho e_i \delta S)}{\partial t} \right] \right\} dx dt \end{aligned} \quad (6.19)$$

The variation of P can be written in terms of the variation of the other flow variables with the help of an equation of state, such as the perfect gas law,

$$P = \rho(\gamma - 1)[e_i - 0.5u^2] \quad (6.20)$$

Now, Eq. (6.19) can be integrated by parts. For the maximization problem, the costate equations, the corresponding boundary (transversality) and initial conditions, and their sensitivity coefficients, respectively, are expressed as

The costate equations are given as

$$\frac{\partial \lambda_1}{\partial t} + u \frac{\partial \lambda_2}{\partial t} + e_t \frac{\partial \lambda_3}{\partial t} + u \frac{\partial \lambda_1}{\partial x} + u^2 \frac{\partial \lambda_2}{\partial x} + [u(\gamma e_t - 0.5(\gamma - 1)u^2)] \frac{\partial \lambda_3}{\partial x} = -(\gamma - 1)(e_t - 0.5u^2) \quad (6.21)$$

$$(1 + u) \frac{\partial \lambda_2}{\partial t} + \rho \frac{\partial \lambda_1}{\partial x} + 2\rho u \frac{\partial \lambda_2}{\partial x} + [(\gamma - 1)\rho u^2 - \rho e_t - P] \frac{\partial \lambda_3}{\partial x} = (\gamma - 1)\rho u \quad (6.22)$$

$$\frac{\partial \lambda_3}{\partial t} + \gamma u \frac{\partial \lambda_3}{\partial x} = -(\gamma - 1) \quad (6.23)$$

The boundary conditions of Eqs. (6.21) - (6.23) are given as

$$\int_0^T \left\{ S[u\lambda_1 + u^2\lambda_2 + (\gamma e_t - 0.5(\gamma - 1)u^3)\lambda_3] \right\}_0^L dt = 0 \quad (6.24)$$

$$\int_0^T \left\{ [\rho S\lambda_1 + 2\rho u S\lambda_2 + S[\gamma \rho e_t - 1.5(\gamma - 1)\rho u^2]\lambda_3] \right\}_0^L dt = 0 \quad (6.25)$$

$$\int_0^T \left\{ S\lambda_3 \right\}_0^L dt = 0 \quad (6.26)$$

The terminal conditions at time T of Eqs. (6.21) - (6.23) are given as

$$\int_0^L \left\{ [S\lambda_1 + uS\lambda_2 + Se_t\lambda_3] \right\}^T dx = 0 \quad (6.27)$$

$$\int_0^L \left\{ S\lambda_2 \right\}^T dx = 0 \quad (6.28)$$

$$\int_0^L \{S\lambda_3\}^T dx = 0 \quad (6.29)$$

The functional derivative coefficients are finally expressed as

$$\begin{aligned} \delta J_a = & \int_0^T \int_0^L \left\{ \rho \frac{\partial \lambda_1}{\partial t} + \rho u \frac{\partial \lambda_2}{\partial t} + \rho e_i \frac{\partial \lambda_3}{\partial t} + \rho u \frac{\partial \lambda_1}{\partial x} + (P + \rho u^2) \frac{\partial \lambda_2}{\partial x} \right\} \delta S dx dt \\ & \int_0^T \int_0^L \left\{ u(P + \rho e_i) \frac{\partial \lambda_3}{\partial x} + P - \lambda_2 \frac{dP}{dx} \right\} \delta S dx dt \end{aligned} \quad (6.30a)$$

Because $S = S(x, x_D)$, one obtains $\delta S = \frac{\partial S}{\partial x_D} \delta x_D$, and Eq. (6.30) can be simplified

as

$$\begin{aligned} \frac{dJ_a}{dx_D} = & \int_0^T \int_0^L \left\{ \rho \frac{\partial \lambda_1}{\partial t} + \rho u \frac{\partial \lambda_2}{\partial t} + \rho e_i \frac{\partial \lambda_3}{\partial t} + \rho u \frac{\partial \lambda_1}{\partial x} + (P + \rho u^2) \frac{\partial \lambda_2}{\partial x} \right\} \frac{\partial S}{\partial x_D} dx dt \\ & \int_0^T \int_0^L \left\{ u(P + \rho e_i) \frac{\partial \lambda_3}{\partial x} + P - \lambda_2 \frac{dP}{dx} \right\} \frac{\partial S}{\partial x_D} dx dt \end{aligned} \quad (6.30b)$$

Eqs. (6.21) - (6.29) are solved for an already known flow solution from the flow analysis and given boundary and terminal conditions, i.e., Eqs. (6.24) - (6.29). From Eq. (6.30), note that the computation of the functional sensitivity requires the prior solutions of the state and adjoint (costate) equations.

6.4 Approach 2: Perturbed State Equations and Performance Indices in Conservative Variables

Unlike the first approach, this approach deals directly with the variation of the conservative fluxes with respect to the conservative field variables. To realize this objective, let us recast Eqs. (6.1), (6.2), and (6.3) in a form amenable to

conservative formulation. If one follows this procedure, the time dependent quasi one-dimensional Euler equations in conservative form are given as

$$\frac{\partial(S\bar{Q})}{\partial t} + \frac{\partial E}{\partial x} - H_s = \bar{0} \quad (6.31)$$

where

$$E = S[\rho u, p + \rho u^2, (p + \rho e_t)u]^T \quad (6.32)$$

$$H_s = H_s(S, \bar{Q}) = \left[0, p \frac{dS}{dx}, 0 \right]^T \quad (6.33)$$

are the flux and the source terms, respectively. For the derivation of the sensitivity, we consider only the steady-state condition, i.e., $\frac{\partial(S\bar{Q})}{\partial t} = 0$. Now, let us define a functional, J , as the integrated force along the given contour S as

$$J = \int_0^L (PS) dx \quad (6.34)$$

Also the residual R is given as

$$R = \frac{\partial E}{\partial x} - H_s \quad (6.35)$$

Then, with Eqs. (6.34) and (6.35), the functional is modified by

$$J_a = \int_0^L (PS) dx + \int_0^L \bar{\lambda}^T R dx \quad (6.36)$$

Consequently, the variation of the functional is expressed as

$$\delta J_a = \int_0^L \left\{ PS + \delta(PS) + \left[(\bar{\lambda}^T + \delta\bar{\lambda}^T)(E_x + \delta E_x - H_s - \delta H_s) \right] - PS - \bar{\lambda}^T [E_x - H_s] \right\} dx \quad (6.37)$$

where $E_x = \frac{\partial E}{\partial x}$. By neglecting the second-order terms and only keeping the linear parts of Eq. (6.37), one recovers the Euler equations in term of the variation of the Lagrange multipliers as

$$\delta\bar{\lambda}^T (E_x - H_s) = \bar{0} \quad \text{in } 0 \leq x \leq L \quad (6.38)$$

Then the variation of the objective functional becomes

$$\delta J_a = \int_0^L \left\{ \delta(PS) + \left[(\bar{\lambda}^T)(\delta E_x - \delta H_s) \right] \right\} dx \quad (6.39)$$

Let us define the following terms for later use:

$$\begin{aligned} A &= \frac{\partial E}{\partial Q} & B_h &= \frac{\partial H_s}{\partial Q} & C &= \frac{\partial P}{\partial Q}, \\ s_x &= \frac{dS}{dx} & M_h &= \frac{\partial H_s}{\partial s_x} \\ \delta S &= \frac{\partial S}{\partial x} \delta x_D & \delta \left(\frac{dS}{dx} \right) &= \frac{\partial}{\partial x_D} \left(\frac{dS}{dx} \right) \delta x_D \end{aligned} \quad (6.40)$$

The insertion of Eq. (6.40) into Eq. (6.39) and further simplification of the resulting equation leads to

$$\delta J_a = \int_0^L \left\{ S \frac{\partial P}{\partial Q} \delta \bar{Q} + P \delta S + \bar{\lambda}^T \left[(A \delta \bar{Q})_x - \frac{\partial H_s}{\partial Q} \delta \bar{Q} - \frac{\partial H_s}{\partial (s_x)} \delta (s_x) \right] \right\} dx \quad (6.41)$$

Integration by parts of Eq. (6.38) gives

$$\delta J_a = \int_0^L \left[-\bar{\lambda}_x^T A - \lambda^T \frac{\partial H_s}{\partial Q} \right] \delta \bar{Q} dx + \left[\bar{\lambda}^T A \delta \bar{Q} \right]_0^L + \int_0^L \left\{ S \frac{\partial P}{\partial Q} \delta \bar{Q} + P \delta S - \bar{\lambda}^T \frac{\partial H_s}{\partial (s_x)} \delta (s_x) \right\} dx \quad (6.42)$$

where A , B_h , C , and M_h are matrices given in Appendix C. If one uses Eqs. (6.40) and considers only the first variation of the functional in Eq. (6.42) to be zero, then one gets the adjoint (costate), boundary conditions and the functional sensitivity equations, respectively, as

$$-A^T \bar{\lambda}_x - B_h^T \bar{\lambda} + SC^T = \bar{0} \quad (6.43)$$

$$\left[A^T \bar{\lambda} \right]_0^L = \bar{0} \quad (6.44)$$

$$\delta J_a = \int_0^L \left[P \delta S - \bar{\lambda}^T M_h \delta s_x \right] dx \quad (6.45)$$

The insertion of the various partial derivatives of S from Eq. (6.6) into Eq. (6.45) gives

$$\frac{dJ_a}{dx_D} = \int_0^L \left[P \frac{\partial S}{\partial x_D} - \bar{\lambda}^T M_h \frac{\partial s_x}{\partial x_D} \right] dx \quad (6.46)$$

6.5 Solution Algorithm and Surface Modification

The state and costate equations are discretized using two vector-splitting methods: Beam-Warming flux-vector-splitting method for the first approach and the Van Leer vector-splitting method for the second approach. In both approaches we have used the speed of sound to serve as a sensor to switch between different flow regimes at every grid point.

After adding an appropriate time term $\bar{\lambda}_t$ into Eq. (6.43), the numerical integrations of the adjoint equations, i.e Eqs. (6.21) - (6.29) and (6.43) - (6.45), are accomplished from the maximum value of L to 0 and from the maximum time value T to 0. To bring this in line with the flow equations, the following spatial and temporal transformations are carried:

$$\zeta = L - x \qquad \tau = T - t \qquad (6.47)$$

Then, the discretized forms of the adjoint equations are first transformed by the above relationships, i.e. Eq. (6.47), and then integrated in time until the convergence criteria are met.

Based upon the steepest descent method, the optimal cross-sectional area can be obtained by the recursive relation, which is given as

$$S^{m+1} = S^m - \varepsilon \frac{dJ_a}{dx_D}$$

$$\text{where } \frac{dJ_a}{dx_D} = \{ \text{Eqn. (6.30b) or (6.46)} \} \qquad (6.48)$$

and ε is the step size.

6.6 Numerical Results and Discussion

As the benchmark of the present variational approach, the thrust was maximized for three different flow regimes. The first regime is a purely supersonic flow with the inflow conditions at $M = 1.5$. The inflow conditions for the second flow regime are identical to those of the first case, but the outflow plane is prescribed as a subsonic flow, approximately $M = 0.43$, to form a shock in the duct. The third flow regime is designed to be a purely subsonic flow with inflow conditions at $M = 0.3$. It is observed that the stability limit for both the flow and costate analyses depends on the type of inflow and outflow conditions. Secondly, even though the flow and the adjoint equations were both hyperbolic partial differential equations, their stability criteria were completely different (refer to Chap. 5).

The convergence history for the flow and costate equations are also different. In the three cases presented, the rate of convergence depends on the type of inflow and outflow conditions imposed at the inlet and exit. Although the time integration of the costate equations is dependent on the fluid flow, its quick convergence is assured once the flow solution has converged to steady state.

The thrust evolution for the three cases considered are presented in Figs. (6.1) - (6.3). Despite the presence of a strong shock at the middle of the flow field, the evolution of the area (Fig. 6.4) and the distributions of the Mach number (Fig. 6.5) and pressure (Fig. 6.6) are all smooth. Also in Figs. (6.7), (6.8), and (6.9) are presented the area, Mach number, and pressure histories, respectively, for the subsonic flow condition. The thrust first increases and then seems to decrease and settle down as the optimization progresses. The initial increase and then decrease of the thrust for the subsonic case may be attributed to the fact that the physics of flow was not accurately modeled for the type of nozzle configuration considered. A much better thrust augmentation is achieved for the

supersonic flow condition (Fig. 6.1) as compared with the other flow conditions. This may be attributed to the noticeable shape change at the upstream location in comparison with the downstream location (Fig. 6.10). One also observes that the downstream Mach number (Fig. 6.11) increases and the static pressure decreases (Fig. 6.12), which results in the increase of the thrust (Fig. 6.1).

To build further confidence in the present variational shape optimization approach, the mass conservation at every cross section of the initial and optimized flows were compared (Fig. 6.13). Except for the shock region, the mass flow rates were found to be constant. The optimized shape produced a sharper and narrower mass jump at the shock area as compared with the initial shape. This may suggest that the shock strength attenuation by the optimized shape is improved as compared with the initial shape.

During the numerical experimentation of the costate equations, the boundary conditions of the first approach were easier to numerically implement, but the boundary conditions of the second approach are superior, especially when there is a flow discontinuity (shock) in the flow field. Apart from this apparent difference, both approaches give identical results for the optimal solution.

6.7 Conclusions

A proof-of-concept study for a new design optimization method based on the variational methods has been conducted. The method has been demonstrated for the quasi one-dimensional Euler equations. The general design optimization incorporates the optimization, CFD analysis, and the adjoint equations analysis. The optimization is based on the steepest descent method, and it is intrinsically coupled with the flow and adjoint solutions.

The thrust maximization for purely supersonic, purely subsonic, and mixed supersonic-subsonic cases presented demonstrate that the optimized shapes

and flow variables are efficiently predicted even with the presence of a strong shock in the flow field. They also suggest that the whole optimization needs relatively small incremental computer time and memory in addition to the CFD analysis and therefore, suggest that the present **variation methods** is an efficient alternative to perform fluid dynamic design optimization for all types of flow regimes.

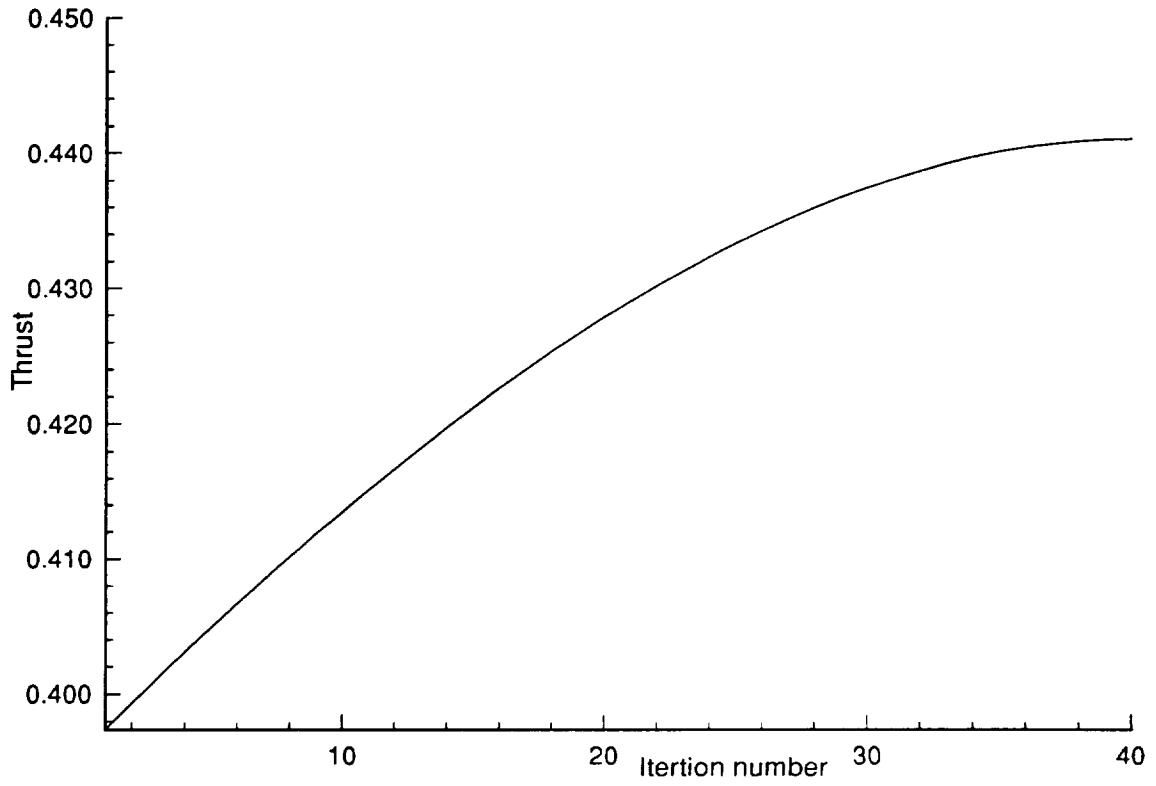


Fig. 6.1 Thrust evolution for supersonic flow.

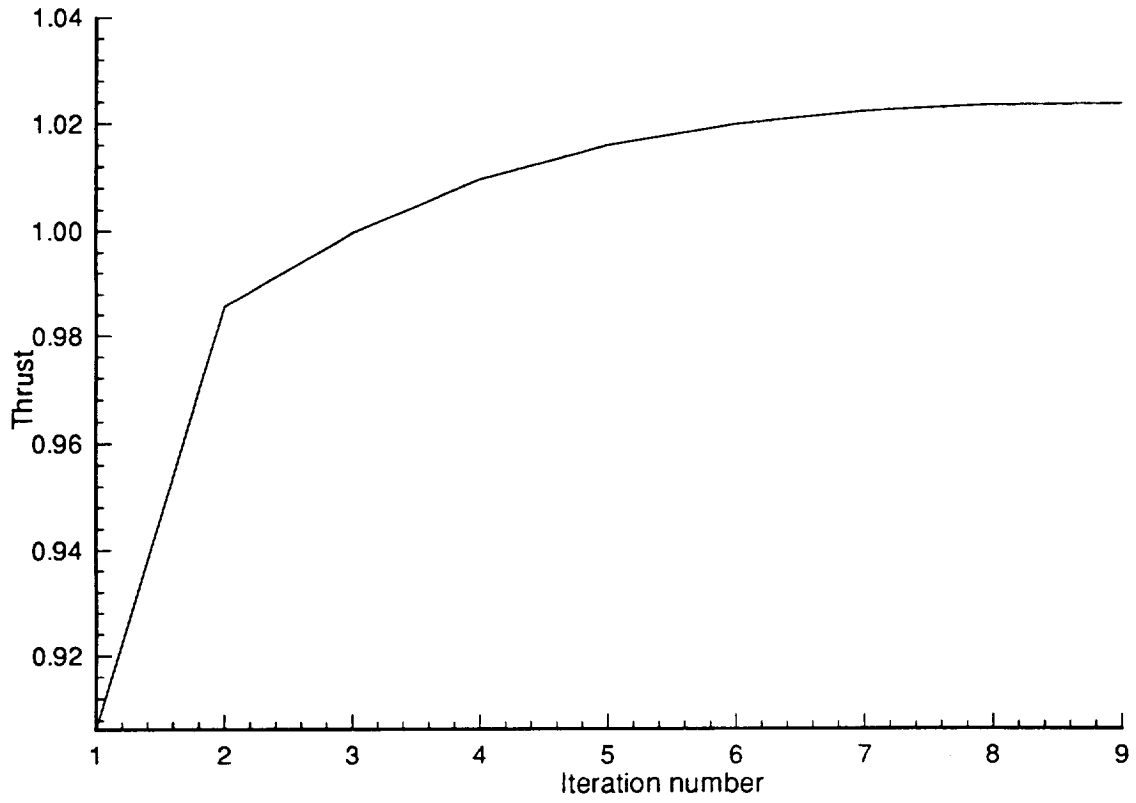


Fig. 6.2 Thrust evolution for shock flow.

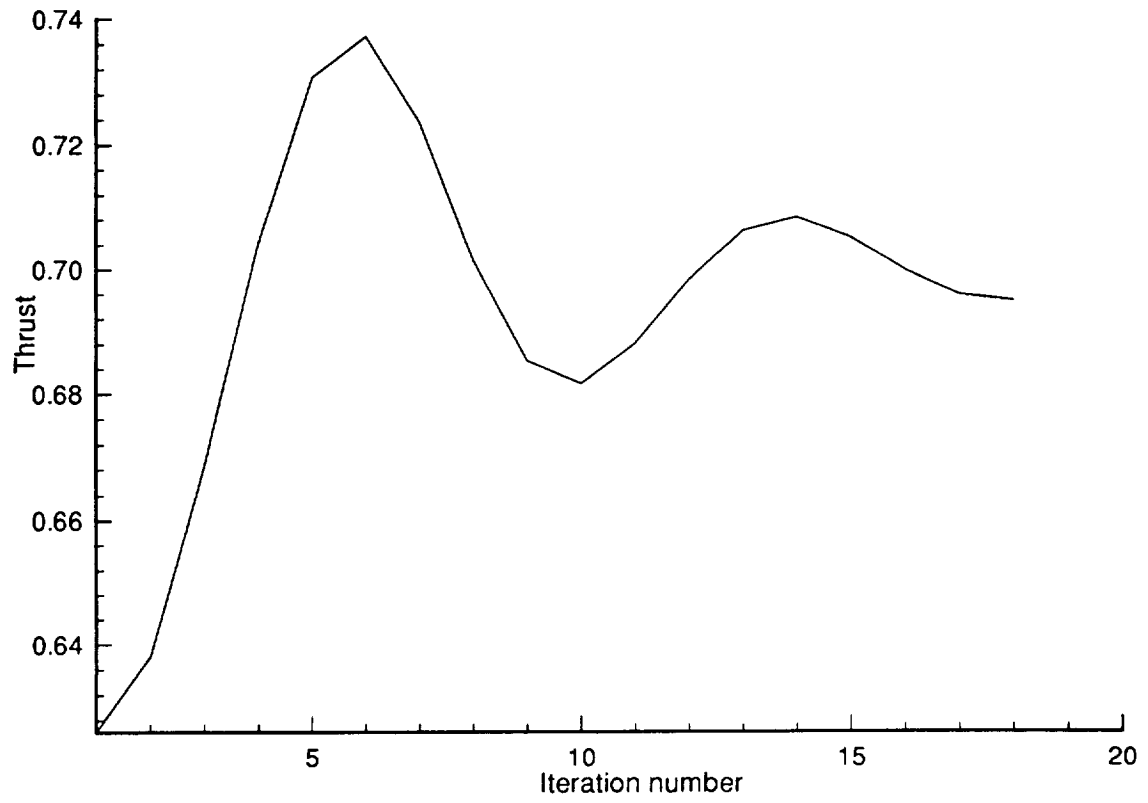


Fig. 6.3 Thrust evolution for subsonic flow.

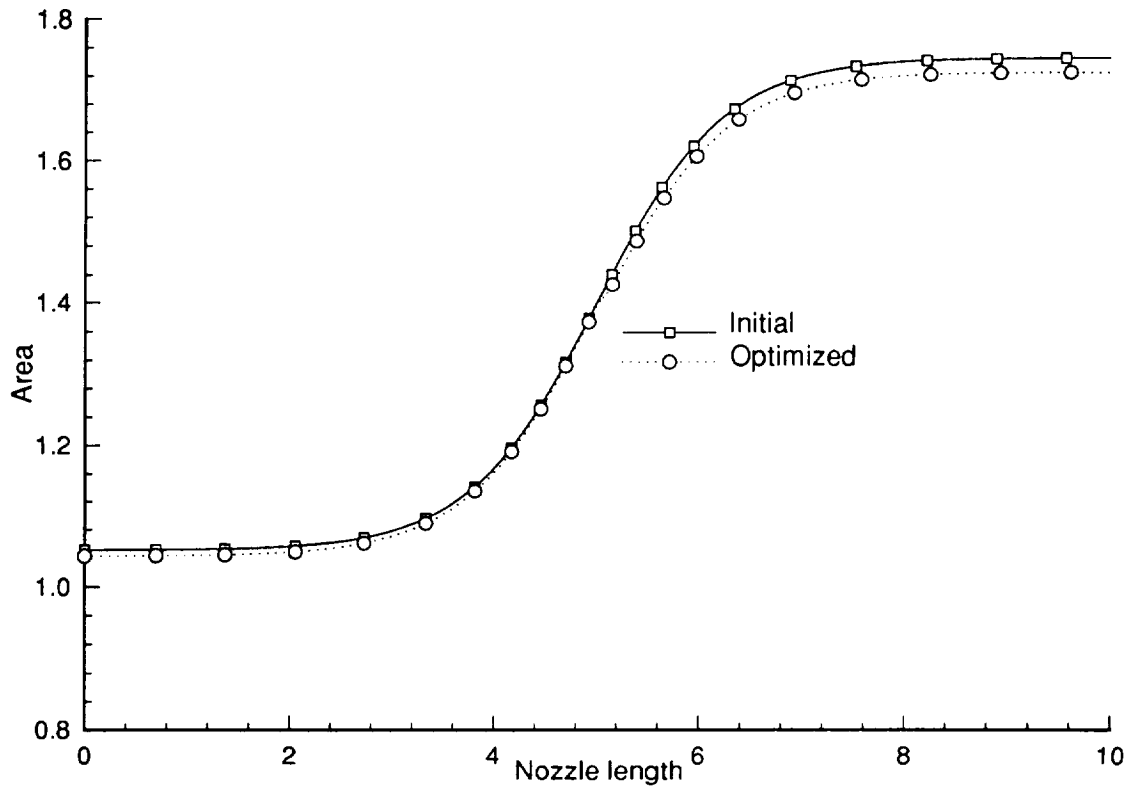


Fig. 6.4 Area evolution for the shock flow.

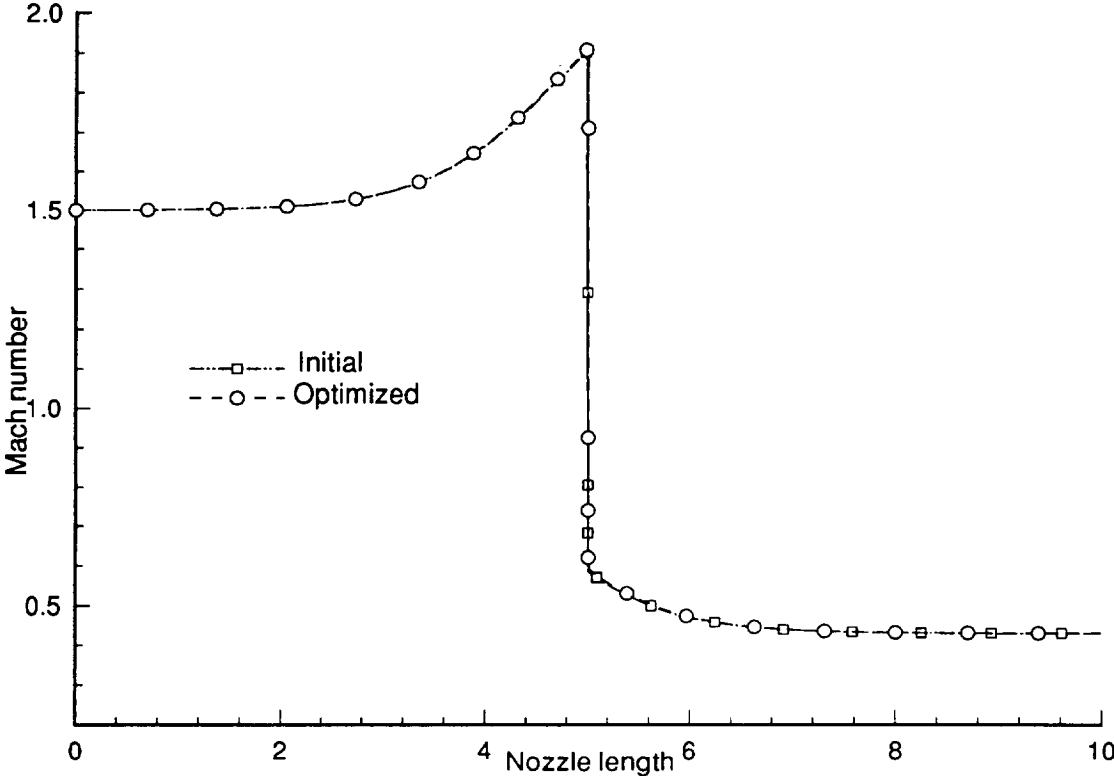


Fig. 6.5 Initial and optimized Mach number distributions for the shock flow.

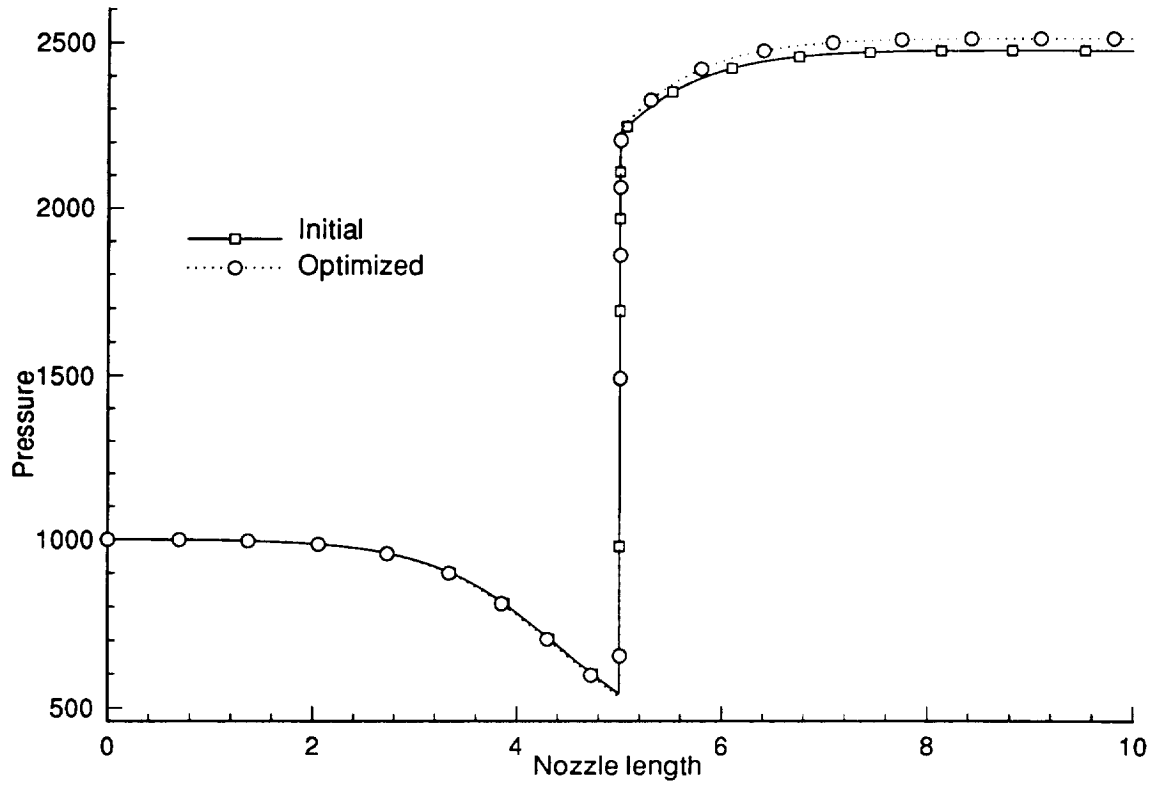


Fig. 6.6 Initial and optimized pressure distributions for the shock flow.

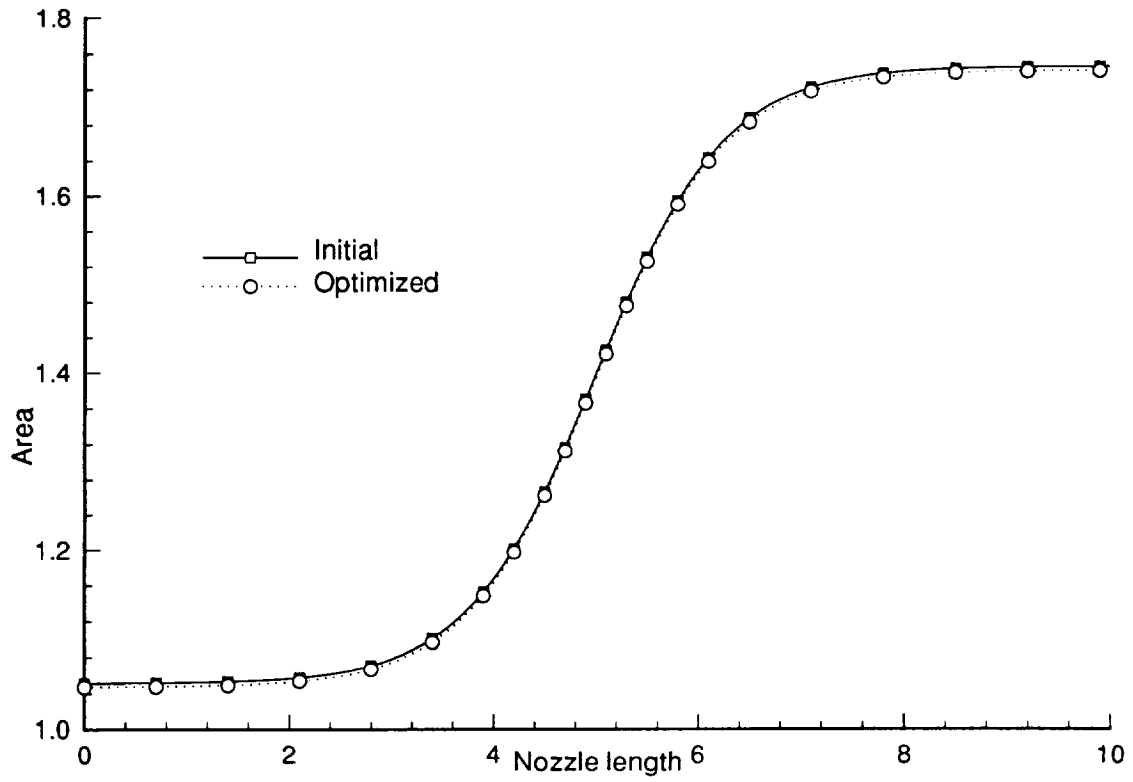


Fig. 6.7 Area evolution for subsonic flow.

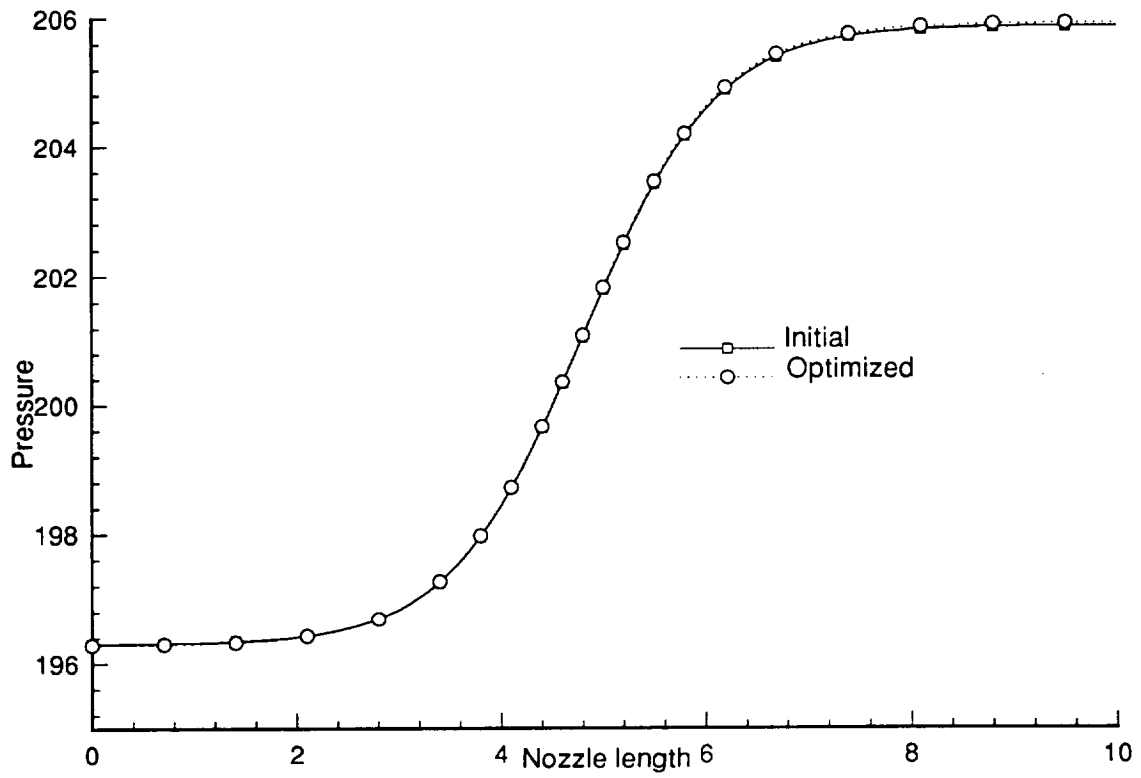


Fig. 6.8 Initial and optimized pressure distributions for subsonic flow.

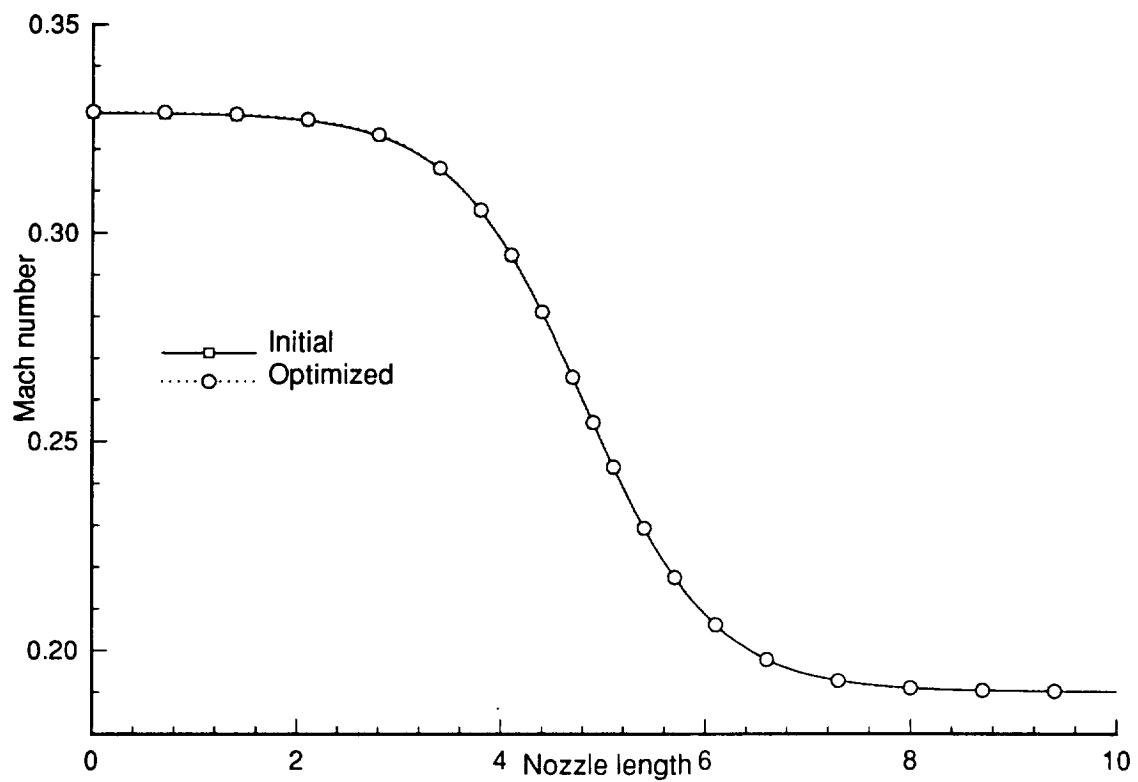


Fig. 6.9 Initial and optimized Mach number distributions for subsonic flow.

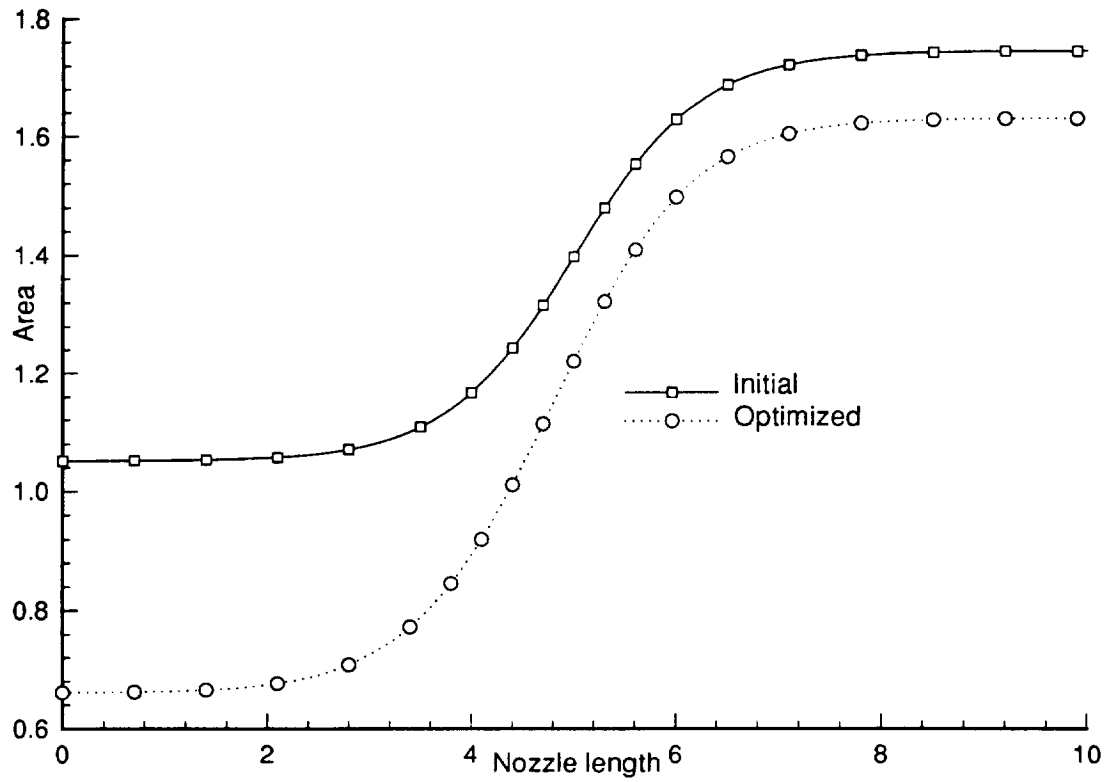


Fig. 6.10 Shape evolution for supersonic flow.

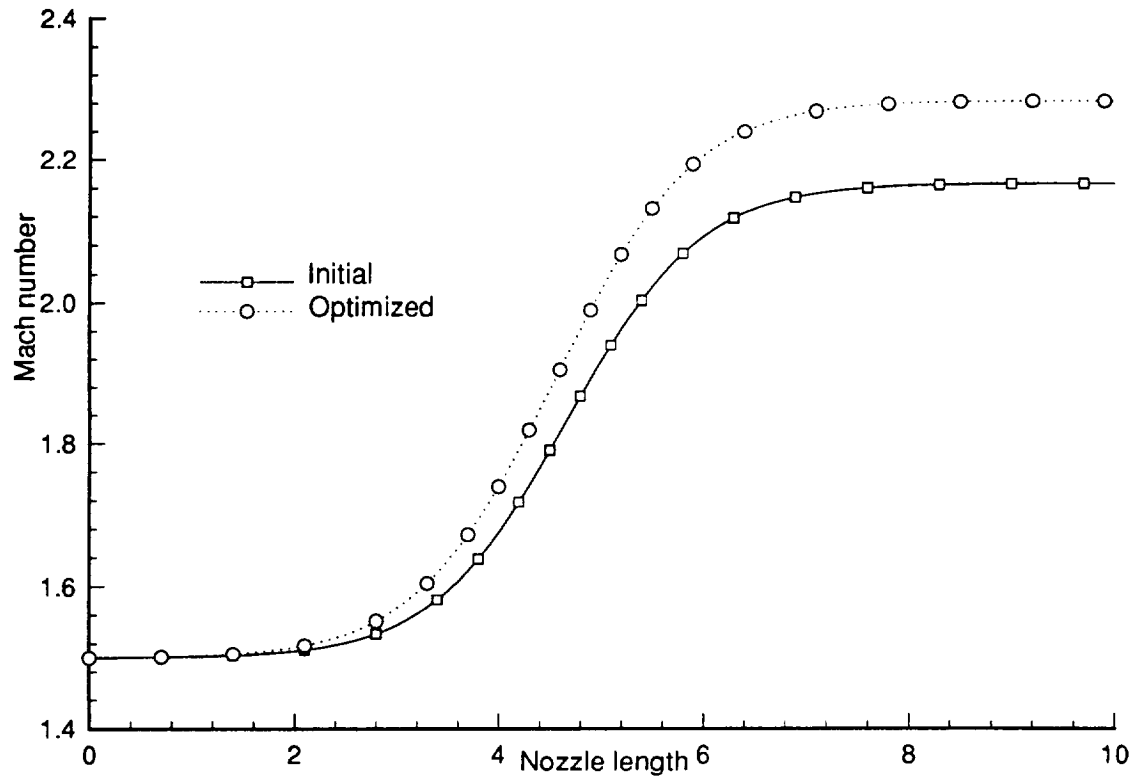


Fig. 6.11 Initial and optimized Mach number distributions for supersonic flow.

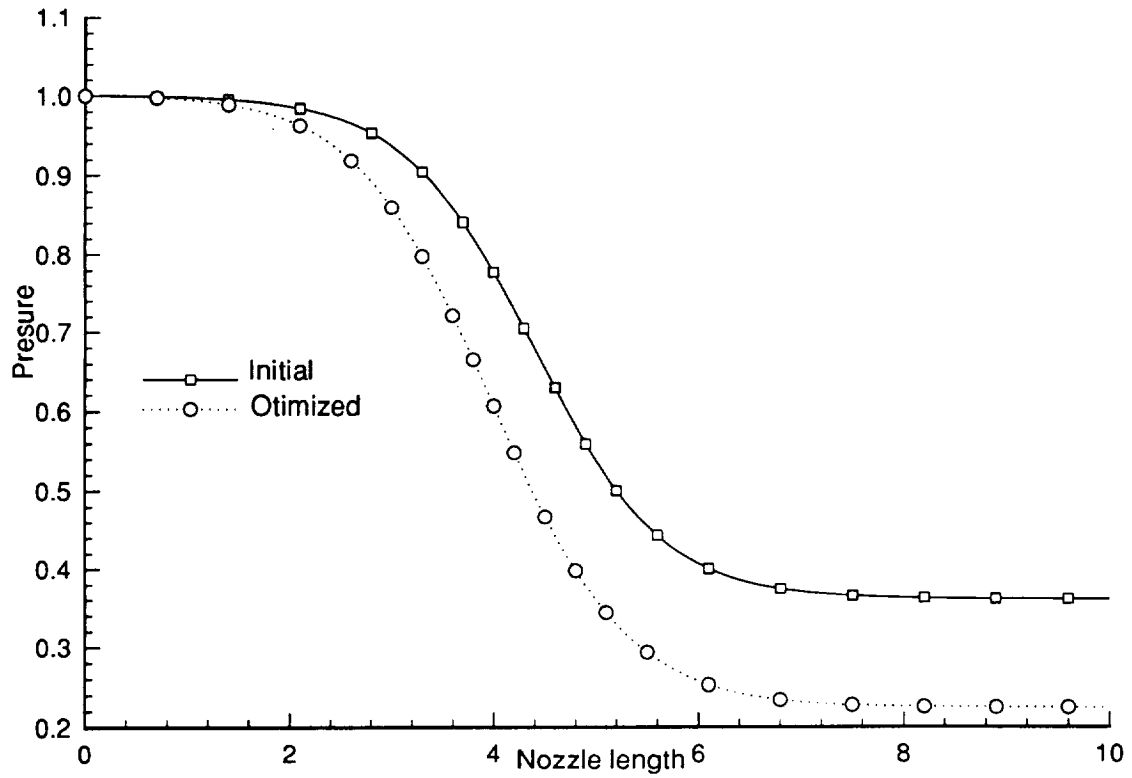


Fig. 6.12 Initial and optimized pressure distributions for supersonic flow.

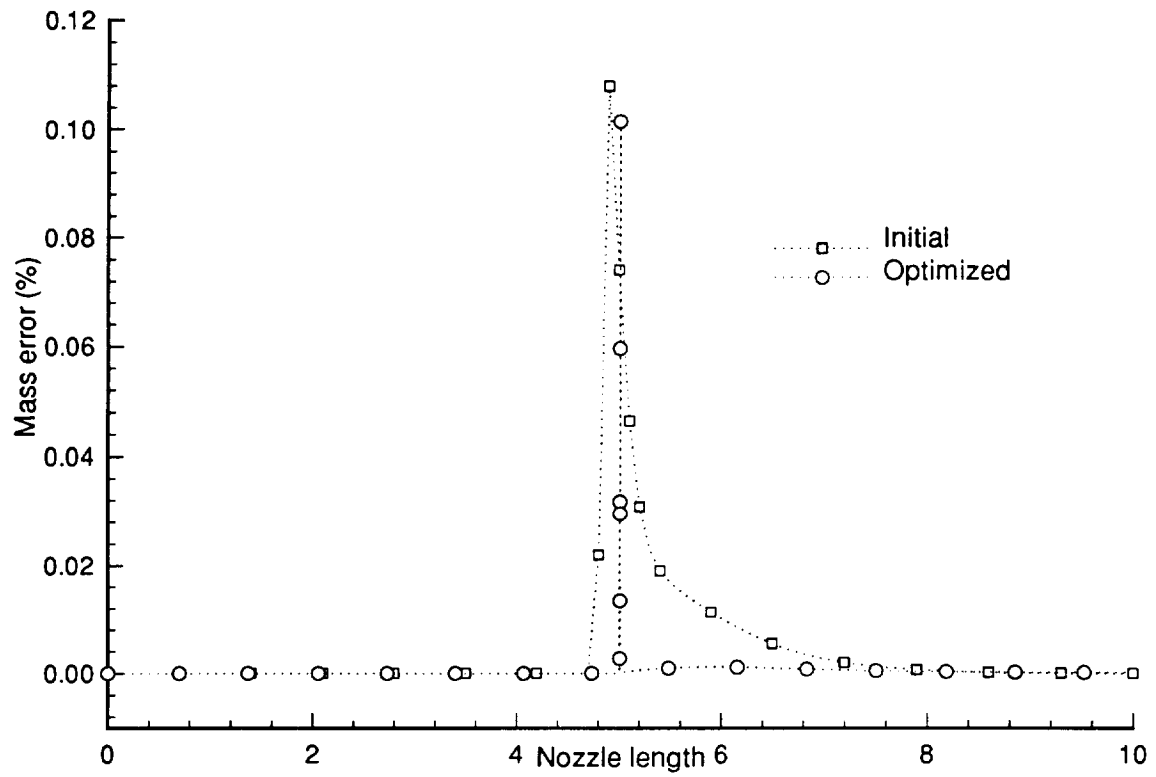


Fig. 6.13 Mass error for the shock flow.

Chapter 7

RESULTS AND DISCUSSION ON DESIGN OPTIMIZATION OF INTERNAL FLOWS USING TWO-DIMENSIONAL EULER EQUATIONS

The main thrust of this chapter is to briefly discuss the the numerical results of the variational sensitivity analysis that are obtained by the use of two-dimensional Euler flow equations. Additionally, the efficiency and accuracy of the variational sensitivity in comparison to the finite difference are analyzed.

7.1 Two-Dimensional Nozzle Optimization Problem Formulation

At least a couple of reasons can be given for choosing the two-dimensional nozzle geometry in order to demonstrate our point of optimization methodology. The first one is that one can easily obtain various types of nozzle geometries by simply using already known analytical expressions for different flow conditions. The second important reason is also the need to develop a scramjet nozzle afterbody for the High-Speed Civil Transport. The third one is the need to develop efficient wind tunnels with optimal shapes for various experimental wind tunnel applications. The optimization problem demonstrated here seeks the optimal shape for the maximum thrust in conjunction with the nonreverse flow condition at the exit. Hence, the example problem is formulated as the maximization of the functional defined by

$$J_{\bar{\Gamma}} = \int_{\bar{\Gamma}} P d\bar{\Gamma} \quad (7.1)$$

with the constraint that the static pressure P at the exit assumes a certain percentage of the ambient pressure p_∞ for maximum expansion at that exit lip of the solid boundary. Therefore, the constraint is mathematically posed as

$$G_j(\bar{Q}, \bar{n}) = \int_{\bar{\Gamma}} \left[\left(1 - \frac{P}{p_\infty}\right) + \left|1 - \frac{P}{p_\infty}\right| \right] d\bar{\Gamma} \leq 0 \quad (7.2)$$

7.2 Two-Dimensional Nozzle Flow

The initial geometry for this internal flow configuration is given in Fig. 7.1. It is a supersonic nozzle where only half of the physical domain is considered with 137 x 69 grid points. It is a convex type of geometry with the smallest area at the inlet and a diverging afterbody for supersonic expansion. The only aerodynamic inequality constraint considered is the criteria on the static pressure at the exit lip of the nozzle to reach a certain percentage of the ambient pressure as a necessary condition to avoid any reverse flow from underexpansion as the shape evolves during the optimization cycle.

To assess the variational methods for sensitivity analysis, computational efficiency and accuracy calculated by variational methods and finite difference are compared. One of the obvious limitations with the finite difference is the uncertainty to *a priori* determine the step size that will give reliable sensitivity derivatives. The magnitude of the stepsize is dependent on how accurate one needs the derivatives to be. If, for instance, one only needs a 10% deviation from the assumed exact derivative, then the step size must be under a 10% range of the derivative. In our case of computing the sensitivity derivatives using the finite difference, we have assigned the step size to be 0.0001.

The x component of the design variables (Bezier control points) are *a priori* computed as being spatially invariable, and the variation of the design variables

is allowed only in the y direction. This apparent limitation of the design variables must not be a hindrance since addition or deletion of any desired design variables in the design domain will produce the same result. To verify this claim, two sets of design variables, in addition to the assumed optimal number of design variables (in this case the optimum is eight design variables), were investigated. The first set was performed by increasing the number of design variables by four and the second one by decreasing it by four from the optimal number of design variables. Here, the optimal number defined as that number of design variables which reproduces the closest shape to that of the initial geometry.

As presented in Table 7.1, the CPU time and memory requirements of complete cycle of optimization for the two additional sets of design variables are almost identical for the two-dimensional optimization case. Therefore, the eight design variables are considered as the optimal number of design variables which produced the desired computational efficiency for our test case. On the other hand, this slight memory increase as the number of design variables increases could be a warning to the eventual computational memory increase as the dimensionality, number of constraints, and design variables increase. The second aspect of the role played by the number of design variables may be the influence on the optimal shape (Fig. 7.2). All three categories of the design variables produced slightly different optimum shapes from each other. Comparing all three shapes (Fig. 7.2), the shape produced by twelve design variables appears to follow the shape produced by the four design variables in the compression area (upstream) and the shape of the eight design variables in the expansion area (downstream). The shape generated by the optimal number of eight design variables shows a slight change of shape upstream, from approximately $x=0.1$ to $x=0.375$, and downstream, from approximately $x = 0.7$ to $x = 1.0$ as compared with the shapes generated by the other sets of design

variables. The shape change in the compression area seems to be more desirable because it produces high-pressure ratios and thereby gives more thrust as one integrates the change of pressure along the changing nozzle shape. The shape change in the expansion region, on the other hand, reduces the ratio of the static pressure to the ambient pressure, which results in less thrust augmentation. This physical phenomena is further reflected in Fig. 7.3 where the optimal thrust of the eighth design variable shape is higher than the other two design variable shapes.

From the parametric studies (four, eight, and twelve design variables) conducted, one may conclude that the eight design variables are the *optimal* number of design variables to sufficiently represent the nozzle shape and at the same time to give a better thrust and computational efficiency.

The evolution of the design variables for the variational methods and the finite difference approach are given in Figs. 7.4 and 7.5, respectively. Except for the second and the seventh design variables, the general trend of the evolution of the design variables in both approaches is similar. In the variational case, the second design variable approaches the first design variable and the seventh one tends to come close to the eighth design variable. In the finite difference case, however, the second and the seventh design variables tend to pull away from the first and eighth design variables, respectively. As shown in Fig. 7.6, due to the movement of the second and the seventh design variables in the opposite direction, the optimal shapes of the variational methods and finite difference are slightly different. As explained in the parametric studies, the decrease of the optimal (as compared with the initial) shape or optimal design variables in the compression region is much more advantageous to the decrease of the optimal shape or optimal design variables in the expansion region for the supersonic flow regime. This is due to the effect that the decrease of the shape in the upstream

results in the substantial gain of high pressure ratio (compare Figs. 7.7 and 7.8) which favors the augmentation of more thrust (Fig. 7.9) in the design process. Figure 7.9 also clearly indicates that the pressure distribution in the expansion region in general and at the lip of the nozzle in particular is within the constraint specification as imposed in the aerodynamical constraint given by Eq. (7.2).

As given in Table 7.2, the accuracy of the variational methods is verified by comparing the variational functional sensitivity derivatives to the functional derivatives of finite difference. If one takes into consideration that the sensitivity coefficients of the finite difference are dependent on the step sizes, then the gradient values obtained by the variational methods are well within the engineering prediction range, except for the second and the seventh sensitivity coefficients. The discrepancy of those two sensitivity values may be associated with the difficulty to properly implement the boundary conditions of the adjoint equations. Despite the differences on these two sensitivity derivatives which correspond to the second and seventh design variables, the optimal shape and thrust of the variational methods are comparable with those of the finite difference as presented in Table 7.3 and Fig. 7.6. It is known that the finite difference uses function evaluations to compute the gradient information while the variational methods solve another set of partial differential equations and sensitivity derivative equations. Due to this, there is a memory increment of approximately 1.3 mega words as shown in Table 7.4. This slight increment in memory is negligible as compared with the other gradient-based sensitivity analysis approaches, such as the discrete sensitivity analysis which requires higher memory allocation for the given optimization problem.

Table 7.1. CPU Time and Memory for Four, Eight, and Twelve Design Variables
With Variational Methods

Design variables	CPU time (sec)	Memory (MGW)
4	868.0463	5.249459
8	864.2226	5.249939
12	866.2128	5.250579

Table 7.2. Sensitivity Derivatives by Variational Methods and Finite
Difference

X_D	Variational methods	Finite difference	Deviation (%)
1	9.1483E-2	9.4441E-2	3.1
2	7.9228E-2	1.1062E-2	86.0
3	-6.6563E-2	-4.7906E-2	28.1
4	-5.5491E-2	-5.9409E-2	6.6
5	-4.6421E-2	-5.3278E-2	12.9
6	-3.8979E-2	-4.6287E-2	15.8
7	-3.2186E-2	-6.9988E-2	53.9

Table 7.3. Initial and Optimal Values of Functional and Constraint for Variational Methods and Finite Difference.

		Variational methods	Finite difference
Initial	Functional	0.045481	0.045481
	Constraint	- 2.10787	-2.10787
Optimum	Functional	0.049958	0.49885
	Constraint	-0.5858	-0.5668

Table 7.4. Efficiency Comparison Between Variational Methods and Finite Difference.

			Variational methods	Finite difference
CPU time (sec)	Complete optimization		865.098	4356.33
	Single analysis	Euler equations		128.23
		Co-state equations	58.59	
Memory (MGW)	Complete optimization		5.25 (with sensitivity eqs.)	3.98 (no sensitivity eqs.)

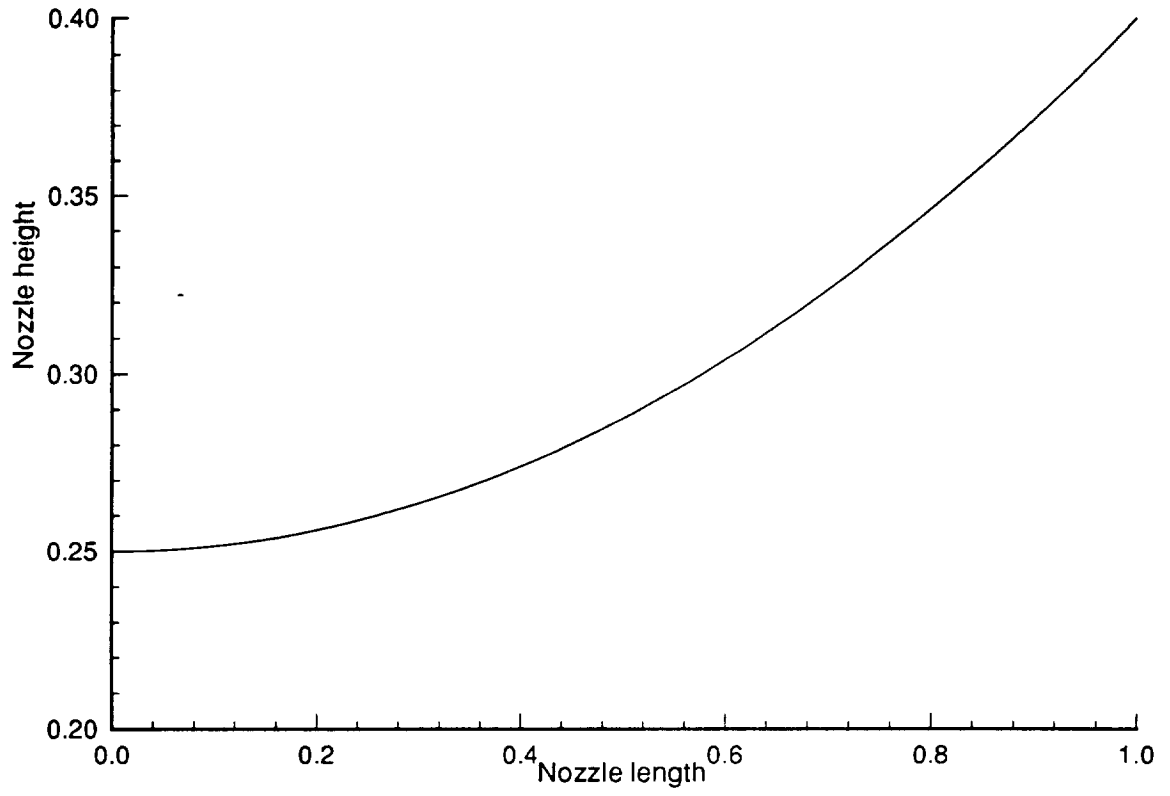


Fig. 7.1 Initial supersonic nozzle shape.

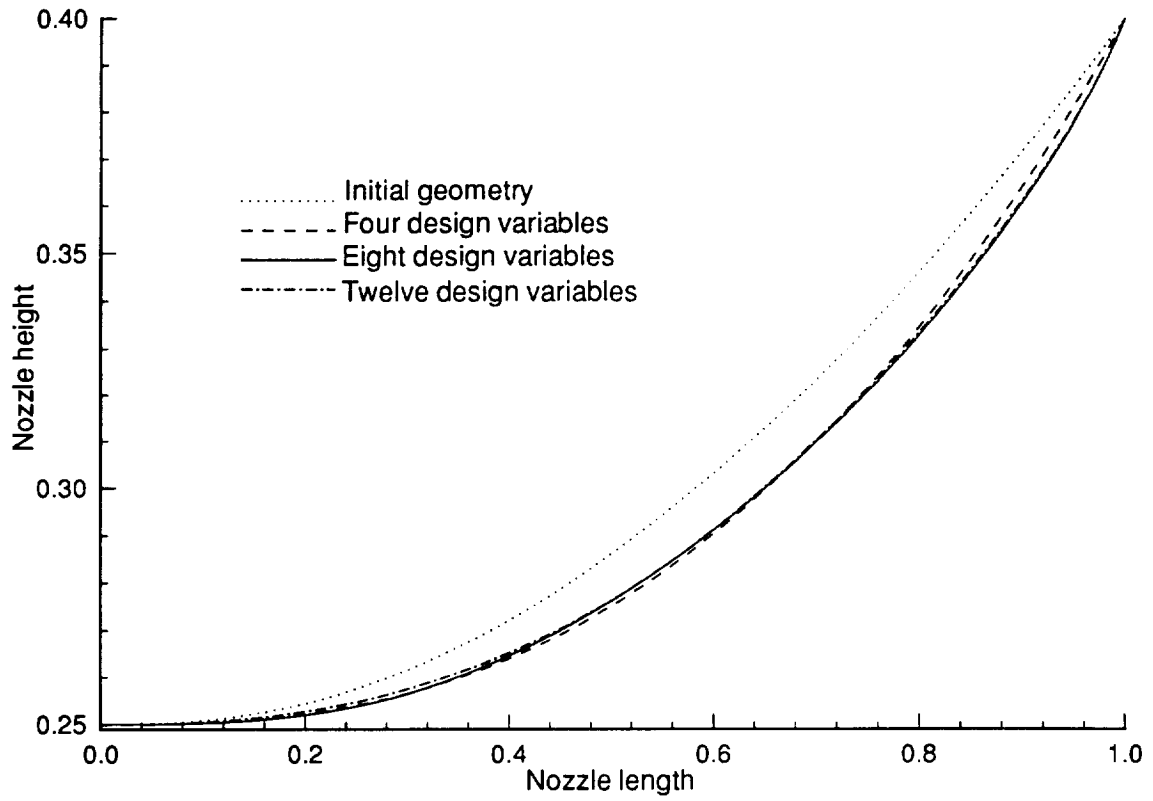


Fig. 7.2 Effect of the number of design variables on the optimal shape.

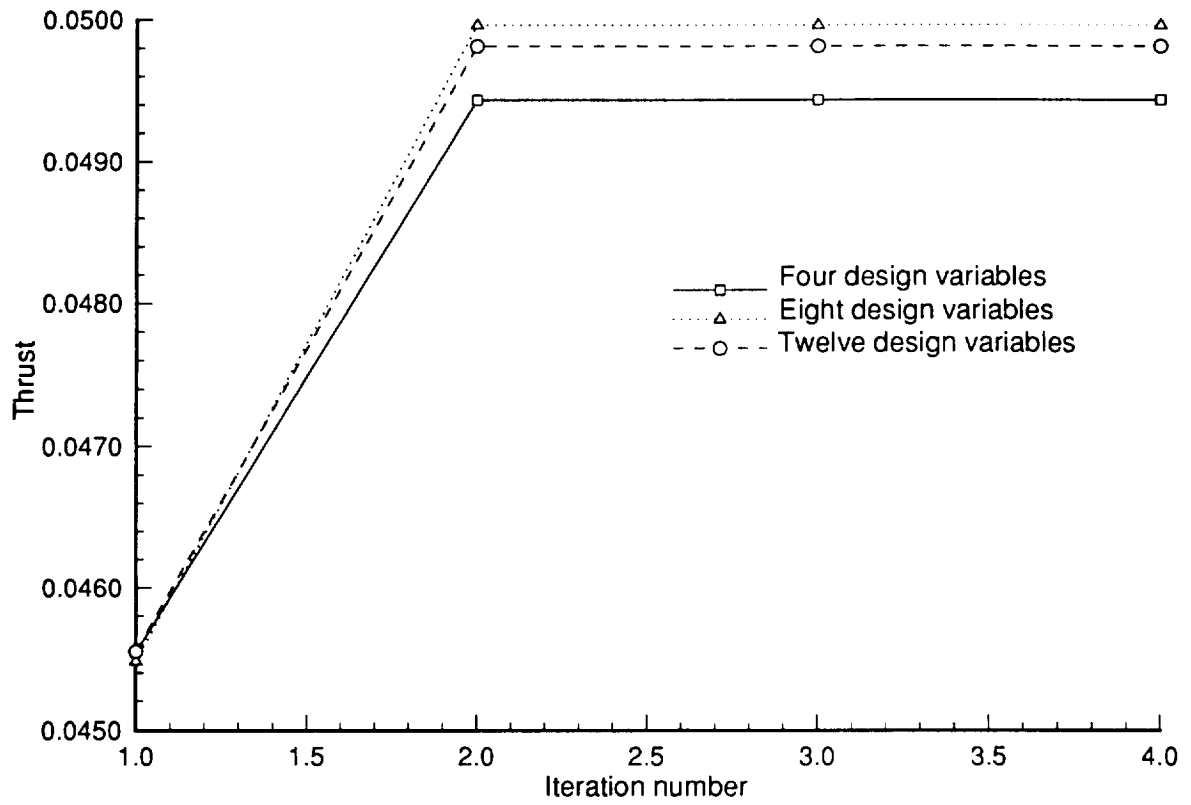


Fig. 7.3 Effect of the number of design variables on the optimal thrust.

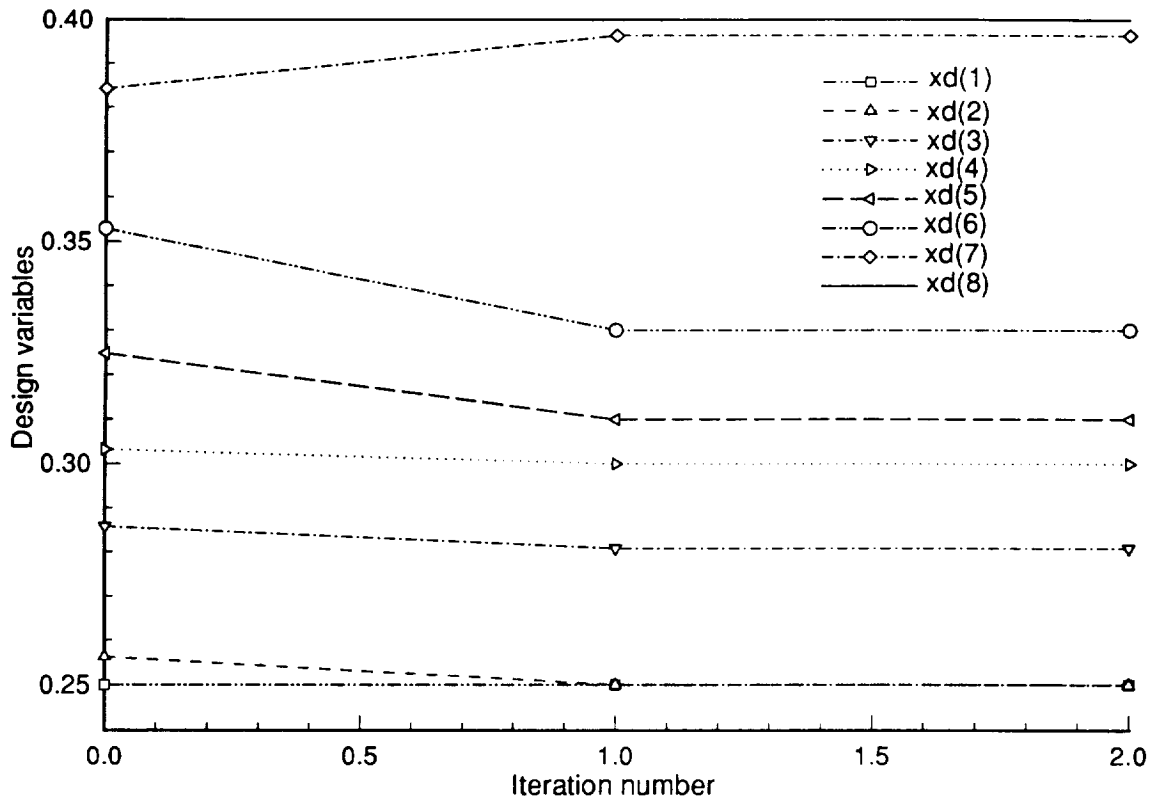


Fig. 7.4 History of the design variables for the variational methods.

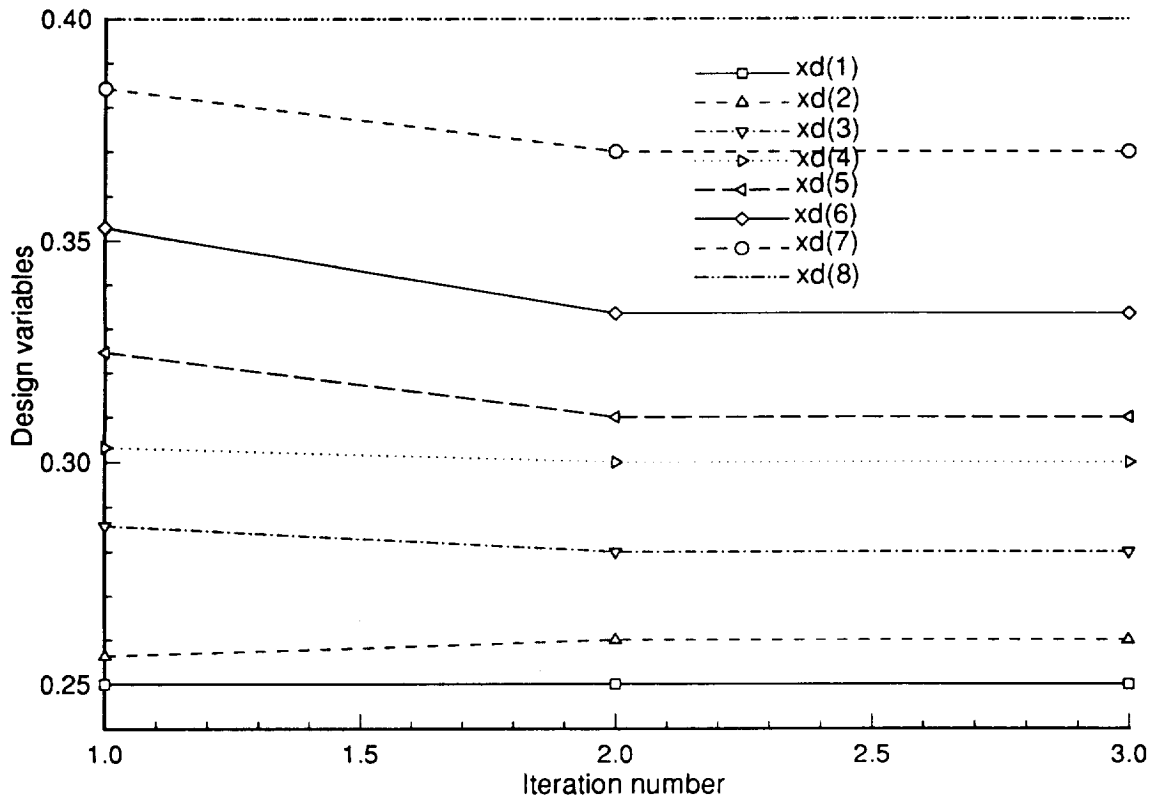


Fig. 7.5 History of the design variables for the finite difference.

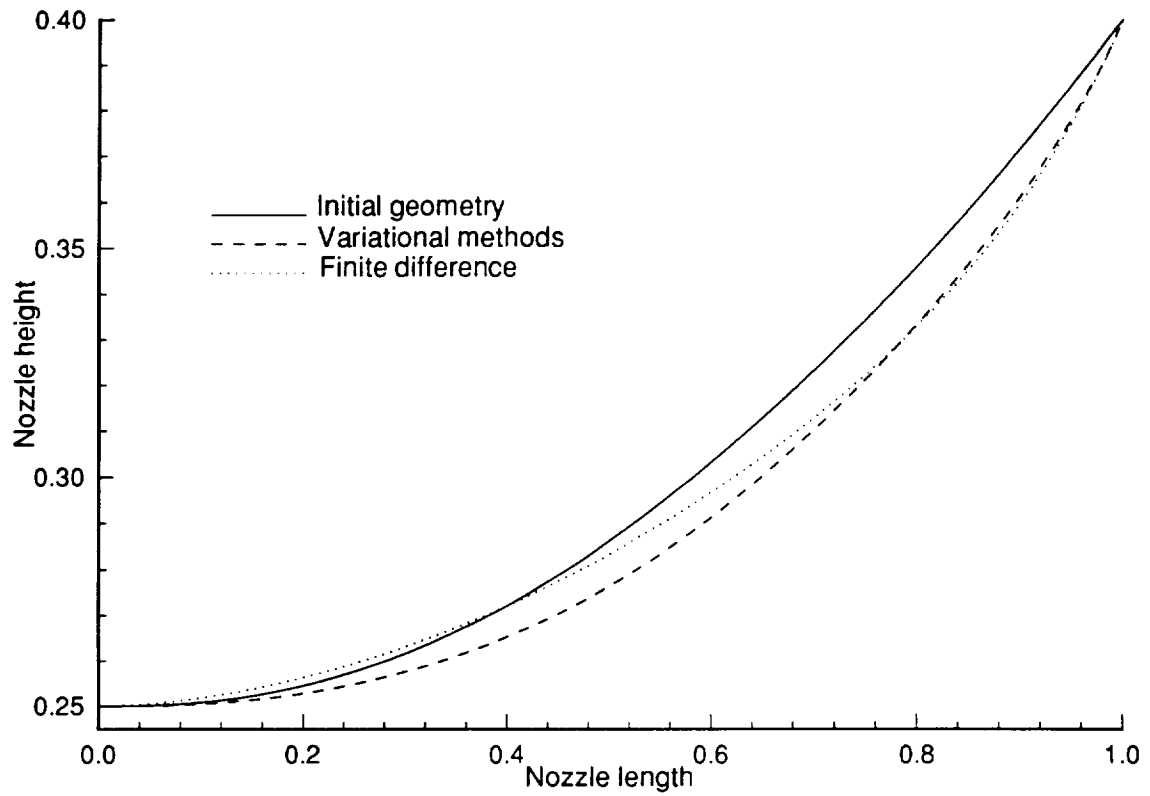


Fig.7.6 Optimal shapes by variational methods and finite difference.

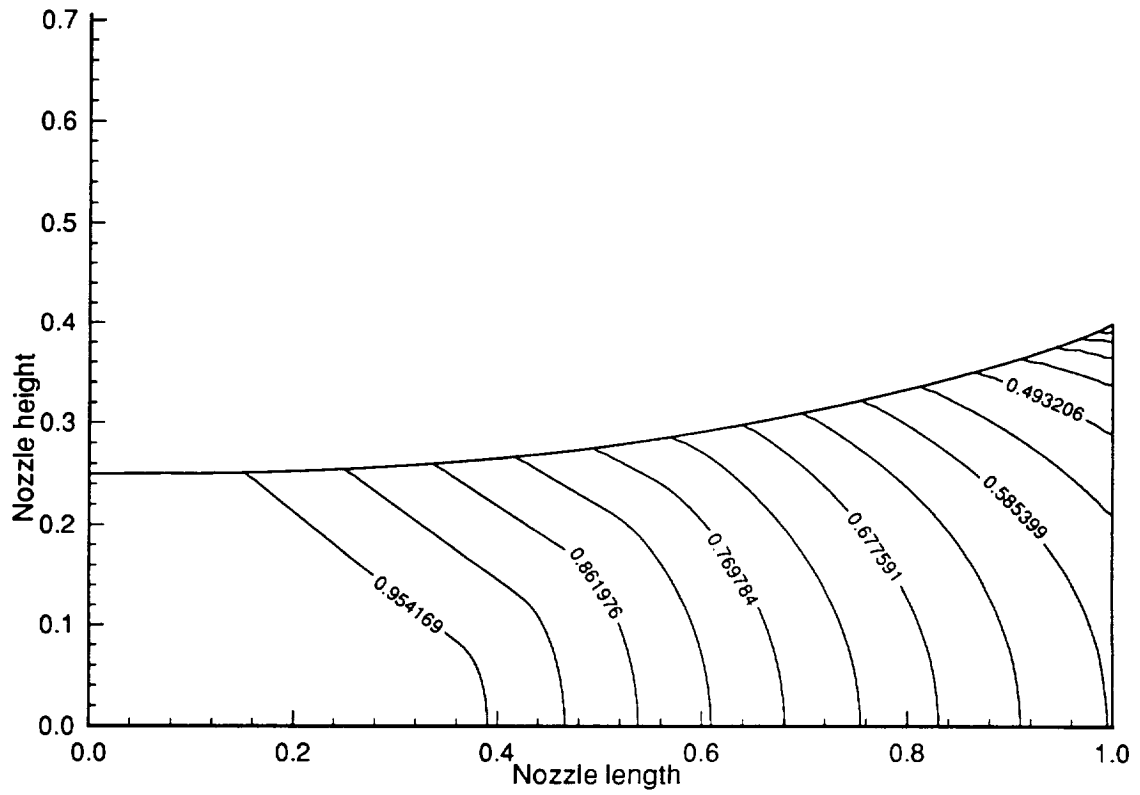


Fig. 7.7 Optimal pressure countour by variational methods.

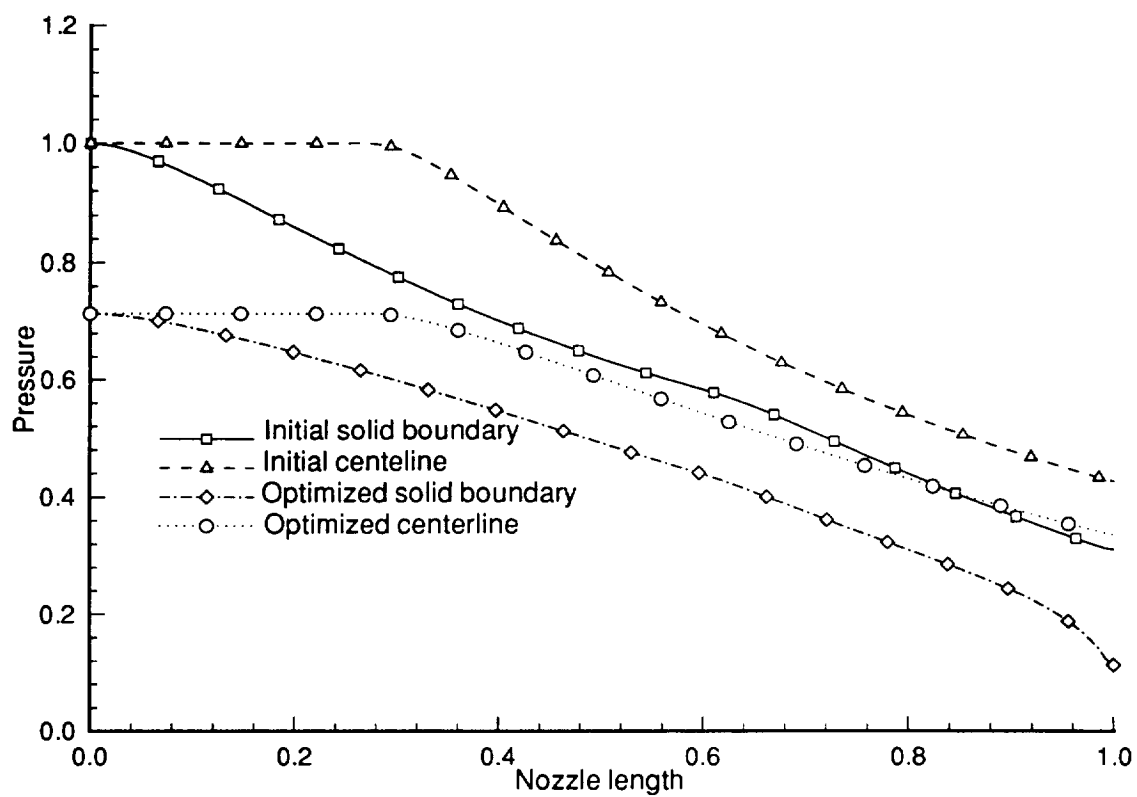


Fig. 7.8 Pressure distributions on the solid and symmetry line by variational methods.

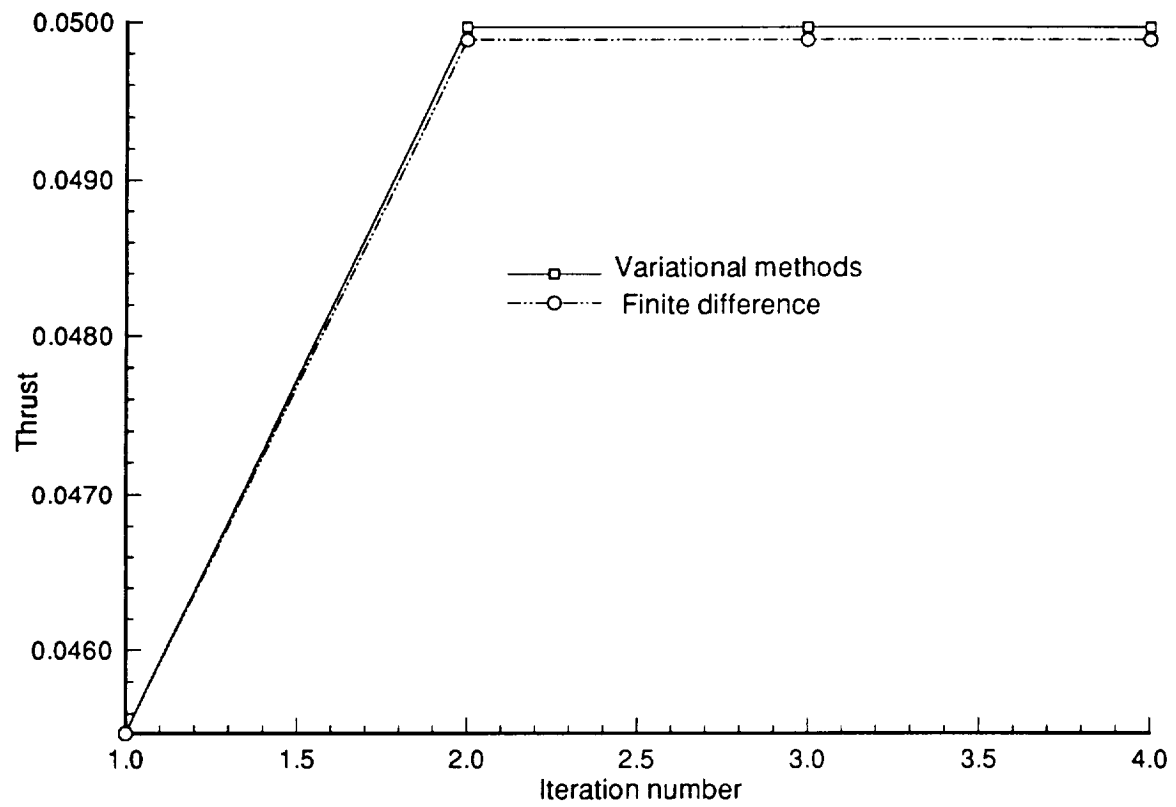


Fig. 7.9 Optimal thrust history by variational methods and finite difference.

Chapter 8

CONCLUSIONS AND RECOMMENDATIONS

A versatile design optimization approach must be independent of: (1) the level of approximations, methods of numerical integration, and discretization of the flow analysis, (2) the grid points and grid sensitivities, (3) the initial design points and solutions, and (4) the flow regimes. In the case considered, starting from the converged solution of the two-dimensional Euler flow equations, the sensitivity derivatives for the optimal solution are derived (See Chap. 3.) The distinctive feature of the variational approach is that the converged solution can be obtained from any level of approximations, methods of numerical integration, and variety of discretizations of the fluid flow. For instance, either the two-dimensional full potential or the two-dimensional Euler equations can be chosen for the level of the flow field approximation. One can also choose either the Beam-Warming, or Van Leer flux-splitting, or Roe flux-differencing, and any implicit or the explicit Runge-Kutta time-advancing method can be adopted. The only requirement in this approach is that the state solution has to completely converge so that the Jacobian matrices that are needed in the costate, transversality, and sensitivity derivative equations are accurately constructed. Even though the Jacobian matrices in the costate equations are transposed, they are the by-product of the converged solution from the state equations, and there is no extraneous effort involved in obtaining them.

The time integration of the costate equations, as described in Chap. 4, requires an understanding of the stability behavior of the costate equations.

Because of the negative entries of the transposed Jacobians, the Von Neumann stability analysis indicates that the costate equations are unstable for the CFL and wave number considered. To make the costate equations stable, the transformation of the costate's computational domain in line with the state's computational domain was undertaken. This unique approach produced a stable costate solution that is necessary in obtaining the sensitivity derivatives of the functional and constraints with respect to the Bezier control points.

Variational methods in sensitivity analysis and shape optimization for aerodynamic applications have been considered. The main components of the approach are the control theory and calculus of variations where the design control is the continuous domain boundary represented by the Bezier control points or design variables, Eqs. (3.5) - (3.7). Because the domain boundary is continuously evolving until it reaches its optimal shape, the contribution of the changing domain and domain boundary are used and incorporated in the derivation of the optimality conditions and sensitivity derivatives through the surface transformation matrix J_s (Appendix A) and curvatures (Eqs. (3.24 and 3.25)). The use of the steady-state solutions of the two-dimensional Euler equations results in the derivation of the costate or the adjoint equations, the boundary or transversality conditions, and the sensitivity derivatives for the generic design optimization problem where the functional and the constraint are defined on the domain boundary. The final numerical computation of the sensitivity derivatives is carried out for the converged state and costate equations.

Since the stable and converged solution of the costate equations is imperative for the successful computation of the sensitivity derivatives and design optimization, a complete stability analysis of the Euler and costate equations is

treated. Based on the findings of the stability criteria, the stable and converged numerical integration of the costate equations is guaranteed only if the domain of integration is transformed in line with the state equations or any other numerical technique which handles the reverse nature of costate equations is adopted.

A two-dimensional nozzle optimization problem was considered, and the application of variational methods to compute the optimal shape for the maximum thrust is presented. During the design process, the supersonic nozzle remained supersonic while improving the performance index or thrust (Table 7.2). Also, while the VM's computational accuracy (Table 7.3) is comparable with the finite difference, its computational efficiency and memory savings (Table 7.4) are found to be substantial. As memory and computational efficiency are the bottle-necks for large two-dimensional and three-dimensional problem in general, variational methods are one of the most viable candidates in solving design optimization problems.

Design optimization requires gradient information of both the functional and constraints. But as the number of constraints increases, the computational intensity and memory may be prohibitive to do any realistic optimization. This can be overcome by converting the constrained problem into an unconstrained problem through the introduction of penalty function methods. This is highly important especially for multidisciplinary optimization where the number of constraints and design variables is high. Therefore, procedures similar to the penalty function methods must be explored to efficiently use variational methods in obtaining sensitivity derivatives. To further build confidence in the proposed approach, two-dimensional internal and external flows with shocks must be investigated. Finally, the concept must be extended to two-dimensional viscous and three-dimensional Euler flows.

REFERENCES

1. Abbott, I. H., and Von Doenhoff, A. E., *Theory of Wing Sections, Including a Summary of Airfoil Data*, Dover Publications, Inc., New York, 1959.
2. Whitcomb, R. T., "Review of NASA Supercritical Airfoils," *9th Congress of the International Council of Aeronautical Sciences (ICAS)*, Haifa, Israel, ICAS Paper 74-10, August 1974.
3. Valarezo, W. O., Dominik, C. J., McGhee, R. J., Goodman, and W. L., Paschal, K. B., "Multi-Element Optimization for Maximum Lift at High Reynolds Numbers," *AIAA Applied Aerodynamics Conference, 9th, Baltimore, MD*, AIAA-91-3332-CP, September 1991.
4. Bateman, H., "Motion of a Compressible Inviscid Fluid," *Proceedings of the National Academy of Sciences of the United States of America*, Vol. 16, September 1930, pp. 816 - 825.
5. Rasmussen, H., and Heys, N., "Application of a Variational Method in Plane Compressible Flow Calculation," *Journal of Mathematics Applications*, Vol. 13, February 1974, pp. 47 - 61.
6. Miele, A., "Variational Approach to Problems of Hypervelocity Flight," Purdue University, Final Report, Report No. A-59-7, June 1959.
7. Miele, A., "The Calculus of Variations in Applied Aerodynamics and Flight Mechanics," Boeing Scientific Research Laboratories, D1-82-0113, June 1961.

8. Miele, A., "The Extremization of Functionals Involving Products of Powers of Integrals and its Application to Aerodynamics," Boeing Scientific Laboratories, D1-82-0162, May 1962.
9. Miele, A., and Cole, J., "A Study of Optimum Slender Bodies in Hypersonic flow with a Variable Friction," Boeing Scientific Laboratories, D1-82-0223, January 1963.
10. Miele, A., "Slender Bodies of Revolution Having Minimum Total Drag at Hypersonic Speeds," Boeing Scientific Laboratories, D1-82-0230, February 1963.
11. Miele, A., "Optimum Airfoils at Moderate Supersonic Speeds, Part I- Preliminary Considerations," Rice University, Aero-Astronautics Report , No. 41, September 1968 (restricted to government agencies and contractors).
12. Biryuk, S. V., and Semenov, Y., "Application of the Method of Langrange Multipliers to Problems of Real-Data Assimilation," *IZVESTIYA Atmospheric and Oceanic Physics*, Vol. 27, No. 12, December 1991, pp. 962 - 967.
13. Le Dimet, F. X., and Talagrad, O., "Variational Algorithms for Analysis of Meteorological Observations: Theoretical Aspects," *Tellus*, Vol. 38A, No. 2, March 1986, pp. 97 - 110.
14. Lebdev, V. N., and Rummyantsev, B. N., "Variational Problem in Flight Between Two Points in a Central Field," *Planet and Space Science*, Vol. 12, June 1964, pp. 639 - 643.
15. Rao, G. V., "Exhaust Nozzle Contour for Optimum Thrust," *Jet Propulsion* , Vol. 28, No. 6, June 1958, pp. 377 - 382.
16. Shmyglevskii, Y. D., *Nekatorye Variatsionaye Zadachi Gazavoi Dinamiki*, Vichislitilnii Sentr AN SSSR, Moskva, 1963.
17. Mikhlin, S. G., *Variational Methods in Mathematical Physics*, Translated by T. Boddington, Pergamon Press, 1964.

18. Thompson, H. D., and Murthy, N. B., "Design of Optimized Three-Dimensional Rocket Motor Nozzle", AIAA No. 65-568, June 1965.
19. Lighthill, M. J., "A New Method of Two-Dimensional Aerodynamic Design," Research & Memorandum 2112, Aeronautical Research Council, April 1945
20. Bauer, F., Garabedian, P., and Korn, D., *A Theory of Super Critical Wing Section with Computer Programs and Examples*, Springer Verlag, 1972.
21. Gils, M., B., and Drela, M., "Two-dimensional Transonic Aerodynamic Design Methods," *AIAA Journal*, Vol. 25, No. 9, September 1987, pp. 1199 - 1206.
22. Carlson, L. A., Ratcliff, R. R., Gally, T. A., and Campbell, R. L., "Inverse Wing Design in Transonic Flow Including Viscous Interaction," *Transonic Symposium; Theory, Application and Experiment*, NASA CP-3020, Vol. 1, part 2, March 1989, pp. 497 - 519.
23. Lee, K. D., and Eyi, S., "Aerodynamic Design Via Optimization," ICAS 90-6.9.1, *17th congress of International Council of Aeronautical Sciences*, September 1990, pp. 1808 - 1818.
24. Lee, J., and Mason, W. H., "A Three-Dimensional Inverse Method for Supersonic and Hypersonic Body Design," AIAA Paper-91-3325-CP, September 1991.
25. Campbell, R. L., "An Approach to Constrained Aerodynamic Design with Application to Airfoils," NASA TP-3260, November 1992.
26. Barger, R. I., and Moitra, A. "On Minimizing the Number of Calculations in Design-by-Analysis Code," NASA TP-2706, June 1987.
27. Whitaker, K. W., Prasanth, R. K., and Markin, R., "Specifying Exhaust Nozzle Contours with a Neural Network," *AIAA Journal*, Vol. 31, No. 2, February 1993, pp. 273 - 277.

28. King, E. G., Freeman, L. M., Whitaker, K. W., and Karr, C. L., "Two-Dimensional Thrust Vectorizing Nozzle Optimization Techniques," AIAA Paper 91-0473, January 1991.
29. Park, J., and Sandberg, I. W., "Universal Approximation Using Radial Basis Function Network," *Neural Computation*, Vol. 3, No. 2, February 1991, pp. 246 - 257.
30. Huddleston, D. H., and Mastin, C. W., "Optimization of Aerodynamic Designs Using Computational Fluid Dynamics," AGARD-CP-463, Paper No. 23, May 1989.
31. Vanderplaats, G. N., "ADS - A Fortran Program for Automated Design Synthesis," Version 1.10, NASA Contractor Report 177985, September 1985.
32. Hicks, R. M., Murman, E. M., and Vanderplaats, G. N., "An Assessment of Airfoil Design By Numerical Optimization," NASA TM X-3092, July 1974.
33. Vanderplaats, G. N., "Approximation Concepts for Numerical Airfoil Optimization," NASA TP-1370, March 1979.
34. Vanderplaats, G. N., "An Efficient Algorithm for Numerical Airfoil Optimization," AIAA Paper No. 79-0079, January 1979.
35. Pittman, J. L., "Supersonic Airfoil Optimization," *Journal of Aircraft*, Vol. 24, No. 12, December 1987, pp. 873 - 879.
36. Elbanna, H. and Carlson, L., "Determination of Aerodynamic Sensitivity Coefficients in the Transonic and Supersonic Regimes" *Journal of Aircraft*, Vol. 27, No. 6, June 1990, pp. 507 - 518.
37. Baysal, O., and Eleshaky, M., E., "Aerodynamic Sensitivity Analysis Methods for the Compressible Euler Equations," *Journal of Fluids Engineering*, Vol. 113, No. 4., December 1991, pp. 681 - 688.

38. Baysal, O., and Eleshaky, M. E., "Aerodynamic Design Optimization Using Sensitivity Analysis and Computational Fluid Dynamics," *AIAA Journal*, Vol. 30, No. 3, March 1992, pp. 718 - 725.
39. Eleshaky, M. E., and Baysal, O., "Airfoil Shape Optimization Using Sensitivity Analysis on Viscous Flow Equations," *Multidisciplinary Applications of CFD*, [Ed: O. Baysal], FED-Vol 129, ASME-Winter Annual Meeting, December 1991, pp. 26 - 36.
40. Burgreen, G. W., and Baysal, O., "Aerodynamic Shape Optimization Using Preconditioned Conjugate Gradient Methods," AIAA Paper 93-3322, July 1993.
41. Burgreen, G. W., and Baysal, O., "Three-Dimensional Aerodynamic Shape Optimization of Wings Using Discrete Sensitivity Analysis," AIAA Paper 94-0094, January 1994.
42. Burgreen, W. G., "Three Dimensional Aerodynamic Shape Optimization Using Discrete Sensitivity Analysis," Ph.D. Dissertation, Old Dominion University, May 1994.
43. Lacasse, M. J., "Implementation of a Multiblock Sensitivity Analysis Method in Numerical Aerodynamic Shape Optimization," Masters Thesis, Old Dominion University, May 1994.
44. Taylor, A. C, III, Hou, G. J.-W., and Korivi, V. M., "Sensitivity Analysis, Approximate Analysis, and Design Optimization for Internal and External Viscous Flows," AIAA Paper 91-3083, September 1991.
45. Newman, P. A., Hou, G. J.-W., Jones, H. E., Taylor, A. C., III, and Korovi, V. M., "Observations on Computational Methodologies for Use In Large-Scale Gradient-Based Multi-disciplinary Design," *Proceedings of the Fourth AIAA/USAF/NASA/OAI Symposium on Multidisciplinary Analysis and Optimization*, AIAA, Cleveland, OH, September 1992, pp. 531 - 542.

46. Korivi, V. M., Taylor, A. C., III, Newman, P. A., Hou, G. J.-W., and Jones, H. E., "An Approximately-Factored Incremental Strategy for Calculating Consistent Discrete Aerodynamic Sensitivity Derivatives," *Proceedings of the Fourth AIAA/USAF/NASA/OAI Symposium on Multidisciplinary Analysis and Optimization*, AIAA, Cleveland, OH, September 1992, pp. 465 - 478.
47. Hou, G. J.-W., Taylor, C. A., III, Korivi, M. V., "Discrete Shape Sensitivity Equations for Aerodynamic Problems," AIAA-91-2259, AIAA/SAE/ASME/ASEE 27th Joint Propulsion Conference, June 24-27, 1991.
48. Korivi, V. M., Taylor, A. C., III, Hou, G. J.-W., Newman, P. A., and Jones, H. E., "Sensitivity Derivatives for Three-Dimensional Supersonic Euler Code Using Incremental Iterative Strategy," *Proceedings, 12th AIAA Computational Fluid Dynamics Conference*, July 1993, pp. 1053 - 1054.
49. Taylor, A. C., III, Newman, P. A., Hou, G. J.-W., and Jones, H. E., "Recent Advances in Steady Compressible Aerodynamic Sensitivity Analysis," *IMA Workshop on Flow Control*, Institute for Mathematics and its Application, University of Minnesota, Minneapolis, November 1992.
50. Lions, L. J., *Optimal Control of Systems Governed by Partial Differential Equations*. Springer-Verlag, New York, Translated by S. K. Mitter, 1971.
51. Pironneau, O., "On Optimum Profile in Stokes Flow," *Journal of Fluid Mechanics*, Vol. 59, Part 1, June 1973, pp. 117 - 128.
52. Glowinski, R., and Pironneau, O., "On the Numerical Computation of the Minimum-Drag Profile in Laminar Flow," *Journal of Fluid Mechanics*, Vol. 72, Part 2, November 1975, pp. 385 - 389.
53. Chen, W H., and Sienfeld, J. H., "Estimation of the Location of the Boundary of a Petroleum Reservoir," *Society of Petroleum Engineers Journal*, Vol. 15, No. 1, February 1975, pp. 19 - 38.

54. Koda, M., Dogru, A. H., and Sienfeld, J. H., "Sensitivity Analysis of Partial Differential Equations with Application to Reaction and Diffusion Process," *Journal of Computational Physics*, Vol. 30, No. 2, February 1979, pp. 259 - 282.
55. Koda, M., "Sensitivity Analysis of the Atmospheric Diffusion Equations," *Atmospheric Environment*, Vol. 16, No. 11, November 1982, pp. 2595 - 2601.
56. Koda, M., " Optimum Design in Fluid Mechanical Distributed-Parameter Systems," *Large Scale Systems*, Vol. 6, No. 3, June 1984, pp. 279 - 291.
57. Koda, M., "Sensitivity Analysis of Descriptor Distributed Parameter Systems," *International Journal of System Science*, Vol. 19, No. 10, October 1988, pp. 2103 - 2114.
58. Meric, R. A., "Finite Element Analysis of Optimal Heating of Slab with Temperature Dependent Thermal Conductivity," *International Journal Heat and Mass Transfer*, Vol. 22, No. 10, October 1979, pp. 1347 - 1353
59. Meric, R. A., "Boundary Element Methods for the Optimization of Distributed Parameter Systems," *International Journal for Numerical Methods in Engineering*, Vol. 20, July 1984, pp. 1291 - 1304.
60. Shubin, G. R. , and Frank, P. D., "A Comparison of the Implicit Gradient Approach and the Variational Approach to Aerodynamic Design Optimization," Boeing Computer Services, April 1991.
61. Hou, J.-W. G., and Sheen, J., "Numerical Methods for Second-Order Shape Sensitivity Analysis with Application to Heat Conduction Problems," *International Journal for Numerical Methods in Engineering*, Vol. 36, February 1993, pp. 417 - 435.
62. Jameson, A., "Aerodynamic Design via Control Theory," ICASE, NASA Langley Research Center, ICASE Report No. 88-64, November 1988.

63. Cabuk, H., Modi, V., "Optimum Plane Diffusers in Laminar Flow," *Journal of Fluid Mechanics*, Vol. 237, April 1992, pp. 373 - 393.
64. Ta'asan, S., Kuruvilla, K. and Salas, M. D., "Aerodynamic Design and Optimization in One Shot," AIAA 92-0025, January 1992.
65. Ibrahim, H. A., and Baysal, O., "Design Optimization Using Variational Methods and CFD," AIAA-94-0093, January 1994.
66. Reuter, J., and Jameson, A., "Control Theory Based Airfoil Design for Potential Flow and Finite Volume Discretization," AIAA 94-0499, January 1994.
67. Kuruvila, G., Ta'asan, S., and Salas, M. D., "Airfoil Optimization by One Shot Method", AGARD-R-803, November 1994, pp. (7-1) - (7-21).
68. Iollo, A., and Salas, D. M., "Contribution to the Optimal Shape Design of Two-Dimensional Internal Flows With Embedded Shocks," ICASE, NASA Langley Research Center, ICASE Report No. 95-20, March 1995.
69. Ta'asan, S., "Pseudo-Time Methods for Constrained Optimizations Problems Governed by PDE," ICASE, NASA Langley Research Center, ICASE Report No. 95-32, May 1995.
70. Iollo, A., Kuruvila, G., and Ta'asan, S., "Pseudo-Time Method for Optimal Shape Design Using the Euler Equations," ICASE, NASA Langley Research Center, ICASE Report No. 95-59, August 1995.
71. Jespersen, C. D., and Pulliam. H. T., "Flux Vector Splitting and Approximate Newton Methods," AIAA-83-1899, July 1983.
72. Anderson, W. K., and Thomas, L. J., "Multigrid Acceleration of the Euler Equations," *AIAA Journal*, Vol. 26, No. 6, June 1988, pp.649 - 654.

73. Demuren, O. A., and Ibraheem, O. S., "On the Stability Analysis of Approximate Factorization Methods for 3D Euler and Navier-Stokes Equations," NASA TM 106314, ICOMP-93-29, October 1993.
74. Borggaard, J. T., "On the Presence of Shocks in Domain Optimization of Euler Equations," *IMA Workshop on Flow Control*, Institute for Mathematics and its Application, University of Minnesota, Minneapolis, November 1992.
75. Rumsey, C., "A Rough-Draft, Temporary CFL3D Code-Description and Input Documentation Manual," NASA Langley Research Center, Personal communication, 1995
76. Hoffmann, K., and Chiang, S.T., *Computational Fluid Dynamics for Engineers*, Vol. 2, Engineering Education System, Wichita, KS, 1993.
77. Hirsch, Ch., *Numerical Computation of Internal and External Flows*, Vol. I and II, 1990.
78. "GASP, Version 2.2, Users Manual," Aersoft Incorporated, January 1993.
79. Beam, R., and Warming, R. F., "An Implicit Finite Difference Algorithm for Hyperbolic Systems in Conservation-Law-Form," *Journal of Computational Physics*, Vol. 22, September 1976, pp. 87 - 110.
80. Van Leer, B., "Flux-Vector Splitting for the Euler Equations," ICASE, NASA Langley Research Center, ICASE Report No. 82-30, September 1982.
81. Jameson, A., "Numerical Solution of the Euler Equations by Finite Volume Methods Using Runge-Kutta Time Stepping Schemes," AIAA 14th Fluid and Plasma Dynamics Conference, AIAA -81-1259, June 1981.
82. Anderson, D. A., Tannehill, J. C., and Pletcher, R. H., *Computational Fluid Mechanics and Heat Transfer*, 1984

83. Eleshaky, M. E., "A Computational Aerodynamic Design Optimization Method Using Sensitivity Analysis," Ph.D. Dissertation, Old Dominion University, May 1992.
84. Gelfand, I. M., and Fomin, S. V., *Calculus of Variations*, Prentice-hall, Inc, 1963.
85. Thibert, J. J., "One Point and Multipoint Design Optimzation for Airplane and Helicopter Application," *Special Course on Inverse Methods for Airfoil Design for Aeronautical and Turbomachinery Applications*, AGARD-R-780, Paper No. 10, November 1990.
86. Mortenson, E. M., *Geometric Modeling*, John Wiley & Sons, 1985.
87. Smith, R. E., and Kerr, P. E., "Geometric Requirements for Multidisciplinary Analysis of Aerospace-Vehicle Design," *4th, AIAA-USAF-NASA-OIA Symposium on Multidisciplinary Analysis and Optimization*, AIAA-92-4773, Cleveland, Ohio, September 1992.
88. Haug, E. I., Choi, K. K., and Komkov, V., *Design Sensitivity Analysis of Structural Systems*, Academic Press, Inc, 1986.
89. Pironneau, O., *Optimum Shape Design for Elliptic Systems*, Springer-Verlag, 1984.
90. Vanderplaats, G. N., and Moses, F. "Structural Optimization by Methods of Feasible Directions," *Computers and Structures*, Vol. 3, July 1973, pp. 739 - 755.
91. Haftka, R. T., and Gurdal, Z., *Elements of Structural Optimization*, Third Revised and Expanded Edition, Kluwer Academic Publishers, 1991.
92. Roe, P. L., "Approximate Riemann Solver, Parameters Vectors, and Difference Schemes," *Journal of Computational Physics*, Vol. 43, October 1981, pp. 357 - 372.

APPENDICES

APPENDIX A

CONTINUOUS DOMAIN IN VARIATIONAL METHODS

Consider the domain $\bar{\Omega}$ and the solution vectors $\bar{\bar{Q}}$ which are transformed from an original domain Ω and from the nominal solution vector \bar{Q} by the following one-to-one mappings [84]:

$$\bar{\bar{X}} = \bar{\Phi}(\bar{X}; \varepsilon) = \bar{X} + \varepsilon \left[\frac{d\bar{\Phi}}{d\varepsilon} \right]_{\varepsilon=0} + O(\varepsilon^2) \quad (\text{A.1})$$

$$\bar{\bar{X}} = \bar{X} + \varepsilon \left[\frac{d\bar{\Phi}}{d\varepsilon} \right]_{\varepsilon=0} + O(\varepsilon^2) \quad (\text{A.2})$$

where ε is a small quantity. Likewise,

$$\bar{\bar{Q}} = \bar{\Psi}(\bar{X}; \varepsilon) = \bar{\Psi}(\bar{X}; 0) + \varepsilon \left[\frac{d\bar{\Psi}}{d\varepsilon} \right]_{\varepsilon=0} + O(\varepsilon^2) \quad (\text{A.3})$$

$$\bar{\bar{Q}} = \bar{Q} + \varepsilon \left[\frac{d\bar{\Psi}}{d\varepsilon} \right]_{\varepsilon=0} + O(\varepsilon^2) \quad (\text{A.4})$$

Now, take only the linear parts of Eqs. (A.2) and (A.4), and one gets

$$\Delta\bar{X} = \bar{\bar{X}} - \bar{X} = \varepsilon \left[\frac{d\bar{\Phi}}{d\varepsilon} \right]_{\varepsilon=0} \equiv \delta\bar{X} \quad (\text{A.5})$$

$$\Delta \bar{Q} = \bar{Q}(\bar{X}) - \bar{Q}(\bar{X}) = \varepsilon \left[\frac{d\bar{Y}}{d\varepsilon} \right]_{\varepsilon=0} \equiv \delta \bar{Q} \quad (\text{A.6})$$

The variation of the solution vector in the usual variational sense (i.e., variation at the same coordinate location) can also be defined as

$$\Delta \bar{\bar{Q}} = \bar{\bar{Q}}(\bar{X}) - \bar{Q}(\bar{X}) \equiv \delta \bar{\bar{Q}} \quad (\text{A.7})$$

Then for the relation between $\delta \bar{Q}$ and $\delta \bar{\bar{Q}}$, the following expression can be established as

$$\begin{aligned} \Delta \bar{Q} &= \bar{Q}(\bar{X}) - \bar{Q}(\bar{X}) \\ &= \bar{\bar{Q}}(\bar{X}) - \bar{Q}(\bar{X}) + \bar{Q}(\bar{X}) - \bar{Q}(\bar{X}) \\ &= (\bar{\bar{Q}}(\bar{X}) - \bar{Q}(\bar{X})) + (\bar{Q}(\bar{X}) - \bar{Q}(\bar{X})) \end{aligned} \quad (\text{A.8})$$

From the Eq. (A.8), $\bar{\bar{Q}}(\bar{X}) - \bar{Q}(\bar{X})$ can be approximated by

$$\bar{\bar{Q}}(\bar{X}) - \bar{Q}(\bar{X}) = \frac{\partial \bar{Q}}{\partial \bar{X}} (\bar{X} - \bar{X}) = \frac{\partial \bar{Q}}{\partial \bar{X}} \delta \bar{X} \quad (\text{A.9})$$

and with Eq. (A.9), Eq. (A.8) becomes

$$\Delta \bar{Q} = \frac{\partial \bar{Q}}{\partial \bar{X}} \delta \bar{X} + \delta \bar{\bar{Q}} \approx \delta \bar{Q} \quad (\text{A.10})$$

Then with Eq. (A.10), $\delta \bar{\bar{Q}}$ is approximated as

$$\delta \bar{\bar{Q}} = \delta \bar{Q} - \frac{\partial \bar{Q}}{\partial \bar{X}} \delta \bar{X} \quad (\text{A.11})$$

Equation (A.10) explains that the total variation of the solution vector $\delta\bar{Q}$ is composed of parts due to the variation of the state vector $\delta\bar{Q}$ and the coordinate transformation $\frac{\partial\bar{Q}}{\partial X}\delta\bar{X}$.

APPENDIX B

DERIVATION OF THE SURFACE TRANSFORMATION JACOBIAN

For a small quantity ε , the transformed space is represented by Eq.(A.1). Then by the chain rule, the surface Jacobian J_s can be obtained as [84]

$$J_s = \frac{\partial \bar{X}_i}{\partial X_j} \approx \delta_{i,j} + \varepsilon \left(\frac{\partial}{\partial X_j} \left[\left(\frac{\partial \Phi}{\partial \varepsilon} \right)_i \right]_{\varepsilon=0} \right) \quad j = 1, 2, \dots, m; \quad i = 1, 2, \dots, n \quad (\text{B.1})$$

where $\delta_{i,j}$ is the Kronecker delta equal to 1 if $i = j$ and 0 otherwise. The second term on the right hand-side of Eq. (B.1) indicates the contribution due to the space transformation. Then, the total change of the area due to the space transformation is the determinant of Eq. (B.1) which is expressed as

$$|J_s| = \left| \delta_{i,j} + \varepsilon \sum_{i=1}^n \left\{ \frac{\partial}{\partial X_j} \left(\left[\left(\frac{\partial \Phi}{\partial \varepsilon} \right)_i \right]_{\varepsilon=0} \right) \right\} \right| \quad j = 1, 2, \dots, m \quad (\text{B.2})$$

Further simplification of Eq. (B.2) gives

$$|J_s| = \left| I + \varepsilon \sum_{i=1}^n \left\{ \frac{\partial}{\partial X_j} \left(\left[\left(\frac{\partial \Phi}{\partial \varepsilon} \right)_i \right]_{\varepsilon=0} \right) \right\} \right| \quad j = 1, 2, \dots, m \quad (\text{B.3})$$

where I is the identity diagonal matrix. because the variation of the boundary is due to the variations of the boundary coordinates and that

$$\epsilon \sum_{i=1}^n \left(\left[\left(\frac{\partial \Phi}{\partial \epsilon} \right)_i \right]_{\epsilon=0} \right) = \delta \bar{X} \quad (\text{B.4})$$

then, Eq. (B.3) can be expressed as

$$|J_s| = |I + \bar{\nabla} \cdot \delta \bar{X}| \quad (\text{B.5})$$

which is the total change of the surface due to the change of the variable domain.

APPENDIX C

VARIOUS MATRICES IN CONSERVATIVE FORMS FROM THE QUASI ONE-DIMENSIONAL EULER FORMULATION.

The various matrices defined for the quasi one-dimensional Euler equations in the Cartesian coordinate systems are as follows:

1. By use of Beam-Warming flux splitting, the approximate Jacobian matrix A is computed as [76]

$$A = S \begin{bmatrix} 0 & 1 & 0 \\ \frac{(\gamma-3)}{2}u^2 & -(\gamma-3)u & (\gamma-1) \\ (\gamma-1)u^3 - \gamma e_i & \gamma e_i - \frac{3(\gamma-1)}{2}u^2 & \gamma u \end{bmatrix} \quad (C.1)$$

2. By use of the Van Leer flux splitting, the exact Jacobian matrix A is computed as [80]

a = local speed of sound

$$E = [E_{1,vL}, E_{2,vL}, E_{3,vL}]^T$$

is the flux vector where the components are defined as

$$E_{1,vL} = pm \cdot \frac{\rho(u + pm \cdot a)^2}{4a} = pm \cdot \frac{(q_2 + pm \cdot a q_1)^2}{4a q_1} \quad (C.2)$$

$$E_{2,vL} = E_{1,vL} \cdot \frac{[(\gamma-1)u + 2 \cdot pm \cdot a]}{\gamma} = E_{1,vL} \cdot \frac{[(\gamma-1)q_2 + 2 \cdot pm \cdot aq_1]}{\gamma q_1} \quad (C.3)$$

$$E_{3,vL} = E_{1,vL} \cdot \frac{[(\gamma-1)u + 2 \cdot pm \cdot a]^2}{2(\gamma^2 - 1)} = E_{1,vL} \cdot \frac{[(\gamma-1)q_2 + 2 \cdot pm \cdot aq_1]^2}{2(\gamma^2 - 1)q_1^2} \quad (C.4)$$

where the parameter to switch between positive and negative contributions is

$$pm = (\pm) \quad (C.5)$$

and \bar{Q} and P are defined as

$$\bar{Q} = [\rho, \rho u, \rho e_t]^T = [q_1, q_2, q_3]^T \quad (C.6)$$

and

$$P = (\gamma - 1) \left[\rho e_t - \rho \frac{u^2}{2} \right] = (\gamma - 1) \left[q_3 - \frac{q_2^2}{2q_1} \right] \quad (C.7)$$

The derivatives of the fluxes with respect to the conservative variables are

$$\frac{\partial E_{1,vL}}{\partial Q_r} = \frac{pm}{4} \left[2 \frac{(q_2 + pm \cdot aq_1)}{aq_1} \frac{\partial(q_2 + pm \cdot aq_1)}{\partial Q_r} - (q_2 + pm \cdot aq_1)^2 \frac{\partial(aq_1)}{\partial Q_r} \right] \quad (C.8)$$

$$\begin{aligned} \frac{\partial E_{2,vL}}{\partial Q_r} &= \frac{[(\gamma-1)q_2 + 2 \cdot pm \cdot aq_1]}{\gamma q_1} \frac{\partial E_{1,vL}}{\partial Q_r} + \\ &\frac{E_{1,vL}}{\gamma} \left\{ \frac{\partial((\gamma-1)q_2 + 2 \cdot pm \cdot aq_1)}{q_1 \partial Q_r} - ((\gamma-1)q_2 + 2 \cdot pm \cdot aq_1) \frac{\partial q_1}{\partial Q_r} \right\} \end{aligned} \quad (C.9)$$

$$\frac{\partial E_{3,vL}}{\partial Q_r} = \frac{[(\gamma-1)q_2 + 2 \cdot pm \cdot aq_1]^2}{2(\gamma^2-1)q_1^2} \frac{\partial E_{1,vL}}{\partial Q_r} + \frac{E_{1,vL}}{2(\gamma^2-1)} \left\{ \frac{2[(\gamma-1)q_2 + 2 \cdot pm \cdot aq_1]}{q_1^2} - \frac{\partial(q_1^2)}{\partial Q_r} \right\} \quad (C.10)$$

Then the Jacobian components are determined from

$$\frac{\partial E_{vL}^\pm}{\partial Q_r} = \left[\frac{\partial E_{1,vL}}{\partial Q_r}, \frac{\partial E_{2,vL}}{\partial Q_r}, \frac{\partial E_{3,vL}}{\partial Q_r} \right]^T \quad (C.11)$$

where r is the index looping from 1 to 3 and the other quantities are defined as

$$B_h = (\gamma-1)s_x \begin{bmatrix} 0 & 0 & 0 \\ \frac{q_2^2}{2q_1^2} & -\frac{q_2}{q_1} & 1 \\ 0 & 0 & 0 \end{bmatrix} \quad (C.12)$$

$$C = (\gamma-1) \left[\frac{q_2^2}{2q_1^2}, -\frac{q_2}{q_1}, 1 \right]^T \quad (C.13)$$

$$M_h = [0, P, 0]^T \quad (C.14)$$

where P is given in Eq. (C.7).

APPENDIX D

TWO-DIMENSIONAL JACOBIAN MATICES THAT ARE USED FOR THE STABILITY ANALYSIS

By use of the Van Leer flux-splitting technique in Cartesian coordinates, the exact Jacobian matrices A and B of the inviscid two-dimensional Euler Equations are computed. To realize this, let us define the field variables, fluxes, and speed of sound in the conservative form as

$$\bar{Q} = [\rho, \rho u_k, \rho e_t]^T = [q_1, q_2, q_3, q_4]^T \quad (D.1)$$

$$a = \left\{ \gamma(\gamma - 1) \left[\frac{q_4}{q_1} - \left(\frac{q_2^2 + q_3^2}{2q_1} \right) \right] \right\}^{1/2} \quad (\text{local speed of sound}) \quad (D.2)$$

$$M_j = \frac{u_j}{a}, \quad (\text{Mach number}) \quad (D.3)$$

where the parameter to switch between positive and negative contributions is

$$pm = (\pm) \quad (D.4)$$

and

$$f_{mass}^{\pm} = pm \cdot \rho \cdot a \cdot \frac{\left(\frac{u_j}{\rho \cdot a} + pm \right)^2}{4} = pm \cdot q_1 \cdot a \cdot \frac{\left(\frac{M_j}{q_1} + pm \right)^2}{4} \quad (D.5)$$

$$f_j^\pm = \left[\frac{(\gamma-1)u_j + 2 \cdot pm \cdot a}{\gamma} \right] = \left[\frac{(\gamma-1)q_j + 2 \cdot pm \cdot a q_1}{\gamma q_1} \right] \quad (\text{D.6})$$

$$f_{j,mom}^\pm = f_{mass}^\pm f_j^\pm \quad (\text{momentum components}) \quad (\text{D.7})$$

$$\begin{aligned} (f_{energy}^\pm)_x &= f_{mass}^\pm \left[\frac{[(\gamma-1)u_j + 2 \cdot pm \cdot a]^2}{2(\gamma^2-1)} + \left(\frac{v^2}{2} \right) \right] = \\ f_{mass}^\pm &\left[\frac{[(\gamma-1)q_j + 2 \cdot pm \cdot a]^2}{2(\gamma^2-1)q_1^2} + \left(\frac{q_3^2}{2q_1^2} \right) \right] \quad (\text{energy in the x direction}) \quad (\text{D.8}) \end{aligned}$$

$$(f_{energy}^\pm)_y = f_{mass}^\pm \left[\frac{[(\gamma-1)u_j + 2 \cdot pm \cdot a]^2}{2(\gamma^2-1)} + \left(\frac{u^2}{2} \right) \right] = \quad (\text{D.9})$$

$$f_{mass}^\pm \left[\frac{[(\gamma-1)q_j + 2 \cdot pm \cdot a]^2}{2(\gamma^2-1)q_1^2} + \left(\frac{q_2^2}{2q_1^2} \right) \right] \quad (\text{energy in the y direction}) \quad (\text{D.10})$$

Then the flux vectors in the x and y directions, respectively, are given as

$$F_{VL} = [f_{mass}^\pm, f_{j,mom}^\pm, f_{energy}^\pm]^T \quad (\text{D.11})$$

The derivatives of the fluxes are

$$\frac{\partial f_{mass}^\pm}{\partial Q_r} = \frac{pm}{4} \left\{ \left(\frac{M_j}{q_1} + pm \right)^2 \frac{\partial [q_1 \cdot a]}{\partial Q_r} + 2(q_1 \cdot a) \left(\frac{M_j}{q_1} + pm \right) \frac{\partial \left(\frac{M_j}{q_1} + pm \right)}{\partial Q_r} \right\} \quad (\text{D.12})$$

$$\frac{\partial f_{mom,j}^\pm}{\partial Q_r} = f_j^\pm \frac{\partial f_{mass}^\pm}{\partial Q_r} + f_{mass}^\pm \frac{\partial f_j^\pm}{\partial Q_r} \quad (\text{D.13})$$

$$\frac{\partial (f_{energy}^\pm)_x}{\partial Q_r} = \left[\frac{[(\gamma-1)q_j + 2 \cdot pm \cdot a]^2}{2(\gamma^2-1)q_1^2} + \left(\frac{q_3^2}{2q_1^2} \right) \right] \frac{\partial f_{mass}^\pm}{\partial Q_r} +$$

$$f_{mass}^\pm \frac{\partial \left[\frac{[(\gamma-1)q_j + 2 \cdot pm \cdot a]^2}{2(\gamma^2-1)q_1^2} + \left(\frac{q_3^2}{2q_1^2} \right) \right]}{\partial Q_r} \quad (D.14)$$

$$\frac{\partial (f_{energy}^\pm)_y}{\partial Q_r} = \left[\frac{[(\gamma-1)q_j + 2 \cdot pm \cdot a]^2}{2(\gamma^2-1)q_1^2} + \left(\frac{q_2^2}{2q_1^2} \right) \right] \frac{\partial f_{mass}^\pm}{\partial Q_r} +$$

$$f_{mass}^\pm \frac{\partial \left[\frac{[(\gamma-1)q_j + 2 \cdot pm \cdot a]^2}{2(\gamma^2-1)q_1^2} + \left(\frac{q_2^2}{2q_1^2} \right) \right]}{\partial Q_r} \quad (D.15)$$

Then, the A and B Jacobian matrices in the x and y directions, respectively are constructed as

$$\frac{\partial \bar{F}_{VL,x}^\pm}{\partial Q_r} = \left[\frac{\partial f_{mass}^\pm}{\partial Q_r}, \frac{\partial f_{j,mom}^\pm}{\partial Q_r}, \frac{\partial f_{energy,x}^\pm}{\partial Q_r} \right]^T \quad (D.16)$$

$$\frac{\partial \bar{F}_{VL,y}^\pm}{\partial Q_r} = \left[\frac{\partial f_{mass}^\pm}{\partial Q_r}, \frac{\partial f_{j,mom}^\pm}{\partial Q_r}, \frac{\partial f_{energy,y}^\pm}{\partial Q_r} \right]^T \quad (D.17)$$

where r is the index looping from 1 to 4, and j from 2 to 3.

APPENDIX E

DERIVATION OF TWO-DIMENSIONAL CONSERVATIVE VAN LEER JACOBIAN MATRICES IN GENERALIZED COORDINATES

Hyperbolic equations such as the Euler equations of the fluid flow, are numerically treated based on the direction of the physical propagation of waves. Therefore, the fluxes and the Jacobian are split into the positive and negative contributions and are discretized according to the sign of the Jacobian matrices. The Van Leer flux-vector-splitting technique in generalized coordinates, which follows this upwinding method and which has the smooth differentiability property at sonic transitions and stagnation points, is used for our flow analysis and co-state equations. For the general derivation of the various terms in the splitting procedure, we define the following quantities:

$$\hat{\zeta}_k = \frac{\zeta_k}{|\nabla \zeta|} \quad (\text{direction cosines, } k = x, y)$$

(E.1)

$$r_{len} = \sqrt{(\hat{\zeta}_x^2 + \hat{\zeta}_y^2)} \quad (\text{cell area}) \quad (\text{E.2})$$

$$U = \frac{\rho(\zeta_x u + \zeta_y v)}{\rho} = \frac{(q_1 \zeta_x + q_2 \zeta_y)}{q_1} \quad (\text{contravelocity}) \quad (\text{E.3})$$

$$\bar{Q} = [\rho, \rho u_j, \rho e_i]^T = [q_1, q_2, q_3, q_4]^T \quad (\text{conservative variables}) \quad (\text{E.4})$$

$$a = \left\{ \gamma(\gamma - 1) \left[\frac{q_4}{q_1} - \left(\frac{q_2^2 + q_3^2}{2q_1} \right) \right] \right\}^{\frac{1}{2}}, \quad (\text{local speed of sound})$$

(E.5)

$$M_\zeta = \frac{U}{a}, \quad \text{Mach number} \quad (\text{E.6})$$

where the parameter to switch between positive and negative contributions is

$$pm = (\pm) \quad (\text{E.7})$$

$$f_{mass}^\pm = rlen \cdot pm \cdot \rho \cdot a \cdot \frac{(M_\zeta + pm)^2}{4} = rlen \cdot pm \cdot q_1 \cdot a \cdot \frac{(M_\zeta + pm)^2}{4} \quad (\text{E.8})$$

$$f_j^\pm = \left[\frac{\zeta_k}{\gamma} (-U + 2a \cdot pm) + \frac{q_j}{q_1} \right] \quad (\text{E.9})$$

$$f_{j,mom}^\pm = f_{mass}^\pm f_j^\pm \quad (\text{E.10})$$

$$f_{energy}^\pm = f_{mass}^\pm \left[\frac{(1 - \gamma)U^2 + 2 \cdot pm \cdot (\gamma - 1)aU + 2a^2}{(\gamma^2 - 1)} + \left(\frac{q_2^2 + q_3^2}{2q_1^2} \right) \right] \quad (\text{E.11})$$

$$\hat{F}^\pm(\bar{Q}) = \frac{|\nabla \zeta|}{J} [f_{mass}^\pm, f_{j,mom}^\pm, f_{energy}^\pm]^T \quad (\text{E.12})$$

$$\frac{\partial M_\zeta}{\partial Q_r} = \frac{1}{a^2} \left[a \frac{\partial U}{\partial Q_r} - U \frac{\partial a}{\partial Q_r} \right]^T \quad (\text{E.13})$$

By the use of Eqs. (E.1) - (E.13), the derivatives of the mass, momentum, and energy with respect to the conservative field variables can be expressed as

$$\frac{\partial f_{mass}^{\pm}}{\partial Q_r} = rlen * \frac{pm}{4} \cdot \left[a(M_{\xi} + pm)^2 \frac{\partial q_1}{\partial Q_r} + q_1(M_{\xi} + pm)^2 \frac{\partial a}{\partial Q_r} + 2aq_1(M_{\xi} + pm) \frac{\partial M_{\xi}}{\partial Q_r} \right] \quad (E.14)$$

$$\frac{\partial f_j^{\pm}}{\partial Q_r} = \left\{ \frac{\zeta_k}{\gamma} \left[-\frac{\partial U}{\partial Q_r} + 2 \cdot pm \cdot \frac{\partial a}{\partial Q_r} \right] + \frac{\partial \left(\frac{q_j}{q_1} \right)}{\partial Q_r} \right\} \quad (E.15)$$

$$\frac{\partial f_{j,mom}^{\pm}}{\partial Q_r} = f_j^{\pm} \frac{\partial f_{mass}^{\pm}}{\partial Q_r} + f_{mass}^{\pm} \frac{\partial f_j^{\pm}}{\partial Q_r} \quad (F.16)$$

$$q22 = \frac{(q_2^2 + q_3^2)}{2q_1^2} \quad (E.17)$$

$$\frac{\partial f_{energy}^{\pm}}{\partial Q_r} = f_{energy}^{\pm} \frac{\partial f_{mass}^{\pm}}{\partial Q_r} + f_{mass}^{\pm} \left\{ 2 \frac{(a \cdot pm - U)}{(\gamma + 1)} \frac{\partial U}{\partial Q_r} + 2 \cdot pm \left[U + 2 \frac{a}{(\gamma - 1)} \right] \frac{1}{(\gamma + 1)} \frac{\partial a}{\partial Q_r} + \frac{\partial q22}{\partial Q_r} \right\} \quad (E.18)$$

With Eqs. (E.14) - (E.18), the general expressions for the split Jacobian in conservative variables can be symbolically represented as

$$\frac{\partial \hat{F}_{VL}^{\pm}}{\partial Q_r} = \left[\frac{\partial f_{mass}^{\pm}}{\partial Q_r}, \frac{\partial f_{j,mom}^{\pm}}{\partial Q_r}, \frac{\partial f_{energy}^{\pm}}{\partial Q_r} \right]^T \quad (E.20)$$

where r is the index looping from 1 to 4 and j from 2 to 3. When the computation is performed in the ξ direction, $\frac{\partial \hat{F}_{VL}^{\pm}}{\partial Q_r}$ denotes the split Jacobian matrices in the

ξ direction, similarly, when the computation is performed in the η direction, $\frac{\partial \hat{F}_{VL}^\pm}{\partial Q_r}$ denotes the split Jacobians in the η direction.